PolyPublie
Polytechnique Montréal

POLYTECHNIQUE MONTRÉAL
UNIVERSITÉ D'INGÉNIERIE

Titre: Title:	Development of Natural Fiber Reinforced Polylactide-Based Biocomposites
Auteur: Author:	Andrea Marcela Arias Herrera
Date:	2014
Type:	Mémoire ou thèse / Dissertation or Thesis
Référence: Citation:	Arias Herrera, A. M. (2014). Development of Natural Fiber Reinforced Polylactide-Based Biocomposites [Thèse de doctorat, École Polytechnique de Montréal]. PolyPublie. https://publications.polymtl.ca/1457/

Document en libre accès dans PolyPublie
Open Access document in PolyPublie

URL de PolyPublie: PolyPublie URL:	https://publications.polymtl.ca/1457/
Directeurs de recherche: Advisors:	Marie-Claude Heuzey, & Michel Huneault
Programme: Program:	Génie chimique

Ce fichier a été téléchargé à partir de PolyPublie, le dépôt institutionnel de Polytechnique Montréal
This file has been downloaded from PolyPublie, the institutional repository of Polytechnique Montréal

https://publications.polymtl.ca

UNIVERSITÉ DE MONTRÉAL

DEVELOPMENT OF NATURAL FIBER REINFORCED POLYLACTIDE-BASED BIOCOMPOSITES

ANDREA MARCELA ARIAS HERRERA

DÉPARTEMENT DE GÉNIE CHIMIQUE

ÉCOLE POLYTECHNIQUE DE MONTRÉAL

THÈSE PRÉSENTÉE EN VUE DE L'OBTENTION

DU DIPLÔME DE PHILOSOPHIAE DOCTOR

(GÉNIE CHIMIQUE)

JUILLET 2014

© Andrea Marcela Arias Herrera, 2014.

UNIVERSITÉ DE MONTRÉAL

ÉCOLE POLYTECHNIQUE DE MONTRÉAL

Cette thèse intitulée:

DEVELOPMENT OF NATURAL FIBER REINFORCED POLYLACTIDE-BASED BIOCOMPOSITES

présentée par : ARIAS HERRERA Andrea Marcela

en vue de l'obtention du diplôme de : Philosophiae Doctor

a été dûment acceptée par le jury d'examen constitué de :

M. CARREAU, Pierre, Ph.D., président

Mme HEUZEY, Marie-Claude, Ph.D., membre et directrice de recherche

M. HUNEAULT, Michel, Ph.D., membre et codirecteur de recherche

M. AJJI, Abdellah, Ph.D., membre

Mme STOEFFLER, Karen, Ph.D., membre

DEDICATION

To my parents, from whom I learned the patience to pursue my dreams

and the perseverance to achieve them.

A mis padres, de quienes aprendí la paciencia para perseguir mis sueños

y la perseverancia para hacerlos realidad.

ACKNOWLEDGMENTS

First and foremost, I offer my sincerest gratitude to my two supervisors; Prof. Marie-Claude Heuzey from Polytechnique Montréal and Prof. Michel Huneault from Université de Sherbrooke. Their patience, guidance and support were key motivations all the time throughout my Ph.D. I am grateful for my inclusion in their NSERC grant.

Marie-Claude has been my guiding beacon through my stay at Polytechnique. I am truly thankful for her openness, receptivity and promptly response to my questions and queries. Michel is a mentor and friend from whom I have learnt scientific rigor and critical thinking. His kindness and dedication to the improvement of my scientific writing has been invaluable.

I would like to thank the rest of the members of the jury: Prof. Pierre Carreau, Prof. Abdellah Ajji, Prof. Martin Lévesque and Dr. Karen Stoeffler for their excellent feedback and suggestions for improving this thesis.

My sincere thanks also goes to Dr. Gilles Ausias, Dr. Abdelkader Bendahou and Dr. Paula Wood-Adams for their encouragement, insightful comments and precious discussions.

Special thanks goes to all the technical and administrative staff of chemical engineering department at Polytechnique Montréal, particularly Mr. Guillaume Lessard, Ms. Claire Cerclé, Ms. Mélina Hamdine and Ms. Weawkamol Leelapornpisit for their technical assistance and valuable knowledge.

My warm thanks to my fellow labmates, to my office colleagues and friends for their understanding and support in the difficult moments; their human qualities and pleasant company have my deepest appreciation.

Finally, my deepest gratitude to my beloved parents, brother and sister; their love goes beyond borders.

RÉSUMÉ

Le polylactide ou PLA est un polymère biodégradable qui peut être produit à partir de ressources renouvelables. Ce polyester aliphatique présente de bonnes propriétés mécaniques similaires à celles du polyéthylène téréphtalate (PET). Depuis 2003, du PLA à haut poids moléculaire est produit à l'échelle industrielle et commercialisé sous forme de grades amorphes et semicristallins pour diverses applications. L'amélioration de la cinétique de cristallisation du PLA est cruciale pour que ce biopolymère devienne compétitif face aux plastiques issus du pétrole et puisse les remplacer. D'autre part, la combinaison de fibres naturelles avec des matrices polymériques issues de ressources renouvelables, afin de produire des polymères composites entièrement biosourcés et biodégradables, a été une tendance marquée dans les activités de recherche au cours de la dernière décennie. Néanmoins les différences liées à la structure chimique, notamment observées dans la nature fortement hydrophile des fibres et le caractère hydrophobe des matrices thermoplastiques, représentent un inconvénient majeur pour les interactions fibre/matrice.

Le but de la présente recherche a été d'étudier les interactions intrinsèques fibre/matrice dans des polymères composites issus de fibres naturelles et du PLA, préparés par un mélange à l'état fondu. Des fibres de lin courtes présentant une longueur nominale d'environ 1 mm ont été sélectionnées comme renfort; par la suite, des biocomposites contenant une charge de fibres faible à modérée ont été préparés par mélange direct des fibres avec la matrice à l'état fondu. La rupture des faisceaux de fibres pendant la mise en forme a conduit à d'importantes réductions dans la longueur et le diamètre des fibres. Le rapport de forme moyen a été diminué d'environ 50%. La cinétique de cristallisation au repos du PLA et des systèmes biocomposites a été examinée sous conditions isothermes et non isothermes. La capacité de nucléation des fibres de lin a été démontrée et la cristallisation du PLA a été effectivement accélérée en présence du renfort. Cette amélioration a été de plus contrôlée par la température à laquelle la cristallisation a eu lieu, la transition de la phase liquide à la phase solide étant thermodynamiquement favorisée par le degré de surfusion. Lors de la cristallisation, les propriétés viscoélastiques devraient être fortement influencées par le développement des cristallites et leur empiètement. La rhéométrie a été choisie comme technique appropriée pour étudier l'évolution de la viscosité complexe et des modules de conservation et de perte lors de la cristallisation du PLA et de ses biocomposites. L'optimisation des conditions expérimentales a été nécessaire afin de compenser adéquatement le

rétrécissement du polymère, qui est un souci majeur pour la reproductibilité des mesures, en particulier à niveaux élevés de surfusion. Cette étude a démontré que la vitesse de cristallisation était accrue en présence des fibres de lin, et ce dans une large gamme de températures de cristallisation. Étant donné que le développement de la cristallisation dans les procédés à échelle industrielle peut différer grandement des études sous conditions au repos, une investigation préliminaire de l'effet de l'écoulement en cisaillement sur la cristallisation du PLA a été entreprise. En utilisant le même intervalle de vitesses de cisaillement, deux ensembles de conditions ont été étudiés, à savoir (1) déformation totale constante, et (2) temps de cisaillement constant. Dans les deux cas, l'accroissement de la cinétique de cristallisation a été démontré par une diminution du temps d'induction, laquelle est devenue plus importante aux vitesses de cisaillement les plus élevés. Environ 75% de réduction du temps d'induction a été observée à 4 s^{-1}, le taux de cisaillement maximal atteint dans cette recherche.

La réduction de la taille des particules de cellulose de l'échelle micro à l'échelle nanométrique a également attiré une attention croissante lors de la dernière décennie. Les réseaux bien dispersés de fibres nanométriques dans des matrices polymères peuvent apporter des améliorations extraordinaires dans la résistance du matériau et modifier les interactions particule/polymère au niveau moléculaire. En conséquence, la cristallisation peut être favorisée à très basses concentrations de renfort. Il est bien connu que la dispersion des nanocristaux de cellulose (NCC) dans les systèmes non aqueux est un défi majeur pour développer davantage ces promesses nanométriques. Dans ce travail, un nouveau procédé composé de deux étapes: le mélange en solution suivi par le malaxage à l'état fondu, a montré d'excellents résultats dans la dispersion de faibles charges de NCC dans le PLA. L'oxyde de polyéthylène (PEO) à bas et haut poids moléculaires a été proposé comme un polymère porteur de nanocristaux et l'encapsulation des NCC dans le PEO a été réussie. La réduction de la taille des agglomérats a été contrôlée par l'augmentation du rapport en poids PEO:NCC. Un effet synergique entre la plastification et le renforcement de la matrice PLA a été clairement mis en évidence par le comportement cristallin des nanocomposites. La méthode de préparation de nanocomposites issus de PLA, NCC et PEO, présentée dans cette thèse, représente un pas en avant dans les applications potentielles de ces nanoparticules dans les matériaux composites verts.

ABSTRACT

Polylactide or PLA is a biodegradable polymer that can be produced from renewable resources. This aliphatic polyester exhibits good mechanical properties similar to those of polyethylene terephthalate (PET). Since 2003, bio-based high molecular weight PLA is produced on an industrial scale and commercialized under amorphous and semicrystalline grades for various applications. Enhancement of PLA crystallization kinetics is crucial for the competitiveness of this biopolymer as a commodity material able to replace petroleum-based plastics. On the other hand, the combination of natural fibers with polymer matrices made from renewable resources, to produce fully biobased and biodegradable polymer composite materials, has been a strong trend in research activities during the last decade. Nevertheless, the differences related to the chemical structure, clearly observed in the marked hydrophilic/hydrophobic character of the fibers and the thermoplastic matrix, respectively, represent a major drawback for promoting strong fiber/matrix interactions.

The aim of the present study was to investigate the intrinsic fiber/matrix interactions of PLA-based natural fiber composites prepared by melt-compounding. Short flax fibers presenting a nominal length of ~1 mm were selected as reinforcement and biocomposites containing low to moderate fiber loading were processed by melt-mixing. Fiber bundle breakage during processing led to important reductions in length and diameter. The mean aspect ratio was decreased by about 50%. Quiescent crystallization kinetics of PLA and biocomposite systems was examined under isothermal and non-isothermal conditions. The nucleating nature of the flax fibers was demonstrated and PLA crystallization was effectively accelerated as the natural reinforcement content increased. Such improvement was controlled by the temperature at which crystallization took place, the liquid-to-solid transition being thermodynamically promoted by the degree of supercooling. During crystallization, viscoelastic properties are expected to be strongly influenced by crystallite development and impingement. Rheometry was selected as a suitable technique to study the evolution of complex viscosity and storage and loss moduli during the crystallization of compounded PLA and PLA-biocomposites. Optimization of experimental conditions was needed for achieving the compensation of polymer shrinkage, which was a major concern for the reproducibility of measurements, particularly at high supercooling level. Fruitful information about the enhanced crystallization rate due to the presence of flax fibers in a wide

range of crystallization temperatures was obtained from this study. Since development of crystallization in industrial processing may differ greatly from quiescent studies, a preliminary investigation of the effect of shear flow on the improvement of PLA crystallization was carried out. Using the same shear rate interval, two different sets of conditions were explored, namely (1) constant total deformation and (2) constant shearing time. In both cases, the crystallization enhancement was evidenced by a decrease in the induction time which became stronger as shear rate augmented. About 75% of reduction was observed at 4 s-1, the maximum shear rate reached in this research.

The size reduction of cellulose particles from micro to the nanoscale has also drawn special attention over the last decade. Well-dispersed nanosized fiber networks into polymeric matrices may bring extraordinary strength enhancement and modify the particle/polymer interactions at the molecular level. As a consequence, crystallization may be promoted at considerably low concentrations of reinforcement. It is well-known that dispersion of cellulose nanocrystals (CNC) in non-aqueous systems is a major challenge for further developments. In this work, a novel two-step process involving solvent-mixing and melt-mixing was found to successfully dispersed cellulose nanocrystals at low weight loadings in the PLA matrix. Polyethylene oxide (PEO) of high and low molecular weight was proposed as a polymer carrier for nanocrystals, and the encapsulation of CNC in this polymer was achieved. Reduction of agglomerate size was controlled by the increase of PEO:CNC weight content ratio in the final nanocomposites. A synergistic effect between plasticization and reinforcement of the PLA matrix was clearly evidenced from the crystallization behavior of nanocomposites. The PLA nanocomposite preparation method presented in this dissertation represents a step forward in the potential applications of CNC in green composite materials.

TABLE OF CONTENTS

LIST OF TABLES

LIST OF FIGURES

INTRODUCTION

The awareness to bridge the gap between industrial development and environmental preservation has become a major quest during the last decades. The integration of sustainability principles into the mainstream of economic growth leads the development of the next generation of raw materials, processes and products. As a result, green polymers and composite materials obtained from renewable and sustainable resources have acquired paramount importance in a vast range of applications, from medicine to transportation. Plants, agriculture residues, straws, bacteria, animal shells, etc. are among the most abundant bio-based resources and their full potential of applications is a matter of ongoing researches.

In this context, natural fibers emerge as a potential alternative to conventional reinforcements such as glass fibers or mineral additives. Due to their low density, natural fibers exhibit specific mechanical properties comparable to those of glass fibers; thanks to this feature the use of cellulosic fibers may represent important reductions of weight in the final compounded product. In addition, natural fibers require less energy for their production which might contribute to have favorable energy balances during the composite production. When natural fibers are embedded in a biodegradable matrix, their biodegradability and non-toxic nature would be an additional advantage at the end of the lifecycle compared to conventional composites. Finally, the availability of natural fibers suggests that in the long term, once commercial production volumes will be broad enough, they will allow to manufacture low cost biocomposites.

Several parameters have an effect on the mechanical properties of the composites. On one hand, the inherent characteristics of the matrix and the reinforcements (elastic modulus, aspect ratio (length/diameter or *l/d*), surface properties, etc.) play an essential role in the whole composite performance. On the other hand, the quality of the fiber/matrix interface is determining in the effective transfer of shear stresses between the matrix and the reinforcement. The current challenge in the biocomposites field is to develop more efficient production methods and optimize formulations to obtain competitive biocomposites compared to materials derived from the petrochemical industry.

Cellulose nanocrystals (CNC) are promising and emerging materials; these are obtained by removing amorphous parts of the cellulosic fiber. As these reinforcements are practically free

from defects, they exhibit elastic modulus close to that of the perfect crystal of cellulose, i.e. 130 GPa. Furthermore, these particles are expected to have an aspect ratio very high, of the order of 30 to 50. Therefore, the composites reinforced with this kind of nanoparticles would show considerable increase in their elastic modulus, without a significant increase in the density of the polymer or a decrease of transparency. An important obstacle to materialize these promising materials is their dispersion in hydrophobic polymer matrices; CNC have a strong tendency to agglomerate due to their highly hydrophilic nature. Another challenge to overcome is to obtain a good fiber-matrix adhesion ensuring the effective transfer of stresses between the matrix and the reinforcement.

In this optic, the first phase of this project is dedicated to the preparation of fully biobased and biodegradable composites by a melt-compounding route. For this, flax fibers are selected as a suitable reinforcement for a semicrystalline commercial grade of polylactide (PLA). A systematic study is performed to examine the synergistic effect of compounding and reinforcement in the inherent fiber/matrix interactions for the PLA-based flax fiber systems. The second phase addresses the melt rheology of reinforced systems and the evolution of viscoelastic properties due to the liquid-to-solid transition taking place during crystallization of the biocomposites. In an effort to explore the potential of well-dispersed nanoreinforcements in the PLA matrix, the third phase is dedicated to the dispersion improvement of cellulose nanocrystals in a melt-compounded process.

The main contributions of this dissertation have been organized in three scientific articles; the first has been published in the journal *Cellulose*. The second and third have been submitted to the journals *Rheologica Acta* and *Cellulose*, respectively.

The present document consists in the following chapters:

- Chapter 1: Literature review
- Chapter 2: Objectives
- Chapter 3: Organization of the articles
- Chapter 4-6: The three articles reporting the main results and contributions of this project
- Chapter 7: General discussion
- Chapter 8: Conclusions and recommendations

CHAPTER 1 LITERATURE REVIEW

1.1 OVERVIEW

A composite material can be understood as the combination of two or more components in order to take advantage of their most favourable characteristics and simultaneously reduce the effect of their less attractive properties. Such combination is often selected to provide atypical enhancements regarding i.e. stiffness, weight, conductivity, thermal stability or cost effectiveness. Composites having exceptional mechanical properties are formed by a reinforcing phase called reinforcement which is embedded in a binder phase called matrix. Polymers, metals and ceramics have been found to be suitable matrices meanwhile fibers, laminates or particulates can act as reinforcements.

Continuous fiber reinforced composites are usually called advanced composites due to the fact that they exhibit the best mechanical performance. They are highly anisotropic and frequently prepared using thermoset matrices. Short fiber reinforced composites can be prepared using the processing methods available for the single matrix. In the case of thermoplastics, this means that processes such as extrusion and injection molding can be applied and composite production at large scale is possible. In short fiber composites the fiber orientation will be determined by the processing method.

Glass fibers are the most common fiber reinforcement in polymer composites. They exhibit diameters between 5 and 20 mm, are round and relatively smooth. Current trends explore the use of natural fibers for composite applications as an alternative to glass fibers. Natural fibers exhibit considerable advantages when compared to glass fibers widely used within the automotive sector. The most significant benefits include reduction in weight and cost when the commercial production will be developed. Substantial environmental benefits may take into account their extensive availability around the world and their potential sustainability. The energy required for the plant growing comes from the sun. Harvesting and subsequent extraction and transportation demand less energy than the production of glass fibers.

The emerging market of biopolymers creates the opportunity to conceive environmentally friendly composites materials. The term biopolymer may refer to biobased polymers,

biodegradable polymers or to plastics exhibiting both features. The term biocomposites involves a broad range of combinations. Composite materials made from non biodegradable polymers like polyolefins and epoxies and natural fibers are called biocomposites which are partially biodegradable. The combination of biopolymers like polylactide (PLA) and polyhydroxyalcanoates (PHAs) and synthetic fibers also come under biocomposites. Composite materials produced from natural fibers and crop-derived polymers are usually termed green composites, fully biobased composites or simply biocomposites.

Some of the growing sectors of potential applications for plant-derived fiber reinforced biocomposite materials are in automotive parts, housing products and packaging. Around 65% of composites produced for automotive and construction applications use glass fiber. Companies specialized in these sectors will notice the potential of biocomposites if they can offer similar or superior performance than conventional composites at lower weight. The hydrophilic nature of natural fibers tends to diminish their potential as reinforcement due mainly to the lack of adhesion between untreated fibers and the polymer matrix. However, such a lack should be understood as a specific issue with certain thermoplastics instead of the polymers in general. However, this fact has not slowed down the growth in applications for natural fibers. For example, the German automotive industry tripled the use of natural fibers between 1995 and 2000. Companies such as BMW, Audi and DaimlerChrysler have led to the development of natural fiber reinforced composites for interior component in several commercial car models; including for example seat backs, door panels, hat racks and dashboards made from natural fiber composites.

1.2 POLYLACTIDE

Polylactide (PLA) is the most promising biodegradable polymer currently produced at a commercial scale. Its industrial production from renewable resources and its compostability are among its most attractive features. The mechanical properties of the PLA are also comparable to those of polyethylene terephthalate (PET), and its melt processing can be performed in conventional equipments used for petrochemical-based polymers [1, 2].

PLA is a thermoplastic biopolymer which can be entirely amorphous or semicrystalline, depending on its stereochemical structure and the undergone thermal history. It has high

mechanical strength and good barrier properties. The first applications of PLA were reserved for biomedical uses [1, 3]. However, since the opening of the NatureWorks[1] plant in 2003, the industrial production of PLA from renewable resources at affordable prices has introduced PLA in the packaging market. The use in the transportation area, however, still remains an industrial challenge.

Regarding some of the physical properties of PLA, the density of the amorphous polymer is 1.25 g/cm^3 and that of crystalline poly(LL-lactide) or PLLA is reported to be 1.29 g/cm^3. Polylactide is insoluble in water, some alcohols and alkanes. In general, it is soluble in dioxane, acetonitrile, chloroform and dichloromethane. PLA is partially soluble at room temperature in toluene, benzene, acetone and tetrahydrofuran (THF) [2]. Table 1.1 presents selected physical and tensile properties of a typical commercial PLA grade.

Table 1.1: Physical properties of a typical commercial PLA grade (4 % D-lactide) [1, 3-5].

Density at 25 °C (g/cm^3)	1.25
Density of the molten polymer (g/cm^3)	1.07
Glass transition temperature (°C)	55
Melting temperature (°C)	165
Thermal conductivity at 48 °C	0.111 W/(m*°C)
Specific heat capacity at 55 °C	1590 J/(kg*°C)
Tensile strength (MPa)	59
Young's Modulus (GPa)	3.5
Elongation at break (%)	7

1.2.1 Chemical structure

The monomer used to polymerize PLA is lactide, a dimer of lactic acid. Lactic acid (2-hydroxypropanoic acid) is a carboxylic acid presenting one asymmetric carbon in the chemical structure. It therefore has two optically active stereoisomers: L(+)-lactic acid and D(-)-lactic acid.

[1] http://www.natureworksllc.com/

Fermentation of carbohydrates results primarily in the L form of lactic acid. Thus, the lactide dimer can take the LL, LD (meso-lactide) or DD forms. When purified monomers LL or DD are used, the PLLA and PDLA are respectively obtained. When the monomers are mixed, the PLA designation is used [1, 3, 6]. Figure 1.1 shows the configuration of the stereoisomers of lactic acid, lactide and the repeating unit of PLA.

The polymerization of lactide to produce high molecular weight PLA is performed by ring opening of the lactide. Direct polycondensation of lactic acid is also possible, but the equilibrium reaction is very sensitive to the presence of water and results in the formation of low molecular weight polymers [1, 3, 6]. However, in the literature the terms poly(lactic acid) and polylactide are used indistinctly, although strictly spoken, commercial PLA is polylactide and not poly(lactic acid).

PLA polymers from pure enantiomers, i.e. poly (LL-lactide) or poly (DD-lactide), are isotactic homopolymers which can reach high degrees of crystallinity. However, most commercial PLA grades are copolymers of LL-lactide with small concentrations of DD-lactide or LD-lactide [7]. These optical impurities cause imperfections in the regularity of the polymer chain and decrease its ability to crystallize and the rate of crystallization [3]. PLA containing more than 10% of stereoisomeric impurities becomes completely amorphous [8]. The racemic mixture (equimolar) of homopolymers of PLA leads to the formation of a crystalline stereocomplex presenting a melting point 50 °C higher than that of the homopolymers [1, 3, 6].

The ability to manipulate the stereochemistry of the macromolecular chain is one of the most important characteristics of polylactide. This allows controlling more or less the rate of crystallization and the degree of crystallinity of the polymer, the mechanical properties and the processing temperatures of PLA [3].

a)

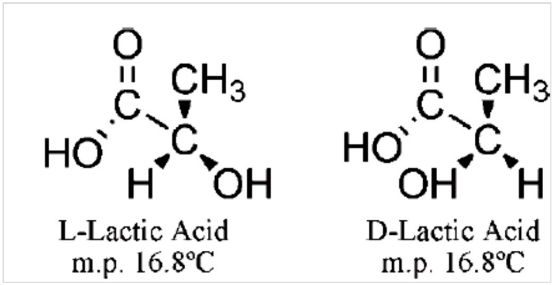

b)

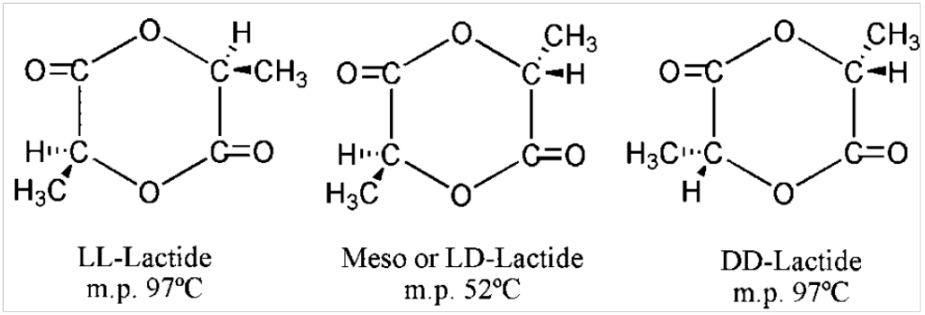

c)

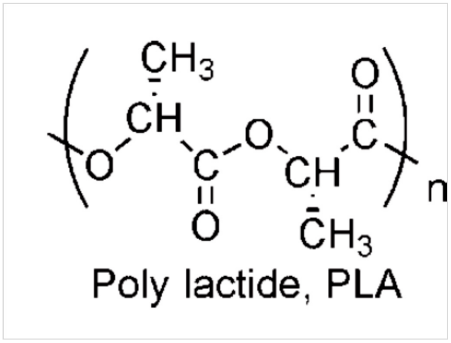

Figure 1.1: Chemical structure of a) isomers of lactic acid, b) isomers of lactide and c) polylactide [1]

1.2.2 Crystallization of PLA

The crystallinity refers to the level of structural order in a solid. In a crystal, the atoms or molecules are placed in a regular and periodic arrangement named lattice cell. In contrast, an amorphous solid is synonymous of structural disorder. In macromolecules, the presence of large side groups and branched chain structures obstruct crystallization. Stereoregularity of macromolecules is almost essential for the formation of crystalline regions.

Crystallization may be initiated by cooling a molten polymer, by annealing above the crystallization temperature, by cooling a polymer solution, or even by a molecular orientation

during processing. The degree of crystallinity depends on the thermomechanical history undergone by the polymer. It will tend to decrease when the imposed cooling of the molten polymer is faster. Mechanical stresses (e.g. the tensile stretching) may orientate the molecules and increase the degree of crystallinity.

Crystallization by cooling of a molten polymer causes the formation of a spherulitic morphology. A spherulite is a set of crystalline "arms" growing in the radial direction; they share the same origin and are interconnected by amorphous regions. Each arm is formed by regularly folded chains in a lamellar structure. The thickness of a lamella is of the order of a few nanometers, while the size of spherulites ranges from microns to millimeters.

For low molecular weight substances, the melting and crystallization occur at the same temperature. In the case of polymers, the crystallization does not occur at a single temperature, but in a temperature range below the melting point (T_m) and above the glass transition temperature (T_g). At this state, the material is designated as supercooled, characterized by a gap of supercooling defined by $\Delta T=T_m^0 - T_c$ (T_m^0 is the melting temperature of the 100% crystalline polymer) [9].

The slow rate of crystallization of PLA is one of the major drawbacks to its industrial application. During polymer processing, the cooling rate of the films or injection-molded parts is very high, which results in low degrees of crystallinity. The addition of inorganic particles, such as sodium salts, clays or talc, increases the density of nucleation points and thus the rate of crystallization [1, 10, 11]. Natural reinforcements such as cellulosic fibers can also act as nucleating agents. The following paragraphs present a brief summary of the highlights of PLA crystallization studies.

Crystallization of polylactide has been extensively investigated by several authors in the last twenty years. As mentioned above, homopolymers of polylactide (PLLA and PDLA) crystallize slowly. The rate of crystallization of PLA depends on its isomeric purity, its molecular weight and the presence of additives such as nucleating agents, plasticizers or a second heterogeneous phase. In general, the crystallization rate and the spherulite size increase in the copolymers (commercial grades of PLA), but the crystal structure becomes disorganized. The maximum rate of crystallisation is achieved in the range 110 °C – 130 °C [12].

The melting enthalpy (ΔH_m) of PLA crystals was evaluated at 93,7 J/g. In semicrystalline PLA, the melting endotherms can reach between 40 and 50 J/g, corresponding to degrees of crystallinity ranging from 37 to 47% [13, 14]. It is worthy to note that samples of very high molecular weight e.g. 400 kg/mol, cannot develop significant degrees of crystallinity due to the reduction of the chain mobility. Samples of molecular weight less than 300 kg/mol develop degrees of crystallinity between 30 and 50% [15].

Crystallization of PLA can be triggered by annealing above 75 °C and below the melting point. Annealing at low temperatures (near T_g) usually induces the presence of two melting peaks. This is due to the quick formation of less perfect crystals with lower melting points, then a recrystallization process to more perfect crystals which melt at higher temperatures [14, 16, 17]. In contrast, the crystals formed at temperatures near the T_m show a single peak at higher melting temperature. This change in the crystallization process occurs gradually as the annealing temperature increases from 100 °C to 140 °C [15].

Kolstad studied the crystallization of copolymers of poly (L-lactide-co-meso-lactide) in a concentration range of meso-lactide from 0 to 9%; the crystallization temperature varied from 85 to 135 °C. He reported an increase of about 40% in the half-time of crystallization for each 1% increment in the concentration of meso-lactide. The lower half-time of crystallization was obtained at 110 °C in all cases. In the same work, Kolstad showed that the addition of talc to copolymers of poly(L-lactide-co-3%meso-lactide) resulted in a decrease of 85% in the half-times of crystallization. In the case of PLLA, the half-time decreased from 180 to 60 seconds for a concentration of 6% talc. Polylactide also lost its ability to crystallize when the concentration of meso-lactide isomer exceeded 15% [18].

Schmidt and Hillmyer examined the crystallization of mixtures of PLLA and PDLA. The equimolar mixture of PLLA and isotactic PDLA leads to the formation of the stereocomplex, whose melting point is ~ 50 °C higher than the homopolymers. At low concentrations of PDLA, this is a nucleating agent more efficient than talc. The authors reported a nucleating efficiency of 56% for a concentration of 6 wt% of PDLA. The same concentration of talc reached only a nucleating efficiency of 32% [19, 20].

The spherulitic growth rate of copolymers strongly depends on the percentage of meso-lactide. At 125 °C, this rate is 4,5 μm/min for PLLA, it decreases to 2,0 and 0,8 μm/min for copolymers of

poly (L-lactide) containing 3,0 and 6,0% meso-lactide, respectively [21]. Baratian et al. reported the decrease in degree of crystallinity and growth rate of spherulites for random copolymers containing 1,5 to 6% of D-lactide [22].

Tsuji and Ikada studied the effect of molecular weight on the crystallization behavior and the crystal morphology of PLLA/PDLLA blends. They found that the spherulitic structure became disordered when the molecular weight of PDLLA increased. They also observed a significant decrease in the melting point with the increment of the PDLLA concentration [13].

Abe et al. examined the crystallization kinetics of PLLA having a molecular weight (M_n) varying between 17 and 300 kg/mol. Figure 1-2a shows the crystallization rate for various molecular weights of PLLA as a function of temperature; as expected, all the curves reached a maximum. The crystallization rate was promoted when the molecular weight decreased. The samples having higher molecular weights had a maximum growth rate of ~4 μm/min; this value increased approximately 4 times for M_n of ~20 kg/mol. According to this study, a commercial polylactide presenting a molecular weight of about 100 kg/mol would exhibit a maximum spherulitic growth rate of ~ 6 μm/min [23].

Using the theory of Hoffman and Lauritzen, several authors have performed a detailed analysis of the kinetics of nucleation and crystallization of PLA and copolymers of PLA [21, 23, 24]. According to this theory, the crystal growth is governed by two variables: the rate of formation of nuclei (*i*) and the growth rate at the surface of the nuclei (*g*). The behavior of *i* with respect to *g* is used to define three different regimes of crystal growth. Thus, when *i* is very small compared to *g*, each crystal layer will have time to form before a new nucleus appears, this is regime I. Abe et al. found that PLLA can have three regimes of crystallization (Figure 1-2b); regimes II and III (below 145 °C) presented a typical spherulitic morphology. Above 150 °C (regime I), the morphology evolved to a hexagonal structure with a decrease in the nucleation density [23]. In contrast, Huang et al. reported the existence of a single regime for meso-lactide copolymers [21].

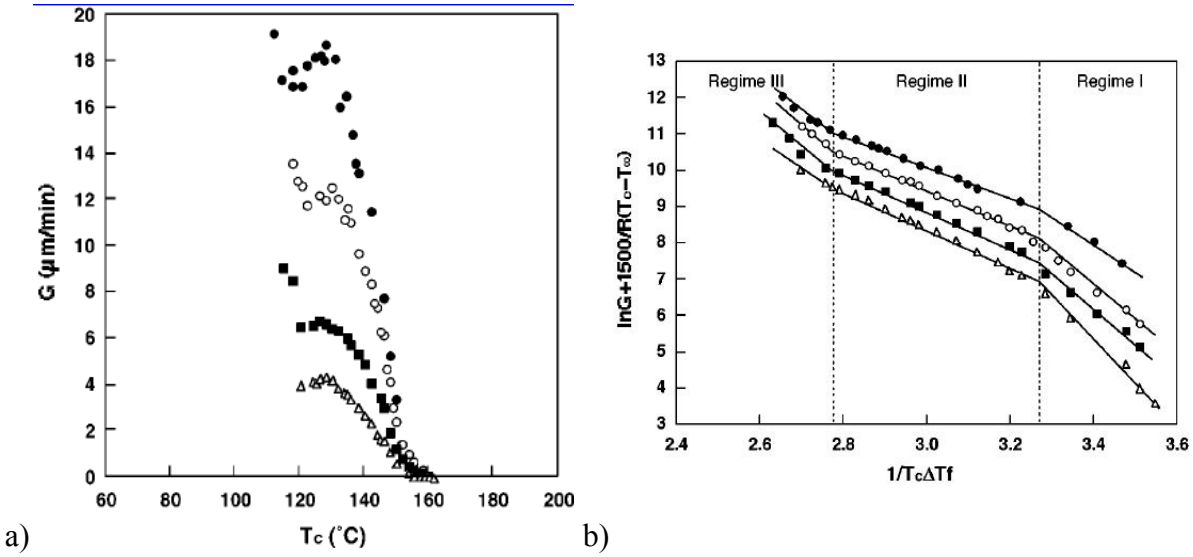

a) b)

Figure 1.2: a) Spherulitic growth rate of PLLA, b) application of Hoffman and Lauritzen equation for different molecular weights of PLA. (•)17 kg/mol, (○)49 kg/mol, (■)89 kg/mol, (△)344 kg/,mol [23]

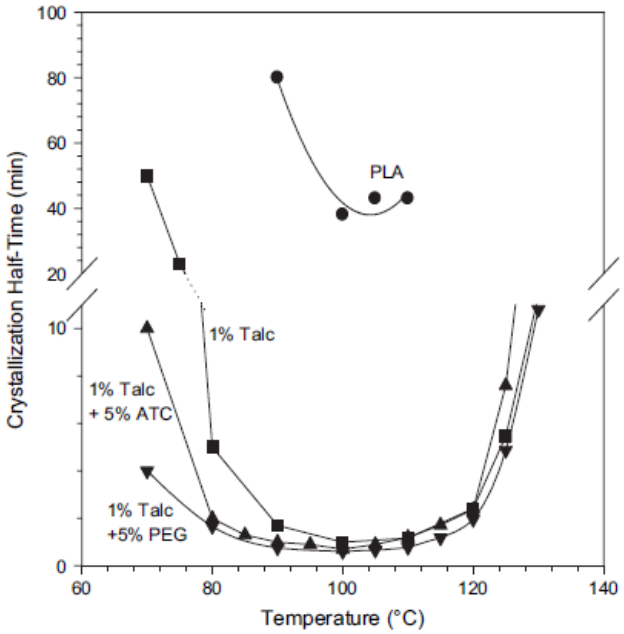

Figure 1.3: Effect of the plasticization and heterogeneous nucleation in the crystallization half-time of PLA under isothermal conditions (PEG: Polyethylene glycol, ATC: acetyl triethyl citrate) [10].

The simultaneous effect of plasticizing and heterogeneous nucleation on the crystallization kinetics of PLA was investigated by Li and Huneault. The use of low molecular weight PEO led to the crystallization of PLA at high cooling rates. The addition of talc to the plasticized matrix could significantly decrease the half-time of crystallization, compared to pure PLA. This fact allowed widening the window of non-isothermal crystallization of commercial PLA containing ~2% D-lactide. Figure 1-3 shows the half-time of crystallization of the various formulations as a function of temperature. Polylactide containing 1% talc and 5% PEG reached a degree of crystallinity of 40% during the cooling step of parts manufactured by injection molding [10].

Regarding the transition temperatures of different stereochemical conformations of PLA, amorphous PLA of high molecular weight shows a T_g of ~58 °C; the transition from the rubbery to the viscous liquid state occurs between 110 and 150 °C, but the processing window is typically around 180-200 °C. The melting temperature of PLLA is 180 °C. This melting point decreases with the increase of D-lactide concentration, for reaching 130 °C at 10% D-lactide. After this concentration, no crystallization occurs. Table 1.2 shows the changes in the melting (T_m) and glass transition (T_g) temperatures for different PLA chain conformations. Table 1.3 reports the variations of the properties of PLA with the stereochemistry, the crystallinity and molecular weight (M_w) for injection molded parts of different isomers of PLA at 195 °C.

Table 1.2: Changes in T_m and T_g according to the stereochemical conformation [3].

PLA structure		**T_m (°C)**	**T_g (°C)**
Poly (L-lactide) or Poly (D-Lactide) isotactic	LLLLLLLL or DDDDDDDD	170 – 190	55 – 65
Random copolymers	Random % of meso or D-Lactide	130 – 170	45 – 65
Stereocomplex PLLA/PDLA	LLLLLL mixed with DDDDDD	220 – 230	65 – 72
Syndiotactic Poly (meso-lactide)	DLDLDLDL	152	40
Heterotactic (disyndiotactic) Poly (meso-lactide)	LLDDLLDDLLDD	-	40

Table 1.3: Mechanical properties of PLA presenting different stereochemical structures and molecular weights [6, 8].

Property	PLLA M_w = 67000	PLLA Annealed M_w = 71000	PDLLA M_w = 114000
Tensile strength (MPa)	59	66	44
Elongation at break (%)	7.0	4.0	5.4
Young's Modulus (MPa)	3750	4150	3900
Maximal tensile strength (MPa)	70	70	53
Flexural strength (MPa)	106	119	88
Impact Izod (not indented) (J/m)	195	350	150
Impact Izod (indented) (J/m)	26	66	18
Rockwell hardness (HR)	88	88	76
Heat deflection temperature (HDT) (°C)	55	61	50
Vicat point (°C)	59	165	52

This section has addressed the numerous investigations focused on understanding and improving the crystallization of PLA. Heterogeneous crystallization has been explored as a mean to enhance the crystallization kinetics of PLA. Significant nucleation rate increase can be reached by the addition of fillers, for example mineral additives such as talc. Further improvements would open the way to control the degree of crystallinity and produce semi- crystallized parts for industrial applications. The use of natural reinforcements may also be considered to retain the biodegradable nature of PLA systems. A description of cellulosic fibers in the scope of polymer reinforcement is provided below.

1.3 CELLULOSE FIBERS

Natural fibers can be classified according to their origin into three main groups: fibers extracted from vegetables, from animals and those from minerals. Vegetable fibers include bast fibers extracted from stems, e.g.: flax, hemp, jute and ramie; fibers from seeds, such as cotton and kapok; and hard fibers extracted from leaves (sisal), trunks (Manila hemp) and shells of certain fruits (coconut) [25, 26]. Animal fibers are extracted from hair, such as animal wool, and some secretions i.e. silk. Figure 1.4 shows a detailed classification of natural fibers.

For applications in polymer reinforcement, it is sought to work with fibers having a structural or protective function in nature, such as vegetable fibers extracted from stems, leaves and fruits, which exhibit interesting mechanical properties [27]. In this document, the terms natural fibers, cellulosic fibers and vegetable fibers are treated as synonyms and refer in particular to those fibers extracted from the stems.

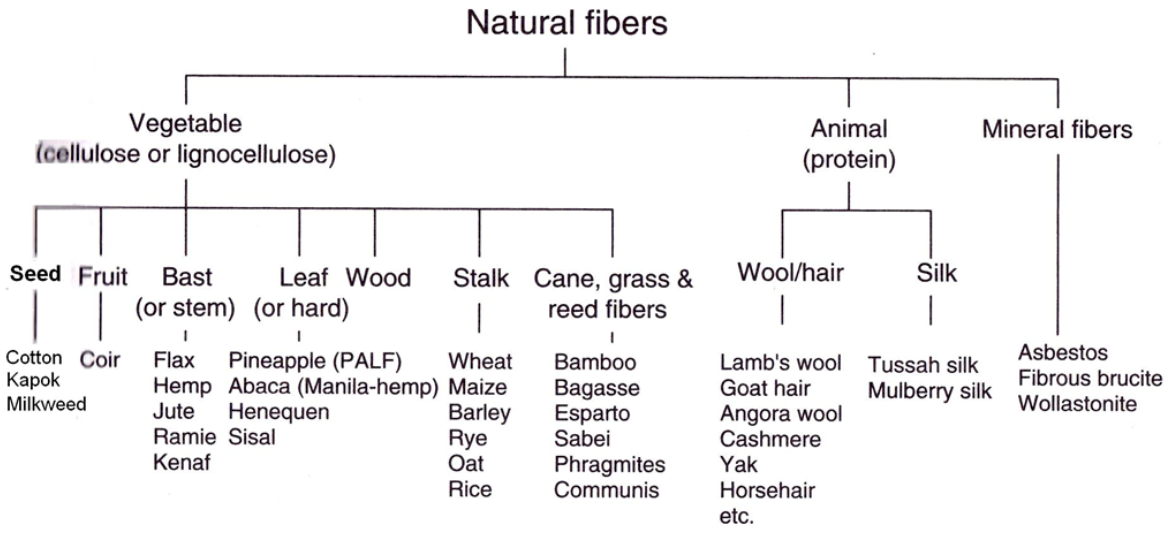

Figure 1.4: Classification of natural fibers according to the origin [26].

1.3.1 Tensile properties

A comparison of the tensile properties of natural fibers and some synthetic fibers commonly used for polymeric reinforcement is presented in Table 1.4. This table also contains a comparison of their specific mechanical properties, which serves to emphasize the advantage of the low density of natural fibers. For example, the Young's modulus of the flax fiber is in the order of 40 GPa, roughly half of that of the glass fiber (70 GPa). However, both present specific modulus of about 30 MPa/(kg/m^3). Due to their natural character, a large variability in the properties reported in the literature can be seen for the same type of fiber. Indeed, the mechanical properties are a function of both the variety and growing conditions of the plant, and the physicochemical treatment during the extraction [25, 26]. Although the mechanical properties of natural fibers are an attractive

feature, a deep look at their properties and physicochemical structure is needed to guide the selection of the most suitable cellulosic reinforcement.

The wide availability at low cost has been reported among the main advantages of natural fibers [26, 28, 29]. However, a natural fiber must be considered truly available if the volume of fibers present on the market is sufficient to produce industrial parts. Natural fibers are biodegradable and it is desirable to keep this feature after the treatments that natural fibers undergo, notably if the development of biodegradable composites is considered. We are therefore interested in fibers whose properties are easily controlled and which nevertheless conserve their mechanical performance. Their non-toxicity and low density are other key points to consider within the selection criteria [28].

Table 1.4: Comparison of tensile properties of natural and synthetic fibers [26, 29, 30].

Fiber	**ρ (g/cm^3)**	**ε (%)**	**E(GPa)**	**σ_u(MPa)**	**$\frac{E}{\rho}\left(\frac{MPa}{kg/m^3}\right)$**	**$\frac{\sigma_u}{\rho}\left(\frac{Pa}{kg/m^3}\right)$**
Flax	1,4 – 1,5	1,2 – 3,2	28 – 80	345 – 1500	20 – 50	230 – 1000
Jute	1,3 – 1,5	1,5 – 1,8	13 – 30	393 – 800	9 –20	393 – 800
Sisal	1,3 – 1,5	2,0 – 7	9 – 38	468 – 700	6 – 25	300 – 460
Ramie	1,5	1,2 – 3,8	44 – 128	400 – 938	30 – 85	260 – 625
Hemp	1,5	1,6	70	550 – 690	45	350 – 460
Glass fiber type E	2,5	2,5 – 3,0	70	2000 – 3500	28	800 – 1400
Glass fiber type S	2,5	2,8	86	4570	35	1800
Aramide	1,4	3,3 – 3,7	63 – 67	3000 – 3150	45	2000

1.3.2 Microstructure

A natural fiber may be described as a microfiber reinforced with crystalline cellulose, amorphous hemicellulose and a lignin matrix. Some authors describe a natural fiber as a composite itself [25, 27]. Table 1.5 shows the chemical composition of cellulose, hemicellulose and lignin in various plants. The percentage of cellulose is between 60 and 80%, the hemicellulose content is near 20% and small amounts of lignin and pectin are also present between the components. Some waxes and water soluble substances are often present at the fiber surface. In general, the tensile strength

and Young's modulus of the fibers increase with the content of cellulose and cellulose crystallinity, while the microfibrillar angle greatly influences the elongation at break [31, 32].

Table 1.5: Chemical composition of selected natural fibers [26, 29, 30, 32].

Fiber	Cellulose (wt%)	Hemicellulose (wt%)	Lignin (wt%)	Waxes (wt%)	Microfibrillar angle (°)
Flax	71	18 – 20	2,2	1,7	5 – 10
Jute	45 – 70	13 – 21	12 – 26	0,5	8
Sisal	47 – 68	10 – 24	7 – 11	2	10 – 20
Ramie	69 – 83	5 – 17	0,6 – 0,7	0,3	7,5
Hemp	57 – 77	14 – 22	4 – 13	0,8	6,2

Cellulose, besides being the most abundant polymer in nature, is the main component of plants and is responsible for the strength and flexibility of plant stems. Cellulose is a polydisperse linear polymer formed by the bonding of D-anhydroglucopyranose units linked by β-1-4-glycoside. Cellulose from wood has a polymerization degree of ~10000 and of ~15000 when the source is cotton [33].

Figure 1.5 illustrates one of the major features of cellulose: its ability to form hydrogen bonds through the three hydroxyl groups that are found in its repeating unit. Hydrogen bonds, both intramolecular and intermolecular, take place in the same plane (along the length of the string) and are responsible for the linear and rigid structure of the polymer chain. This allows the formation of molecule layers bounded together by van der Waal forces, such as illustrated in Figure 1.5 [29, 33, 34].

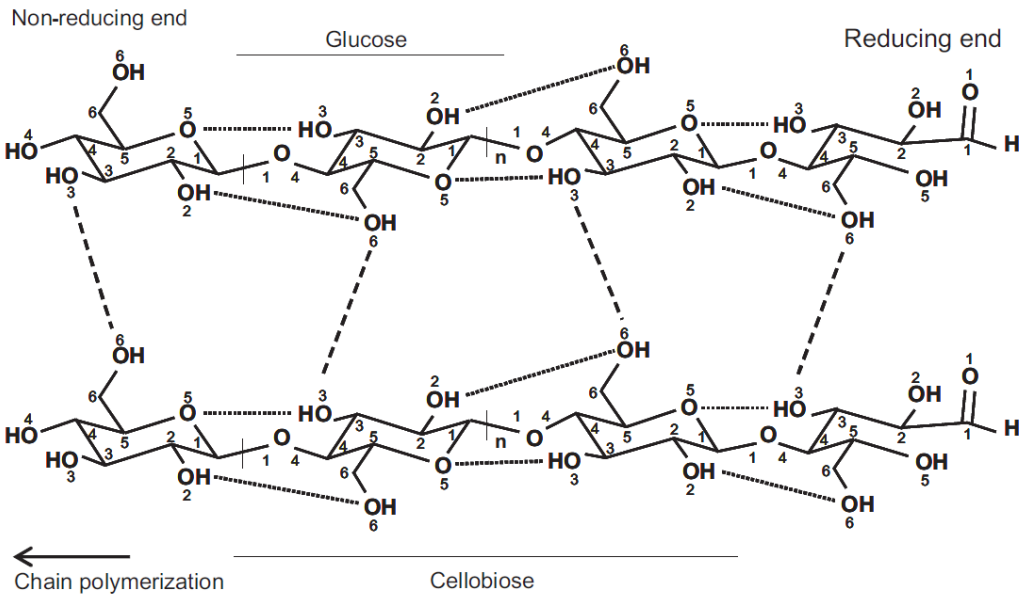

Figure 1.5: Representation of intermolecular and intramolecular hydrogen bonding in cellulose [34].

The cellulosic fibers are located in the stem of the plant, between the bark and the wood. Figure 1.6a shows a cross section of the stem of the flax plant. As illustrated in the figure, the fibers form bunches or bundles, arranged in a circular disposition around the wood. In the case of flax and hemp, the bundles are stuck to each other in the longitudinal direction, so that the fibrous bunches have a length equal to that of the stem. The cross section of the flax stem has around 20-40 bundles, each one composed of about 20-40 fibers [28, 35]. Figure 1.6b shows schematically the hierarchical structure of natural fibers. In fact, each bundle is at the same time, a hierarchical arrangement of fibers, microfibers and microfibrils. In mature plants, fibers represent about 25% of the dry mass of stems. The extraction of the individual fibers is made through physical processes.

It is generally accepted that the microstructure of an elementary fiber (single fiber) is composed by a first wall (often named S1) surrounding the two side walls (S2 and S3). The first layer has a thickness less than 1 micron, while the secondary layer (S2) has a similar thickness to the diameter of the fiber. This layer is formed by a series of long cellulose microfibrils arranged helically to the axis of the fiber. The angle between the axis of the fiber and the microfibrils is

referred as the microfibrillar angle. A complete discussion about the organization and microstructure of single cellulose fibers can be found in references [26, 36].

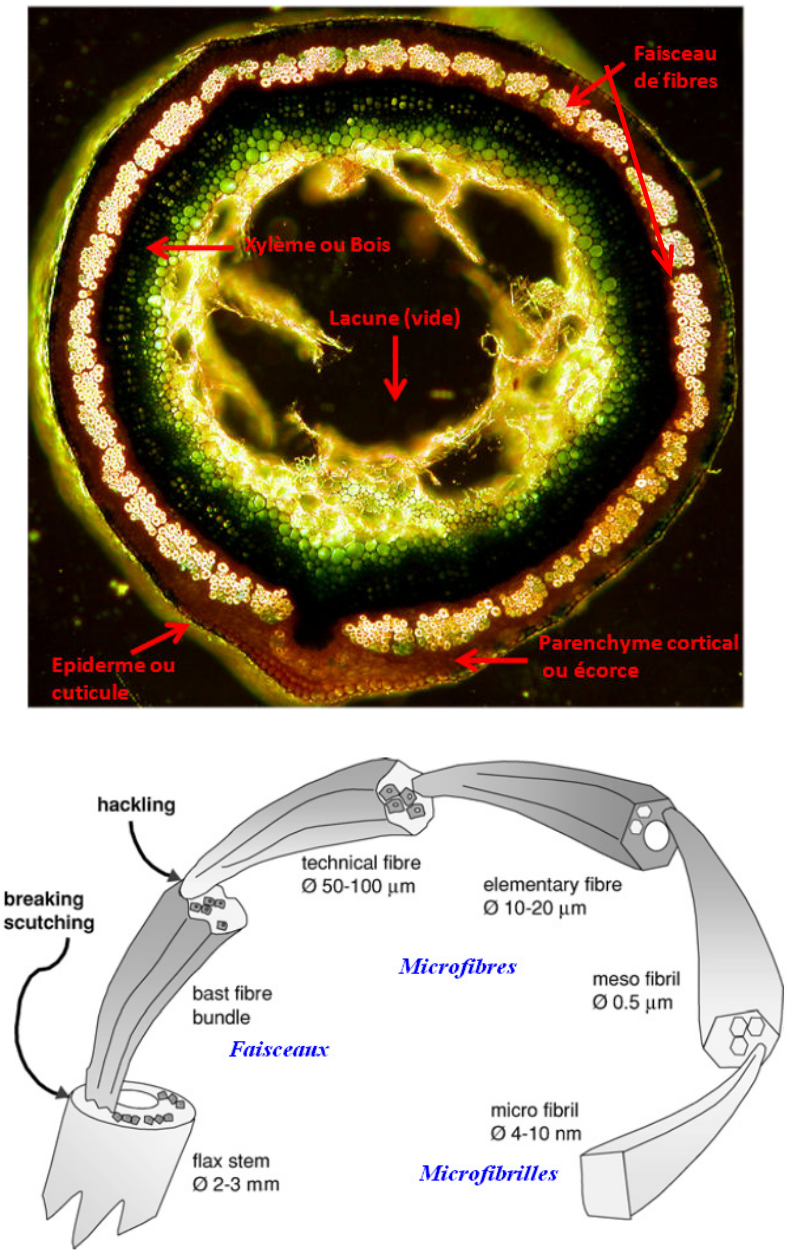

Figure 1.6: a) Transversal section of the flax stem[2], b) representation of the hierarchical structure of cellulose fibers [37].

[2] Printed in: http://fr.wikipedia.org/wiki/Lin_cultiv%C3%A9.

Figure 1.7a shows a sketch of the microstructure of a natural fiber. Figure 1.7b exhibit an AFM micrograph showing clearly the cellulose microfibrils between amorphous areas (highlighted with yellow arrows). A microfiber has a length between 1 and 100 mm and a diameter between 20 and 100 microns [28, 35]. Their structure is similar to that of a composite wherein the matrix is mainly composed of hemicellulose and lignin and the reinforcement would be a set of crystalline cellulose microfibrils helically oriented in the microfibrillar angle. As one reduces the size of the fiber, through physicochemical methods, the amorphous components are eliminated and the fraction of crystalline cellulose is increased [38]. In fact, the reinforcement potential of a natural fiber depends on the crystallinity of the microfibrils and the microfibrillar angle. The smaller the angle, the higher the rigidity and strength of the fiber. The higher the angle, the higher the elongation at break [25].

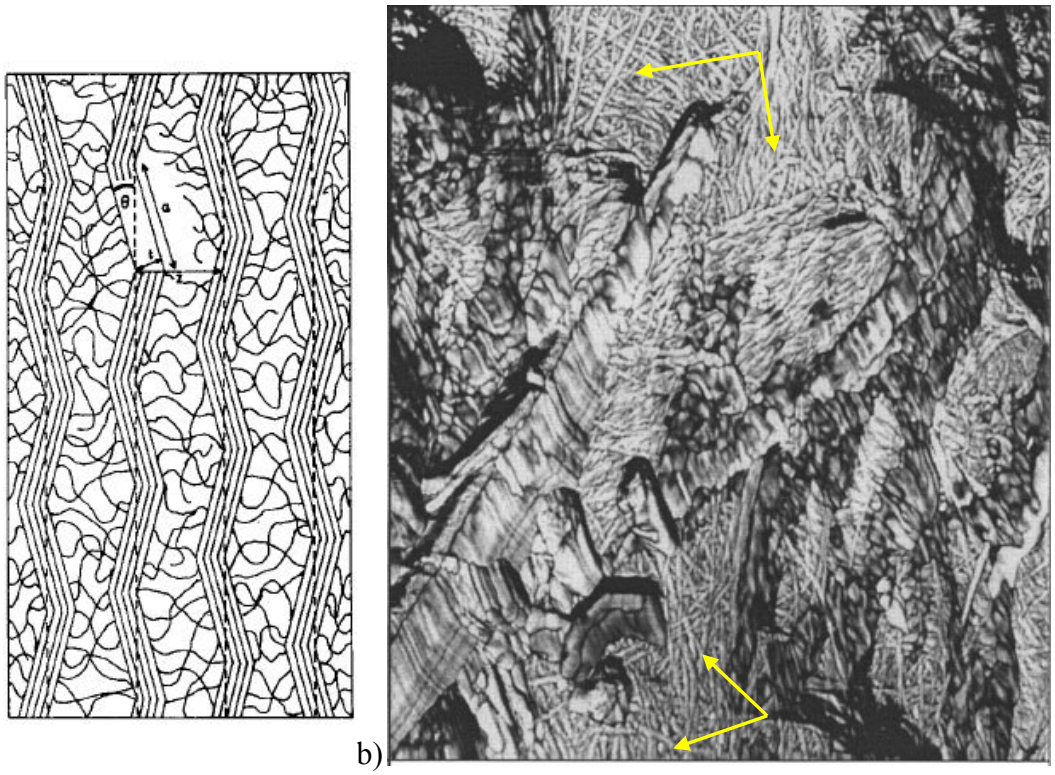

Figure 1.7: a) Sketch of the microstructure of a single natural fiber, b) AFM micrograph of a flax fiber (scanned section of 25 μm^2) [29, 39].

The cellulose microfibrils are long and flexible nanofibers composed of thin strands of crystalline cellulose attached to each other by amorphous areas. Their diameter are of the order of a few nanometers and their length may reach several microns [40]. They can be extracted from natural fibers via multistep physicochemical processes. The first step removes the amorphous matrix and the following steps break the chemical bonds between microfibrils. An additional stage removes amorphous bonds and then separates the strands to expose crystalline cellulose [41, 42]. There is no standardized nomenclature to differentiate these two types of nanoparticles obtained after the first and second stages. However, in recent years the terms "cellulose nanofibers (CNF)", "microfibrils" or "microfibrillated cellulose (MFC)" have been assigned very often to the first type, while the words "cellulose nanocrystals (CNC)", "cellulose nanowhiskers (CNW)", "cellulose monocrystals" or "nanocrystalline cellulose (NCC)" are generally used for the second type. Table 1.6 summarizes some important parameters of cellulose nanocrystals (CNC) and cellulose nanofibers (CNF).

Table 1.6: Comparison of selected properties of CNC and CNF.

Nanoparticle	**CNC**	**CNF**
Diameter (nm)	5 – 15	5 – 50
L/D ratio	20 – 70	100 – 200
Elastic modulus (GPa)	137	78
Tensile strength (GPa)	10	-
References	[43-45]	[40, 46, 47]

Nanocrystalline cellulose can be obtained also from aerobic bacteria such as *Gluconacetobacter*, which is extensively found in the fermentation of sugars and plant carbohydrates. As opposed to CNC and CNF nanoparticles extracted from cellulose sources, bacterial nanocellulose (BNC) is secreted as a polymer in the form of hydrogel during aerobic fermentation processes in aqueous systems. It is composed of a nanofiber network enclosing up to 99% of water. BNC has been found to be a very pure cellulose with high crystallinity, high weight-average molecular weight and good stability. The terms nanocellulose refers to the three different classes of nanoparticles presented above, namely CNC, CNF and BNC. Figure 1.8 presents the morphology of different nanocelluloses.

a)

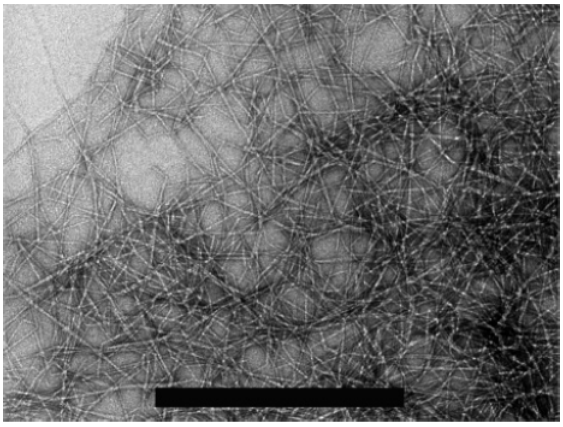

b)

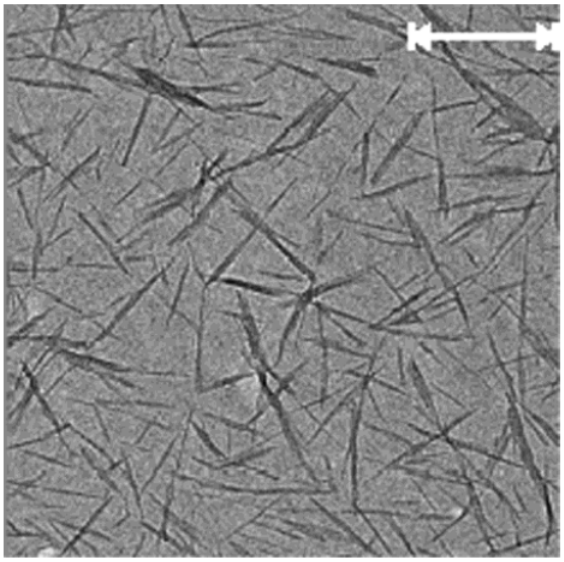

c)

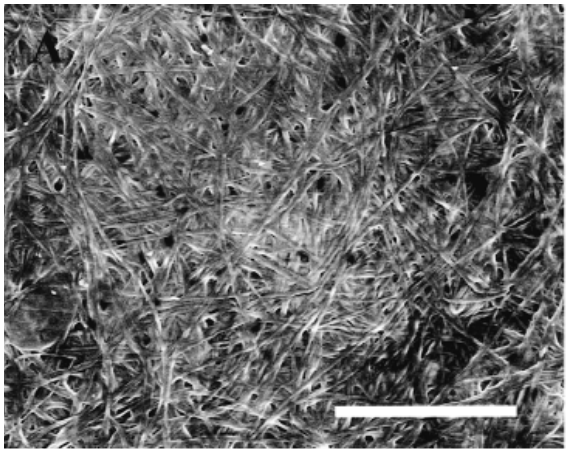

Figure 1.8: Morphology of a) MCF analyzed by TEM, scale bar of 0.5 μm [48]; b) CNC observed by TEM, scale bar of 400 nm [49] and c) BNC analyzed by SEM, scale bar of 3 μm [50].

The physical properties of nanosized cellulose differ greatly from those of the microscopic fibers. As the size of the particle gets reduced, the number of structural defects decreases significantly and mechanical properties rise proportionally. The ratio between the particle surface and the loading fraction becomes very high and the polymer/particle interactions come to be one of the most important parameters to control for tailored polymer composites. At the nanoscale, the particle/particle interactions are also strongly pronounced, the hydrophilic nature of cellulose turns in a splendid feature for applications involving aqueous systems but it is a huge drawback when the hydrophobic materials are privileged. The potential of cellulose based nanomaterials has attracted the attention of researchers all around the world; interesting reviews covering diverse aspects such as physical properties, extraction methods, surface modification and a wide range of potential applications can be found in references: [51-55].

1.4 BIOCOMPOSITES

Among the natural fibers, flax and hemp fibers have been explored increasingly by researchers in the last decade. Thanks to their high strength and their commercial availability, the preparation of biocomposites based on PLA/flax fibers and PLA/hemp fibers has become a promising alternative to traditional composites. However, their widespread use will depend on the development and understanding of fiber/matrix interactions and their control during process at industrial scale. We present here a synthesis of scientific progress in this field.

The research works published explore mostly laboratory methods such as compression molding or film casting. Few studies report the biocomposites processing from intense melt-mixing and similar conditions to those used on the industrial scale. Different approaches found in the scientific literature review examine the macroscopic behavior of the composites, wherein the characterization of tensile properties and the determination of T_g and T_m are often the explored parameters.

Table 1.7 shows the reinforcement ratio of tensile properties of various composites based on PLA. The Young's modulus of pure PLA is around 3,5 GPa. The composite modulus increases linearly with the percentage of natural fibers. However, at the same level of natural fibers, the reinforcement ratio (the ratio between the composite and matrix properties) is very variable. In the case of tensile strength, in general, biocomposites exhibit slight increases compared to the

virgin matrix, whose strength is about 50 MPa. Some studies even report slight decreases in this property [56-60].

The elongation at break of biocomposites decreases in comparison with the neat thermoplastic matrix. The value remains very close to the elongation at break of the fiber, regardless of the percentage of reinforcement added to the system [56-58]. Flax fiber has an elongation of ~3.0% [61].

Bodros et al. used compression molding to prepare flax fiber based composites randomly distributed. They evaluated several unsaturated polyester thermoplastic matrices with reinforcing levels between 10 and 30% of flax fiber which presented two different average lengths: 10 and 50 mm. The authors concluded that for isotropic composites, the elastic modulus and the tensile strength are independent of the length of the fibers, as long as this is greater than the critical length[3] [59]. Huber and Müssig reported a critical length of 3,2 mm for fiber flax [62].

The processing of biocomposites in the molten state generates both the fragmentation and the disintegration of fiber bundles, resulting in the decrease in the length and diameter of the fiber compensated by a better distribution of the reinforcement. Le Duigou et al. showed that the Young's modulus of PLA/30% flax fiber biocomposites remains constant with decreasing the aspect ratio of the fibers from 9,1 to 6,5 during the injection of the composite [63].

Table 1.7. Comparison of reinforcement ratios (property of the biocomposite/property of the matrix) of PLA/flax fiber systems as reported in literature.

Matrix	Fiber	Processing method	Young Modulus	Strength at break	Elongation at break	References
PLA	Flax – 30%	Extrusion	2,5	1,1	0,5	[58]
PLA	Flax – 30%	Injection molding	2,0	1,2	-	[60]
PLA	Flax – 30%	Compression molding	2,7	1,5	0,5	[59]
PLLA	Flax – 30%	Compression molding	2,9	1,6	0,6	[59]
PLLA	Flax – 20%	Injection	1,8	0,9	0,6	[63]

[3] The critical length is the minimum length of fiber needed for having a reinforcing effect in the composite.

PLLA	Flax – 30%	Injection	2,0	0,9	0,5	[63]

Although the mechanical characterization of biocomposites shows significant increases in the Young's modulus and the strength of the material, the microscopic analysis of the fracture surfaces show fiber loosening and pull out during traction, low wetting at the fiber/matrix interface and weak interfacial adhesion [64, 65]. These observations explain the lack of reproducibility of reinforcement ratios (property of the biocomposite/property of the matrix), the necessity of high fiber concentrations (between 30 and 40%) for having a considerable improvement in mechanical properties, and highlight the fact that a part of the fiber potential is being neglected.

The impact of the fiber/matrix interface in the macroscopic behavior of biocomposites is mentioned by most of the authors. They recognize that the microscopic interactions in the vicinity of the fiber play a key role in the strengthening mechanism of the biocomposite [56, 58, 66]. The modification of the fiber surface and the functionalization of the matrix are the most explored routes to improve the fiber/matrix adhesion. In the end, the whole reinforcement effect will be the result of phenomena at the interface (microscopic scale) and in the bulk system (macroscopic scale). Some of the most recurrent treatments to improve the fiber/matrix interface are listed below [28, 30, 67]:

- An alkali treatment (mercerization) to remove lignin, pectin and waxes located at the outer surface of natural fibers. This treatment may lead to the increase of the surface roughness, the activation of reactive groups and the thermal stabilization of the fibers;
- Chemical grafting of different molecules such as silanes, isocyanates, and carboxylic acids, in order to partially modify the chemical composition of the surface of the fibers and promote chemical bonding with the polymer;
- Functionalization of polymers; instead of modifying the fiber surface by a chemical compound, it is possible to directly functionalize the polymer thus it acts as a compatibilizing agent. In this case, a functional group capable of reacting with cellulose is added to the polymeric chain. Examples are polypropylene or polylactide modified with maleic anhydride;

- Physicochemical treatments such as ozonation, cold plasma and electron beam irradiation;
- Heat treatments at temperatures higher than 180 ° C. These types of treatments, carried out under an inert atmosphere, seek for the partial elimination of hemicellulose and lignin, which may improve both the stability and performance of natural fibers.

Mercerization is one of the most popular and easiest treatments to perform. It involves removing waxes and other substances deposited on the fiber surface through washing with sodium hydroxide. This treatment activates the hydroxyl groups at the surface of the fiber and increases the porosity of the fiber. Shanks et al. reported remarkable increases in the storage modulus of composites based on mercerized flax fibers. The authors interpreted this as an indication of improved interfacial adhesion [64].

PLA grafted with maleic anhydride (PLA-g-MA) was proposed as a coupling agent for several fiber/matrix systems. Some authors have also studied its plasticizing effect in polylactide. Indeed, the anhydride groups of MA may interact with the hydroxyl groups of the fiber, promoting chemical bonding between the fiber and the matrix. SEM micrographs showed a significant improvement in the fiber/matrix interface, as illustrated in Figure 1.9. The empty spaces around the fiber, characteristic of low interfacial adhesion, were significantly reduced by the presence of PLA-g-MA and the kenaf fibers appear covered by the matrix. The fracture surfaces were also more homogeneous [66].

The grafting of functional groups on the fiber surface requires a careful control of the chemical reaction (concentration, time, temperature, medium) and physical processes (agitation, drying, heating) taking place during grafting [30, 67]. Silanes are the most common agents used for grafting, certainly due to their role in the industry of glass fibers [68]. They have been increasingly used in the production of polypropylene/modified natural fibers based composites [39, 69, 70]. Very few studies have looked at chemical modification at the surface of natural fibers and the analysis of their potential applications in the industrial development of biocomposites.

Some authors proposed that the fiber surface modification may cause chain scission of polylactide, given the presence of reactive functional groups such as hydroxyl (-OH) or amine (-

NH_2). The possibility of substance release due to the fiber degradation during melt processing is also mentioned and it could affect the thermal stability of PLA [63].

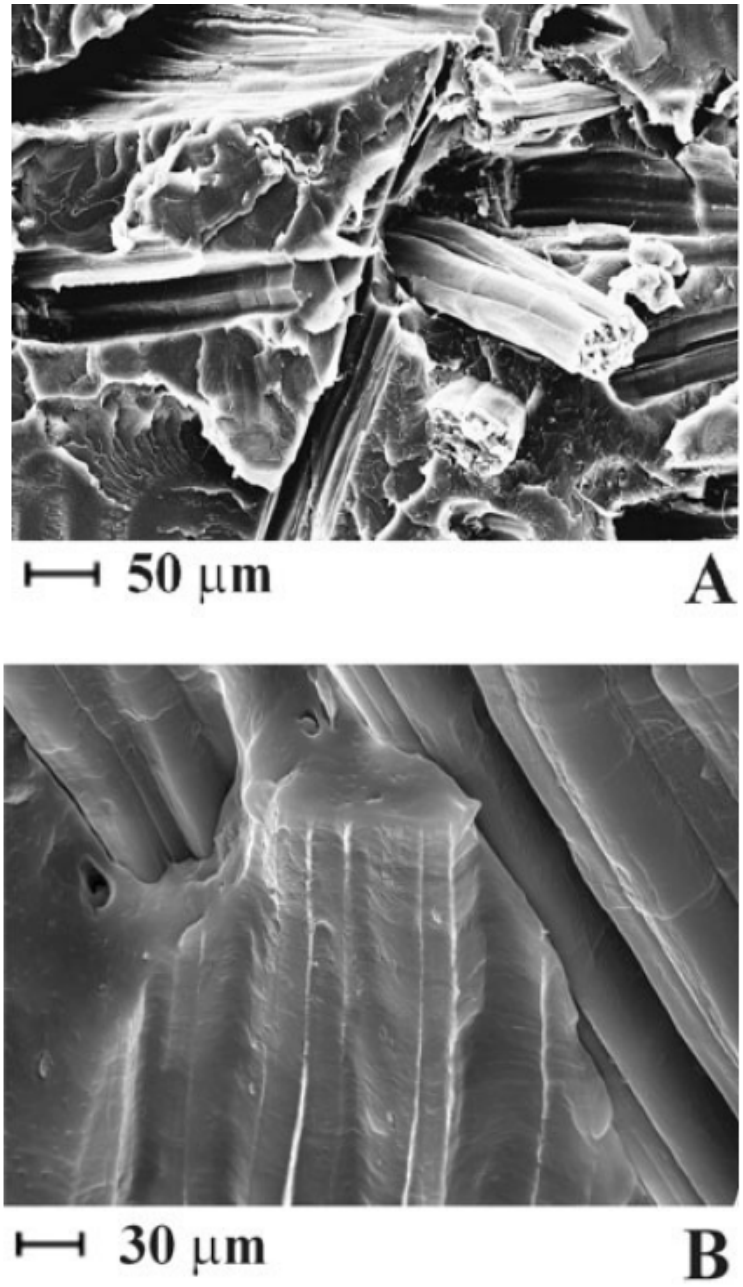

Figure 1.9: SEM micrographs of biocomposites a) PLA/30 wt% kenaf fiber and b) PLA/30 wt% kenaf fiber/5 wt% PLA-g-MA [66].

The transition to nanosized cellulose particles such as cellulose nanofibers and cellulose nanocrystals, CNF and CNC respectively, opens two main possibilities. First, the small size and high aspect ratio of these nanoparticles involve a considerable increase of the fiber/matrix interaction surface. Second, their high elastic moduli allow high expectations about the development of enhanced performance nanocomposites. These advantages may lead, at small concentrations of nanoreinforcements, to excellent mechanical performance greater than those of microcomposites, while maintaining the transparency of the matrix.

The majority of studies examining the reinforcement potential of cellulose nanoparticles have explored hydrophilic matrices and mixing techniques based on suspension of CNC of CNF in polymer solutions. For example, nanocomposites based on a latex matrix showed significant improvements in the storage modulus at concentrations lower than 10% of reinforcement. The modulus exhibited high stability below and above the glass transition temperature of the nanocomposites [71]. In systems based on hydrophobic matrices, the highly hydrophilic nature of the cellulose nanoparticles leads to weak interactions at the fibre/matrix interface; therefore dispersion problems and particles agglomeration are often observed. This is the case of polylactide and polyolefins based nanocomposites prepared by melt-mixing methods. At this level, several approaches have been implemented with the aim of improving the hydrophilic/lipophilic balance of such nanocomposites. In all cases, the mechanical properties show very small gains over the virgin matrix and sometimes even detrimental properties are reported when compared to neat PLA [72-75].

1.5 CRYSTALLIZATION OF BIOCOMPOSITES

In the case of composites based on semicrystalline polymers, the presence of the fibers may modify the crystallization of the neat matrix. The heterogeneity and roughness at the fiber surface may promote changes in the nucleation and crystal growth phases and guide the development of morphologies different that the radial spherulitic growth. Between several microscopic phenomena conditioning the fiber/matrix interactions, crystallization might modify the quality of the interface and, therefore, the macroscopic behavior of the biocomposite.

Considering the case of a single microfiber embedded into a thermoplastic matrix, at the molecular level, the fiber surface is a location with high probability of heterogeneous nucleation

and subsequent growth of spherulites. In fact, if there is a high density of active nuclei lengthwise the fiber/matrix interface, the spherulitic development will be restricted in the axial direction. Consequently, a columnar morphology surrounding the fiber will be developed, and this phenomenon is called transcrystallization. The presence of this crystalline layer has been reported in several composites based on synthetic fibers. Figure 1.10 shows the development of this columnar crystalline morphology for the PP/flax fiber system, where spherulites in the bulk polymer are growing simultaneously [76, 77].

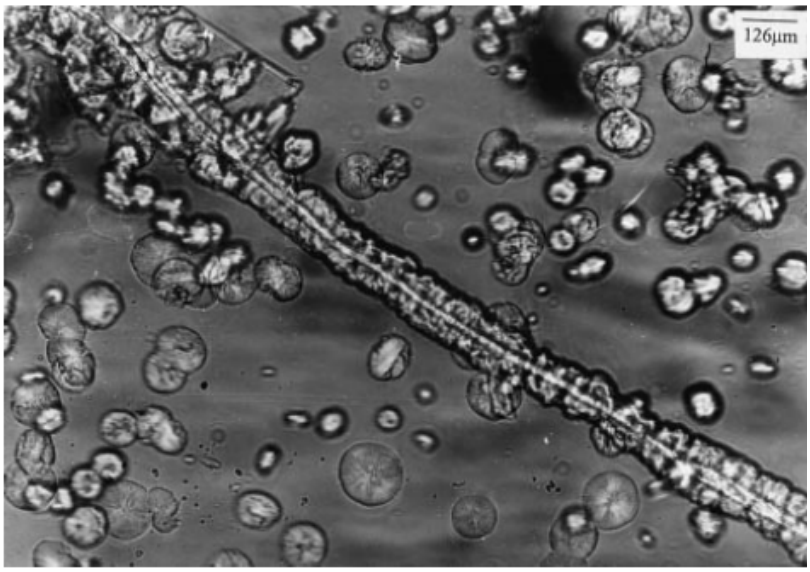

Figure 1.10: Micrograph of a flax fiber embedded in i-PP during isothermal crystallization at137 °C [76].

The fiber roughness plays an important role in the heterogeneous nucleation density, the nucleation rate and the morphology of the transcrystalline layer: rough surfaces result in a high density of nuclei while smooth surfaces do not develop transcrystalline layers [78]. Wang and Liu suggested that according to the surface heterogeneity, different kinds of nuclei may be developed [79]. Most authors indicate that the extraction and purification of natural fibers is a key factor in the transcrystalline behavior.

Zafeiropolus compared the development of transcrystalline layers for four different kinds of flax fibers in isotactic polypropylene (i-PP). Figure 1.11 shows the comparison of the developed morphologies for non-modified and chemically modified flax fibers with stearic acid. In both cases, transcrystalline layers presented variable thicknesses and low growth rates. Considering the thickness, symmetry and homogeneity of the obtained transcrystalline layer, the best result in terms of homogeneity of the transcrystalline layer was obtained with the dew-retted[4] fiber (non shown) [76].

Regarding the influence of surface treatments on the transcrystalline behavior, there is not a clear trend in the scientific literature. Some evidence indicates that mercerization and chemical grafting prompt the fiber roughness and the transcrystallization behavior into the composite. In contrast, other studies show the vanishing of transcrystalline layers due to surface modification. Biagiotti et al. found that this kind of morphology, clearly developed around untreated fibers, disappeared in the treated ones. The authors attributed this behavior to the clean fiber surfaces obtained after chemical treatments [69].

[4] Dew retting is a process employing the action of micro-organisms and moisture on plants to dissolve or rot away much of the cellular tissues and pectins surrounding bast-fibre bundles.

a)

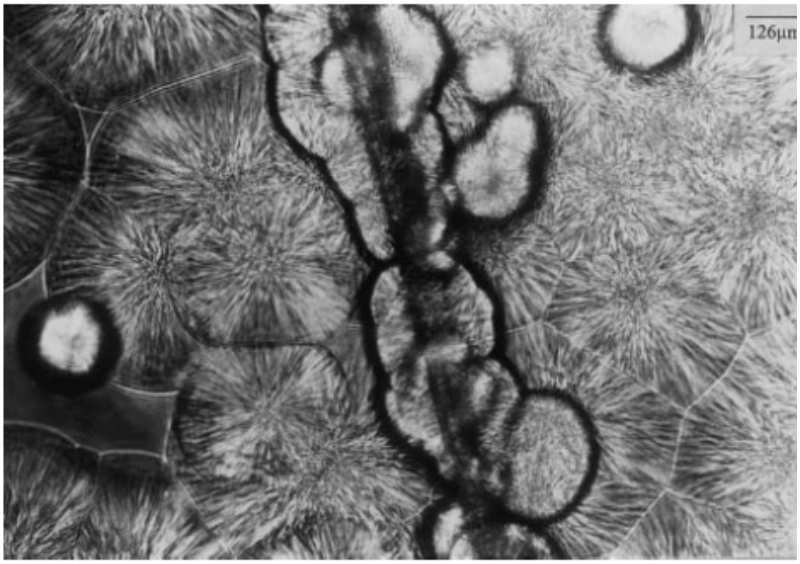

b)

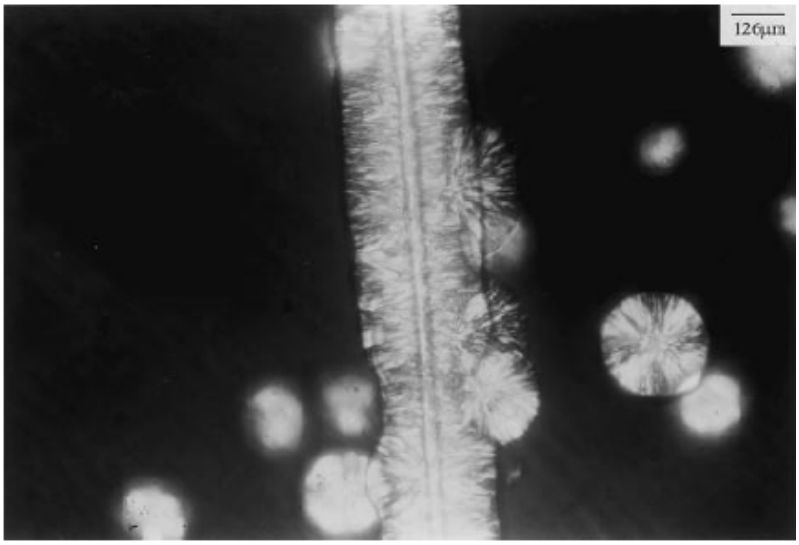

Figure 1.11: Micrographs showing the transcrystalline layer for a) iPP/non-modified flax fiber at 137 °C and b) iPP/flax fiber modified with stearic acid at 145 °C [76].

Transcrystallized layer might have a major effect in the response under loading of biocomposites. Zafeiropolus has reported fragmentation tests of crystallized and non-crystallized films of i-PP containing an embedded single flax fiber. Figure 1.12 shows a micrograph of the film after the fragmentation test. The crack of the composite started in the bulk polymer and extended through the transcrystalline layer for finally reaching the fiber itself. The interlamellar crack is indicated by yellow arrows on the figure. This evidence suggests that transcrystallization improves the

adhesion at the fiber/matrix interface; however, the general contribution of this particular morphology in the performance of biocomposites remains a field of discussion [80].

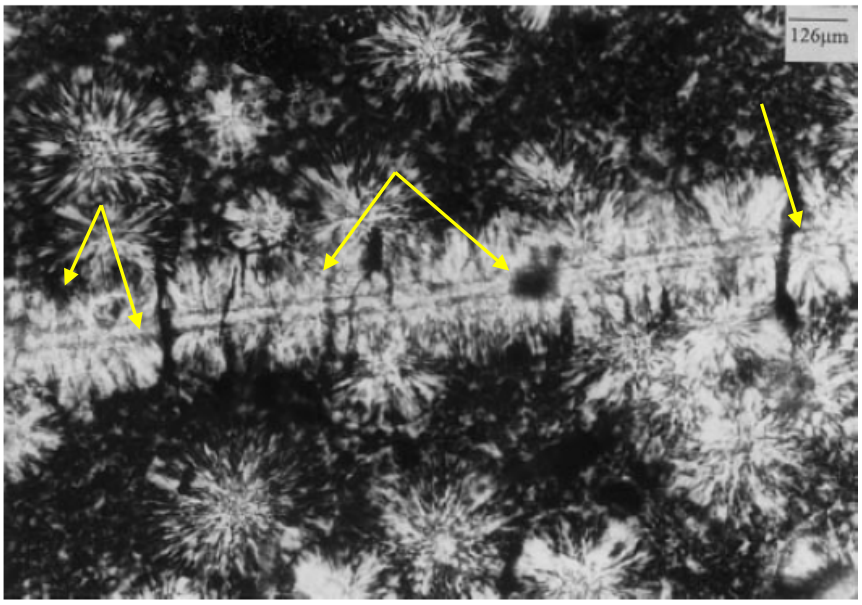

Figure 1.12: Micrograph of a flax fiber embedded in i-PP after a fragmentation test [76].

As it has been pointed out in previous paragraphs, the scientific approaches dealing with the development of biocomposites have not deeply explored the remarkable effects surrounding the fiber/matrix interface. For example, transcrystallization has not been explored in the case of PLA-based cellulose fiber composites. The study of the crystallization for PLA biocomposites is limited to a rough analysis of the thermal transitions using techniques such as differential scanning calorimetry (DSC) and dynamic mechanical analysis (DMA).

Oksman et al. studied the thermomechanical behavior of non-crystallized and crystallized biocomposites based on PLA/flax fiber by DMA. The storage modulus of previously crystallized biocomposites was very stable during the transition to the rubbery state. Storage modulus of non-crystallized specimens showed a smaller drop than the neat matrix for temperatures surrounding the T_g. When the temperature reached ~80 C, the modulus started recovering for finally reaching a value close to that of the crystallized sample [58]. This behavior was attributed to the improvement of the cold crystallization rate due to the presence of natural fibers in the PLA matrix. At the beginning of the modulus drop, the chain mobility is modified by the presence of the reinforcement, which allows the polymer chains to reach the nucleation fronts. Hence, after

the crystallization starts, the elastic modulus of the material recovers and starts increasing. Chain relaxation takes place at higher temperatures and the tangent delta curve does not show the characteristic peak [81].

Mathew et al. reported crystallization temperatures (T_c) slightly higher than the matrix for composites based on PLA/cellulose fiber. This was attributed to the nucleating ability of the reinforcement and it is in agreement with the studies of Shanks et al., whom reported an increase in T_c for biocomposites prepared with mercenerized flax fibers in a similar matrix. The authors concluded that the treated fibers promoted preferential heterogeneous nucleation at the fiber surface [64, 76, 81]. The presence of multiple melting peaks, which is associated to the presence of different sized crystal populations, was also observed.

Le Duigou et al. reported a degree of crystallinity of 47% for biocomposites reinforced at 30 wt% flax fibers, as compared to 37% for the neat matrix. The authors explained this increase by the decrease in molecular weight of PLA during processing; however, they also considered the heterogeneous nucleation at the fiber surface as an explanation for this increase [63].

Finally, processing of biocomposites at an industrial scale involves that both main components, i.e. the matrix and the natural fibers, undergo high shear stresses and important heating and cooling rates which have a direct effect on the crystallization of the systems and the fiber/matrix interactions. Also the orientation of the reinforcement and post-processing steps play a key role in the morphology of the systems and the associated final properties.

1.6 SUMMARY

Polylactide has raised a lot of interest as a potential replacement for petroleum-based polymers. The thermomechanical behavior of PLA is highly controlled by the development of crystalline structures. Presence of additives such as talc or nanoparticles greatly accelerates the crystallization kinetics of PLA. The understanding of PLA crystallization from a fundamental point of view may help the development of tailored properties for commercial applications. Natural fiber reinforced-PLA biocomposites are promising materials to replace conventional composites based on synthetic fibers. However, the highly hydrophilic nature of natural fibers results in poor surface wetting when hydrophobic matrices are used. Despite the efforts to improve fiber/matrix interactions, successful approaches have been rarely reported in the

literature. Besides their reinforcement functionality, natural fibers may act as nucleating agents when semicrystalline polymers are used in the preparation of biocomposites. However, such aspects have not been thoroughly investigated for PLA-based biocomposites.

Nanosized cellulose fibers have attracted the attention of ongoing researches around the world. These nanoparticles may greatly strengthen polymers at very low contents when a perfect dispersion at the nanoscale is reached. Nevertheless, their highly hydrogen bonding nature hampers the development of enhanced nanocomposites based on hydrophobic matrices.

CHAPTER 2 OBJECTIVES

Taking into account the current state of knowledge on biocomposites, and considering the necessity to enlarge the understanding of this new generation of materials, the main objective of this research is:

To develop fully biobased and biodegradable composites based on PLA and cellulosic reinforcements with enhanced crystallization and through a melt-compounding route.

To reach this goal, three specific objectives are defined, namely:

1. To evaluate the effect of flax fiber content on the crystallization behavior and thermomechanical properties of PLA-biocomposites processed by melt-compounding. The potential of PLA-g-MA as a compatibilizer is examined as well.
2. To investigate the melt rheology (hence processability) of PLA-flax fiber systems and the evolution of viscoelastic properties in the presence of crystallization by means of rheometry. Considering that polymer composites are subjected to important deformation during processing, a study of the shear-flow induced crystallization of PLA is also carried out.
3. To develop a melt-mixing-based process that achieves adequate dispersion of cellulose nanocrystals (CNC) in PLA, and to characterize the mechanical properties of this nanocomposite.

CHAPTER 3 SUMMARY OF ARTICLES

The main results from this research are presented in the form of three articles which are the subject of the following chapters.

Melt compounding of fully biodegradable composites based on PLA and flax fiber reinforcement and their characterization are the main focus of the first article, presented in Chapter 4. This article has been published in the scientific journal *Cellulose* in 2013 (impact factor = 3.476). Bundle breakage due to the shear forces to which the fibers are subjected during compounding is analysed. The effect of low to moderate flax fiber concentrations in the quiescent crystallization of PLA is evaluated under isothermal and non-isothermal conditions. Avrami equation is used to model the crystallization kinetics and the temperature presenting the highest crystallization rate is identified for all systems. The addition of PLA-g-MA as a means to enhance the fiber/matrix interactions is evaluated and tensile and thermomechanical properties of compatibilized and non-compatibilized systems are measured.

In Chapter 5, the investigation of quiescent and shear flow-induced crystallization of PLA and based flax fiber composites by means of rheometry is carried out. This second article has been submitted to *Rheologica Acta* in June 2014 (impact factor = 1.626). A broad range of supercooling is analysed in the case of quiescent conditions, meanwhile the lowest value of supercooling is chosen for the shear-flow induced crystallization study. Optimum experimental conditions are identified in order to control the polymer shrinkage promoted by fast cooling and transition from liquid to solid phase during experiments. Fruitful information about the nucleating potential of flax fiber is obtained by following the progress of rheological properties in the presence of crystallization. Induction times for all conditions are obtained using a simple empirical model based on the normalized differences of experimental and predicted viscosities. In the case of shear-flow-induced experiments, total deformation and shearing time are the controlled parameters and their effect on the rise of rheological curves is clearly evidenced.

In an effort to melt-compound entirely biobased and biodegradable composites using nanosized reinforcement, a novel two-step route involving solvent-mixing and melt-mixing is developed. The dispersion enhancement of cellulose nanocrystals (CNC) upon melt-mixing conditions is the primary purpose of the last article, which is presented in Chapter 6. This article has been

submitted to *Cellulose* in June 2014. First, CNC are successfully encapsulated in a hydrophilic polymer miscible with the PLA matrix using a solvent-mixing method. The product obtained from the first step after water elimination is melt-blended in the PLA matrix. A deep look on the nanocomposite morphology brings fruitful information about the dispersion of the nanoreinforcement, which is controlled by the weight ratio between the polymer carrier and CNC. Evidence of well-dispersed systems is also obtained from thermal transitions such as crystallization and dynamic mechanical analysis.

CHAPTER 4 ARTICLE 1 – THERMOMECHANICAL AND CRYSTALLIZATION BEHAVIOR OF POLYLACTIDE-BASED FLAX FIBER BIOCOMPOSITES[5]

Andrea Arias [1], Marie-Claude Heuzey [1], Michel Huneault [2]*

1: Chemical Engineering, Center for applied research on polymers and composites – CREPEC, École Polytechnique de Montréal. Montréal, Canada

2: Chemical and Biotechnological Engineering Department, Center for applied research on polymers and composites – CREPEC, Université de Sherbrooke. Sherbrooke, Canada

** Corresponding author: marie-claude.heuzey@polymtl.ca*

Abstract

In this work, the rheological, thermal and mechanical properties of melt-compounded flax fiber-reinforced polylactide composites were investigated. The effect of compounding on fiber length and diameter, and the relationship between fiber content and the crystallization behavior of the biocomposites, at various temperatures, were also examined. After melt-compounding, fiber bundles initially present were, to a large extent, broken into individual fibers and the fiber length was decreased by 75%, while the aspect ratio was decreased by nearly 50%. The crystallization half-time was found to decrease with increasing flax fiber content, and showed a minimum value at 105 °C for all systems. The elastic modulus was increased by 50% in the presence of 20 wt% flax fibers. The addition of maleic anhydride-grafted polylactide had a positive effect on the mechanical properties of the biocomposite. This system is particularly interesting in the context of sustainable development as it is entirely based on renewable resources and biodegradable.

Keywords: *Polylactide, flax fiber, biocomposite, crystallization, mechanical properties*

---

[5] *Published in Cellulose (2013) 20:439-452DOI 10.1007/s10570-012-9836-8*

4.1 INTRODUCTION

The quest for materials with a reduced environmental impact motivates the development of new biodegradable composites that can represent alternatives to traditional polymer composites materials, which mostly consist of glass fibers and petrochemical-based polymers. Therefore, the manufacturing techniques, recycling and final disposal of biocomposites need to be developed or improved. Using natural fibers as reinforcement for polymeric materials has been a subject of rising interest over the last decade. Natural fibers present many advantages, including biodegradability, renewability and comparable specific mechanical properties to synthetic fibers. Composites based on natural fibers can achieve a weight reduction, leading to lower energy requirements during processing and lower costs in the final application. Availability of natural fibers for the composite industry is an important challenge; currently the markets for natural fibers are mostly concentrated in textile and food applications [1]. Flax fiber is one of the most widely used fibers in Europe and North-America; it presents a specific elastic modulus between 20 and 50 (m^2/s^2) and its specific tensile strength ranges from 250 to 1000 (m^2/s^2) [2].

Working with natural fibers involves several challenges. The high hydrophilicity of natural fibers leads to poor compatibility with the commonly hydrophopic synthetic polymers. This, in turn, generally results in poor fiber wetting, poor dispersion, i.e. the presence of bundles and fiber agglomerates, and in weak fiber-matrix adhesion. In addition, it promotes water uptake by the extruded or injection-molded end-products [3]. Different interfacial modification routes have been investigated to increase hydrophobicity and improve interfacial properties. Chemical modification of the fiber surface involves the grafting of molecules presenting functional groups compatibles with the matrix [4, 5]. Another possible route is to modify the matrix properties by the use of surfactants or of polymeric compatibilizer such as maleic anhydride-grafted polymers [6, 7]. In addition to the fiber-matrix interfacial challenge, natural fibers present particular characteristics compared to conventional fibers. For example, the fiber diameter distribution is much wider and the surface roughness is sensitive to the fiber preparation technique.

Polylactide (PLA) is a biodegradable thermoplastic polymer, which can be produced from renewable resources. Polylactide with high molecular weight for commercial applications is produced by ring-opening polymerization of lactide, a dimer of lactic acid. The stereochemical structure of PLA can be modified to yield amorphous or semicrystalline polymers depending on

the *L* or *D*-isomer content used in the polymerization. However, PLA commercial grades are usually synthesized based on *L*-lactide with small contents of *D*-lactide [8, 9].

The mechanical and thermal properties of PLA are strongly related to crystallinity. Its thermal resistance is limited by its low glass transition, around 60 °C, unless it contains a certain level of crystallinity [10]. Fully crystallized poly *L*-lactide (PLLA) samples showed higher tensile modulus and strength than amorphous samples. At equal molecular weight, the tensile modulus and impact resistance increased by 20 and 100%, respectively [11]. In terms of heat deflection temperature (HDT), the value reported for crystallized PLLA was 30 ^{o}C higher than that of amorphous PLA [12]. However, PLA crystallization is typically very slow. For example, a semicrystalline commercial grade containing 2% *D*-lactide presented a crystallization half-time of approximately 40 min [13]. For several applications, increasing the rate of crystallization is desired. Adding mineral nucleating agents such as talc and clay and more recently N,N-ethylenebis(12-hydroxystearamide) (EBHSA) and bio-based orotic acid [14, 15] is considered as a viable route to improve the crystallization kinetics and decrease the time to achieve PLA crystallization.

The growth of PLA spherulites has been thoroughly studied using optical microscopy. The maximum spherulite growth rate has been observed between 105 and 125 °C, depending on the *D*-lactide content, molecular weight and processing conditions [16-19]. In the presence of fibers, spherulitic growth can be accompanied by the growth of a transcrystalline layer on the surface of fibers. This has been shown in polypropylene (PP) composites for synthetic fibers such as Kevlar, PET, PTFE and carbon fibers [20]. The origin of transcrystallinity is not clear but several phenomena can nucleate crystallization on the surface of fibers. These include epitaxial growth based on similar crystalline lattice sizes, preferential adsorption of the polymer on the fiber surface or thermally-induced polymer orientation due to mismatch in thermal expansion between the fiber and matrix material [20].

Wood fibers, microcrystalline cellulose and cellulose fibers have been shown to increase the crystallization temperature of PLA upon cooling [21]. This is indicative of a nucleating ability. Among these wood-based additives, wood fibers were found to have the strongest effect in terms crystallization temperature shift. A transcrystalline layer over the wood fibers was clearly shown

while little or no transcristallinity occurred on the surface of microcrystalline cellulose or on the cellulose fibers [21].

The effect of flax fibers and their surface treatment on the crystalline development in PLA composites has also been investigated [22]. It was found that the presence of the flax fibers did not modify the crystallization temperature (T_c) significantly (less than 5 ^oC). The T_c changes were not sensitive to the type of surface treatment. Optical micrographs did not provide clear evidence of transcrystallinity either.

The effect of flax fibers on the crystalline development in PP has also been investigated. It was possible to grow important transcrystalline layers on the surface of flax fibers. Transcrystallinity is an important feature in composites because it can improve stress-transfer between the matrix and the fiber [23]. Zafeiropoulos suggested that surface roughness plays a decisive role in the growth of the transcrystalline layer. Unmodified flax fibers developed a non-homogeneous layer; whereas stearic acid treated flax fibers presented a thinner but homogeneous transcrystalline layer. However, in another study on silane-modified fibers and using maleated polypropylene, transcrystallinity development was found only for untreated fibers [24].

Mechanical performance of PP- and PLA-natural fiber composites has been widely investigated [25-28]. Properties of composites were found to depend on fiber characteristics, fiber orientation, fiber-matrix interface and matrix crystallinity. The most relevant fiber characteristics include their aspect ratio, their tensile properties and their thermal stability [28, 29]. It is noteworthy that the reported composite properties were highly variable from one study to another. At 30 wt% of flax fibers, the elastic modulus of PLA-based composites has been shown to range from 6,8 to 9,0 GPa (as opposed to ~ 3 GPa for neat PLA) [30-32]. Also at 30 wt% of flax fibers, the tensile strength showed an increase of about 10% as compared to neat PLA, whose strength is of the order of 50 MPa. However some studies reported a slight reduction of this property, usually explained by the poor stress transfer across the interface, which means that there is practically no interfacial bonding between the reinforcing fiber and the polymer matrix [30, 31, 33]. PLA elongation at break was also shown to decrease with the addition of natural reinforcements such as flax fibers and microcrystalline cellulose (MCC) [29, 32]. Several authors agree on the idea that any fiber can act as a weak point for fracture initiation. The elongation at break of flax fiber composites remained close to the elongation at break of the fiber (~ 3 %) [34], regardless of the

reinforcement content added to the system, hence making PLA slightly more brittle (typically ~ 6 % for neat PLA).

The aim of this work is to investigate the effect of processing and compatibilization on the properties of flax-fiber reinforced PLA biocomposites. This system is entirely based on renewable resources and is fully biodegradable; hence it represents a "green" alternative to traditional thermoplastic polymer composites. The addition of maleic anhydride-grafted PLA (PLA-g-MA) is intended to improve the fiber-matrix interaction. The crystallization behavior in quiescent isothermal and non-isothermal conditions of PLA-based biocomposites, prepared with low to moderate weight fractions of flax fibers, is investigated. Thermal, rheological and mechanical properties of the uncompatibilized and compatibilized PLA-flax fiber systems are also examined.

4.2 EXPERIMENTAL

4.2.1 Materials

The polylactide (PLA) used in this work was obtained from NatureWorks LCC. It is a semi-crystalline grade (PLA 4032D) comprising around 2% D-lactide. Flax fibers, cut to a nominal length of 1 mm, were kindly supplied by LIMATB (France). Maleic anhydride-grafted polylactide (PLA-g-MA) was prepared in a twin-screw extruder using 2 wt% maleic anhydride and 0.25 wt% of a peroxide initiator, following a procedure reported earlier [13] The extent of maleation of the PLA-g-MA sample was quantified by a titration method [35, 36]. The content of MA was found to be 0,8 wt%.

4.2.2 Samples preparation

PLA-flax fiber composites were prepared by melt mixing in an internal mixer (C.W. Brabender Plasticorder) under a nitrogen atmosphere. For all composites, the mixing time was performed for 7 min at 60 rpm and 180 °C. The nominal flax fiber content was set at 1, 5, 10 and 20 wt%. The PLA-g-MA content used was 20 wt%. Two different batches of each blend (25 g) were prepared to verify reproducibility. PLA pellets and flax fibers were previously dried at 80 °C for 24 h under vacuum. For comparison purposes, neat PLA was also processed using the same thermo-mechanical cycle and will be referred to as "compounded PLA".

As-received and compounded PLA, as well as PLA-based biocomposites, were compression molded in a heated press from Carver Laboratory at 180 °C for about 10 min under a nitrogen atmosphere. Pressure was increased slowly from 0 to ~ 14 MPa. After compression molding, the samples were quenched using a water cooled press and stored in a dessicator before subsequent testing. The preparation method was chosen in order to obtain an isotropic distribution of the flax fibers in the matrix and to avoid orientation effects.

4.2.3 Characterization techniques

4.2.3.1 Microscopy

As-received flax fibers and 60 μm thick PLA-based biocomposite films containing 5 wt% of flax fibers were observed using a Zeiss Axioskop 40 optical microscope in transmission mode. The size and state of dispersion of flax fiber before and after blending were evaluated. Diameter and length averages were calculated based on 110 fibers for dry fibers, and 210 fibers in PLA composite films.

4.2.3.2 Thermogravimetry (TGA)

Thermogravimetric analyses were performed using a TGA Q500 from TA Instruments. The measurements were carried out at a heating rate of 10 °C/min in an air atmosphere with a flow rate of 60 mL/min. Temperature ranged from 30 to 700 °C. The sample's weight was approximately 15 mg.

4.2.3.3 Rheological characterization

The rheological properties of PLA (as-received pellets and compounded) and PLA-based biocomposites with flax fiber contents of 1, 5 and 10 wt%, were evaluated at 180 °C using a stress-controlled Gemini rheometer (Malvern Instruments) and a 25 mm parallel-plate flow geometry. Measurements were performed in oscillatory mode in the linear viscoelastic region. Dynamic properties were monitored as functions of time to examine the thermal stability and behaviour of the samples. A thermal soak time of 4 min was used prior to the oscillatory measurements. Time sweep tests were carried out a frequency of 6,28 rad/s for 10 min. Frequency sweeps were performed in the linear viscoelastic regime, from low to high and high to low frequencies ranging from 0,1 to 100 rad/s, over an overall duration of 12 min.

4.2.3.4 Differential scanning calorimetry (DSC)

The thermal characteristics of PLA and PLA-based composites were examined using differential scanning calorimetry (DSC Q1000 from TA Instruments) under a helium atmosphere. A sample size of approximately 10 mg was used. Before all DSC tests, the thermal history was removed by heating the samples from 30 to 200 °C and maintaining at 200 °C for 3 min. The non-isothermal characterization was carried out by cooling the samples from 200 down to 30 °C using cooling rates of 2, 5 and 10 °C/min and then re-heating from 30 to 200 °C at a heating rate of 10 °C/min.

In the case of the isothermal tests, samples were cooled from 200 °C to different crystallization temperatures T_c: 90, 100, 105, 110, and 120 °C, at a rate of 50 °C/min. The samples were then maintained at this temperature until the crystallization was completed. Finally, the samples were heated back from the crystallization temperature to 200 °C at a heating rate of 20 °C/min to measure the melting enthalpy.

4.2.3.5 Mechanical characterization

Tensile testing was performed according to ASTM D638 for tensile properties of plastics using an Instron universal testing machine. Measurements were carried out using standard type V dog-bone shaped samples with a crosshead speed of 1 mm/min, and using a load cell of 5 kN. Six specimens were tested for each formulation.

4.2.3.6 Dynamic mechanical thermal analysis (DMTA)

Dynamic mechanical thermal analysis was performed in a dual cantilever bending mode by using a DMA 2980 from TA Instruments. The measurements were conducted at 1 Hz at a heating rate of 2 °C/min from room temperature to 130 °C. The test specimens were 2 mm thick, 35 mm long and 12 mm wide.

4.3 RESULTS AND DISCUSSION

4.3.1 Thermal stability of fibers

The thermal stability of the flax fibers was evaluated using the TGA technique. Figure 4.1 shows the relative weight drop (left ordinate) and the weight drop first derivative (right ordinate) as functions of temperature in air. Three different rapid weight loss regions can be identified. A first

one, accounting for about 5% weight loss occurs between room temperature and about 100 °C. This weight loss can be associated to residual moisture loss. The second important weight loss, accounting for more than 50% of the total loss, takes place between 220 and 380 °C. This weight loss region is in the degradation interval of the flax fibers and is most commonly associated to the first steps of hemicelluloses and cellulose depolymerization. A third region can be distinguished from the second one when observing the first derivative peaks. The third weight loss region, above 400 °C, accounts for the final 40% weight loss. This weight loss can be associated to the final stages of degradation of cellulose and hemicelluloses. Flax fibers present a complex chemical structure based on crystalline and amorphous cellulose regions contained into a lignin-hemicellulose matrix [2]. During thermal degradation, several parallel reactions take place. Thermal decomposition starts with hemicelluloses, closely followed by lignin and subsequently by cellulose [37]. It has been pointed out that in an inert atmosphere, hemicellulose degrades preferentially from 200 to 325 °C, lignin from 280 to 400 °C and cellulose from 300 to 400 °C [38, 39]. These intervals can shift in the presence of oxygen. Consequently, the second peak in Figure 4.1 represents the superposition of three depolymerization reactions. Several authors have indicated that the third peak corresponds to the further degradation of residues and aromatic substances [40, 41]. Considering these results, the flax fibers should withstand compounding with the PLA matrix at 180 °C under a nitrogen atmosphere.

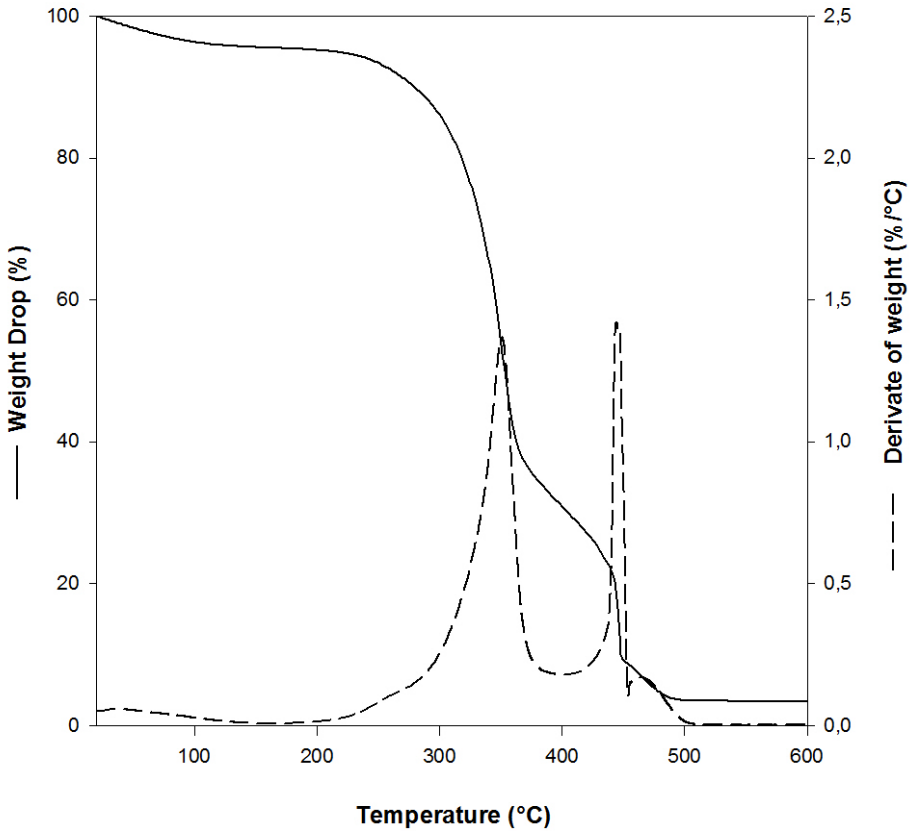

Figure 4.1: Thermogravimetry results for flax fibers.

4.3.2 Fiber morphology

Since fiber attrition and breakup during processing is a major concern, it is important to verify the fiber dimensions and aspect ratio after compounding. Figure 4.2 shows the optical micrographs of as-received flax fibers (4.2a, b) and a PLA-biocomposite film with 5 wt% of flax fibers (4.2c, d). The as-received flax fibers are in the form of bundles and single fibers, with an approximate length of 1 mm (the original nominal length). In comparison, the flax fibers in the composite show less fiber bundles and more single flax fibers, with length below 300 μm (Fig. 4.2c, d).

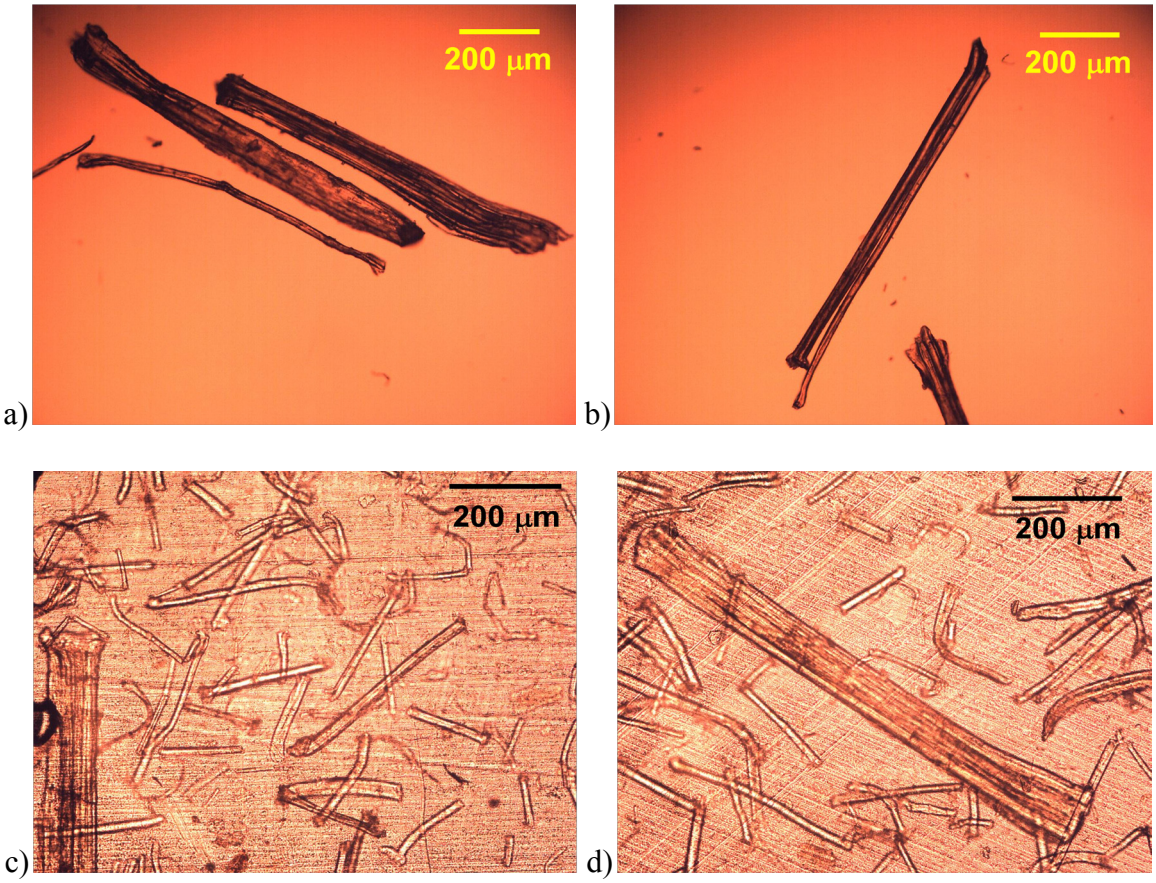

Figure 4.2: Optical micrographs of: a), b) as-received flax fibers and c), d) 5 wt% PLA-flax fiber composite film, 60 μm thick.

Figure 4.3 presents the length, diameter and aspect ratio distributions of the flax fibers before and after compounding. The length distribution of the as-received flax fibers (Fig. 4.3a) varied from 875 to 1275 μm, with a weighted mean length of 1015 μm. More than 80% of fibers were found between 975 and 1075 μm in length. After compounding, the distribution of fiber length varied from 75 to 475 μm, and the weighted mean length decreased by about 75%, reaching 250 μm. The fiber diameter, shown in Figure 4.3b, exhibited a bimodal distribution before compounding. The first mode around 30 μm probably represents the single fiber population in the sample, which accounts for ~ 60% of fibers. The remaining ~40% of fibers had a mode centered on 110 μm that is associated to the bundle population. After compounding, the diameter presented a narrow unimodal distribution, where more than 95% of the fiber diameters were below 40 μm and the presence of bundles was negligible. The aspect ratio of the as-received flax fibers before compounding (Fig. 4.3c) showed a wide distribution. Its value varied from 4 to 76, and it

presented a weighted mean around 28. After compounding, the aspect ratio distribution became narrower so that 70% of the compounded flax fibers exhibited an aspect ratio between 10 and 20. Because the length, diameter and aspect ratio decreased during compounding, it was clear that breakup occurred simultaneously in the longitudinal and transverse directions. However, a more homogeneous distribution was observed in the cases of diameter and aspect ratio after compounding. Flax fiber attrition has been reported earlier in PLA [42] and polypropylene composites [43]. In PLA, flax fiber length was shown to decrease from ~5 to 1 mm after twin screw extrusion. Similar effects have been reported for cellulose nanocomposites; mean length of ramie whiskers has shown a decrease of 50% after extrusion film process [44].

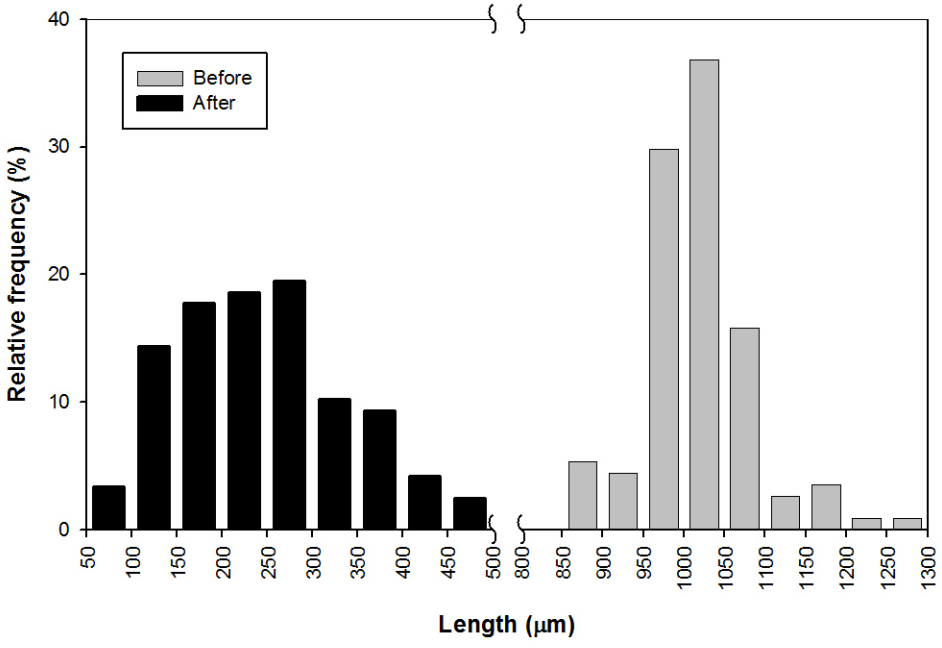

a)

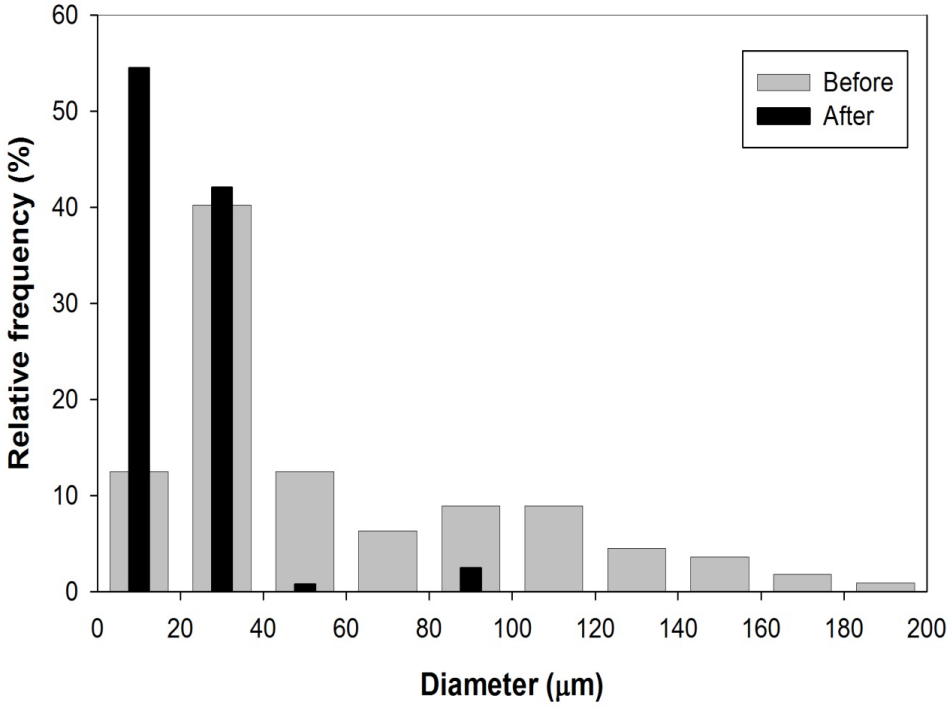

b)

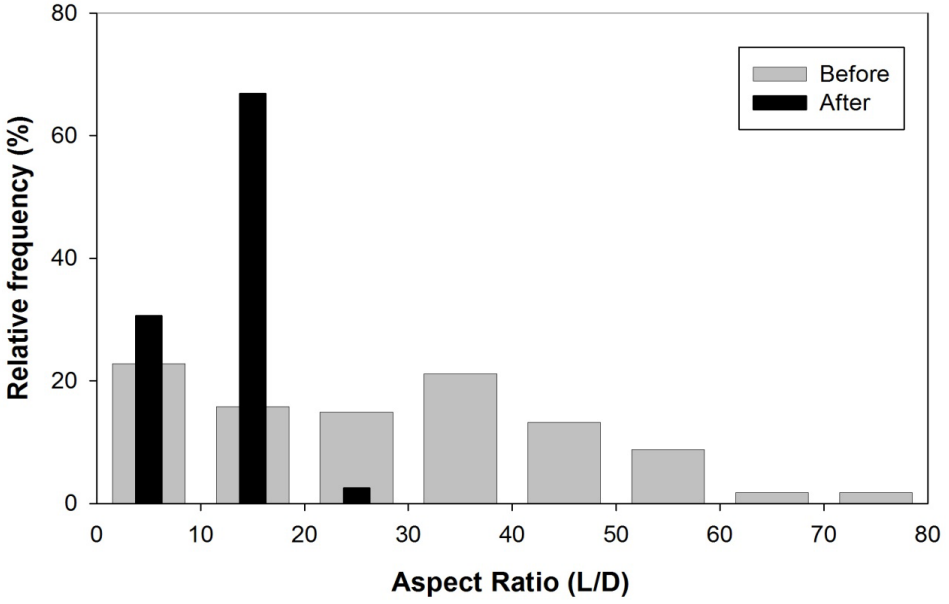

c)

Figure 4.3: Distribution of flax fiber dimensions before and after compounding: a) length, b) diameter, and c) aspect ratio.

4.3.3 Rheology

It is well known that the presence of water and high temperature lead to the random scission of PLA chains, decreasing molecular weight and thus viscosity [45]. Considering that flax fibers are hydrophilic, it is difficult to completely eliminate their water content. This residual water can have an impact on the hydrolytic chain scission of PLA. Since molecular weight and viscosity are intimately linked, rheological measurements were used as a mean to investigate PLA thermal degradation at processing temperature. Figure 4.4 presents the complex viscosity at 180 °C as a function of time, for as-received and compounded PLA and various PLA-flax fiber based composites. The viscosity of the compounded PLA was initially around 3000 Pa.s. It was relatively stable up to 200 s and then dropped slightly, loosing around 5% of its value after 600 s. A similar test was carried out on the as-received PLA. The initial viscosity of the pellets was around 4400 Pa.s, but its drop was slightly more important than for compounded PLA, it decreased ~ 2% per minute, reaching 3600 Pa.s after 600 s. The difference between the as-received and compounded PLA viscosity can be associated to chain scission during compounding, and also in a potential plasticization of the PLA by low molecular weight degradation products such as lactic acid or lactic acid oligomers. These low molecular weight products are known to efficiently plasticize PLA [46].

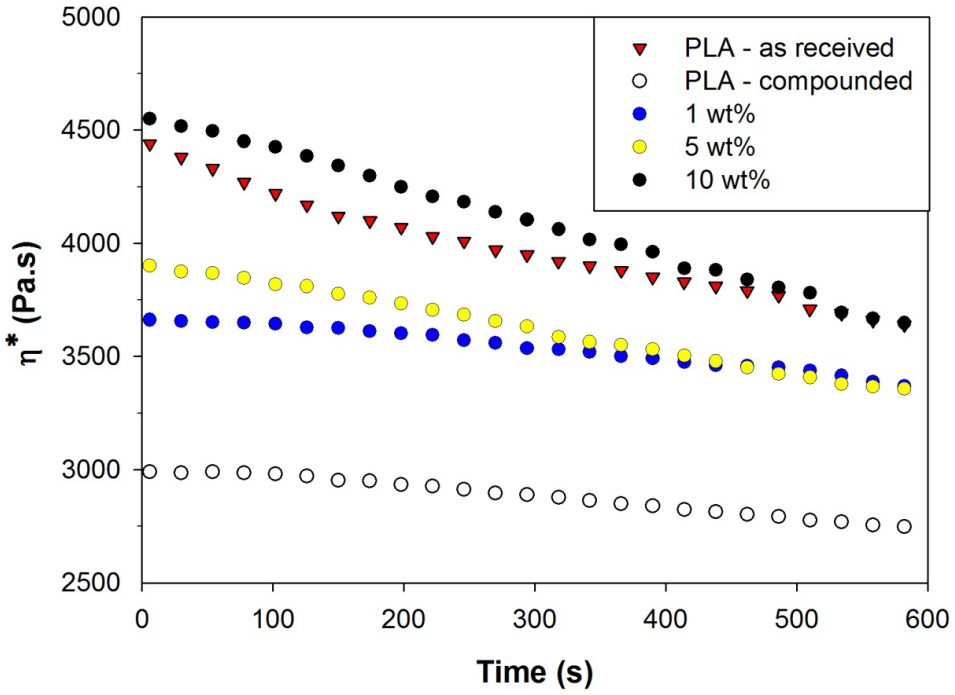

Figure 4.4: Time sweep at 180 °C for as-received and compounded PLA and PLA-based flax fiber composites with various fiber contents.

Figure 4.4 also shows that the complex viscosity increased with fiber content. At 10 wt% of flax fibers, the initial viscosity of the composite was close to 4500 Pa.s, which somewhat exceeds the as-received PLA viscosity. It also represents a 50% increase in comparison with compounded PLA. However the composite's viscosity showed a slightly more important drop with time. On average, the complex viscosity of compounded PLA, as well as 1 and 5 wt% flax fiber composites, dropped by ~ 1% per minute. This value increased to around 2% per minute for the PLA-10 wt% flax fiber composite. It is noteworthy, however, that the residence time in most polymer processing operations is much shorter than the time sweeps in this investigation (14 min, including thermal soak time) or than the laboratory mixing/molding time (7 min mixing and 10 min compression molding). Molecular weight loss during compounding in industrial conditions may therefore be smaller than the effect found in this investigation, depending on the specific thermomechanical history. Considering that the PLA viscosity is a function of molecular weight to the power 3.4 [47], the viscosity drop between the as-received and the compounded PLA can be associated with a 8% drop in average molecular weight over 10 min. In the high molecular

weight range, the mechanical properties of polymers are not expected to differ significantly for such a change in average molecular weight [11].

Figure 4.5 shows the complex viscosity of PLA and PLA-based composites as a function of frequency at 180 °C. As-received and compounded PLA presented a shear-thinning behaviour characterized by a plateau viscosity at low frequency, followed by a power-law decrease as frequency increases. PLA-based composites also exhibited non-Newtonian behaviour. At low frequency, viscosity increased slightly as flax fiber content increased; composite at 10 wt% exhibited a complex viscosity close to 5000 Pa.s at 0,1 rad/s, and there is no indication of a plateau in this frequency range. This phenomenon may be associated with the formation of a fiber network; however, this hypothesis requires further investigation.

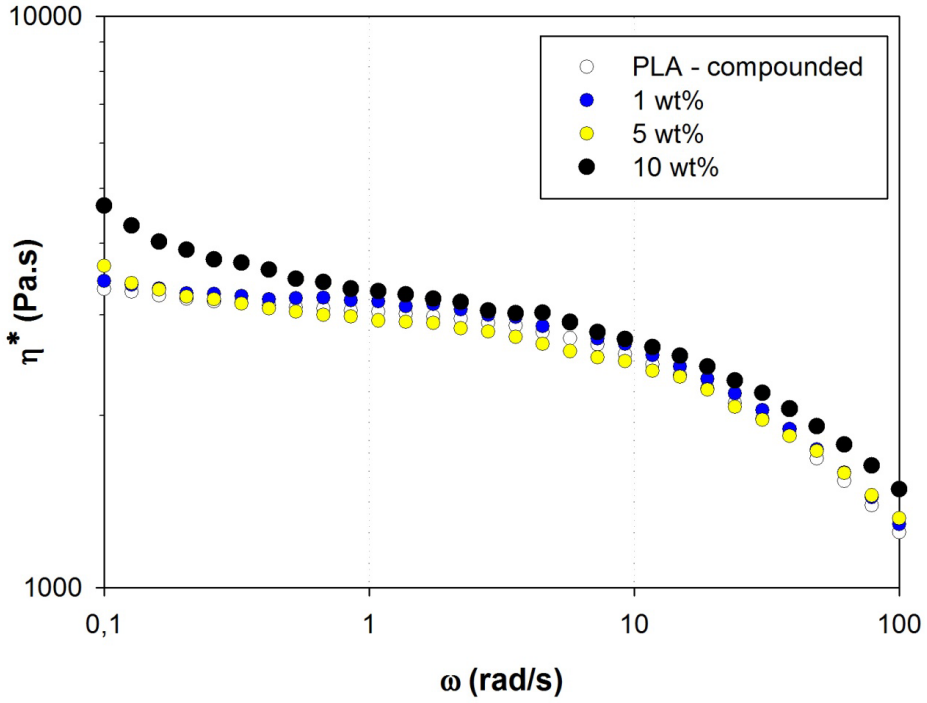

Figure 4.5: Complex viscosity at 180 °C for PLA-based composites and compounded-PLA.

4.3.4 Crystallization

Isothermal crystallization tests were carried out between 90 and 120 °C. The relative degree of crystallinity as function of time is shown in Figures 4.6 and 4.7 for compounded PLA and PLA-based composites, respectively. Figure 4.6 compares the relative degree of crystallinity of compounded PLA for different crystallization temperatures. Isothermal crystallization of as-received PLA pellets at 105 °C is also shown for comparison. All curves have the expected sigmoidal shape. The PLA-compounded samples at 100, 105 and 110 °C showed very similar behaviour and exhibited a faster crystallization than the samples crystallized at 90 and 120 °C. In terms of crystallization half-time, $t_{1/2}$, defined as the time required to reach half of the final crystallinity, the compounding steps leads to a $t_{1/2}$ drop from ~ 40 min to ~ 4 min at 105 °C. One potential reason that could explain such a boost in crystallization rate may come from the decrease in polymer viscosity described in the previous section. The general increase in polymer chain mobility, either by a general average molecular weight reduction during compounding or to a plasticization effect coming from low molecular weight degradation products may considerably speed up the crystalline growth rate.

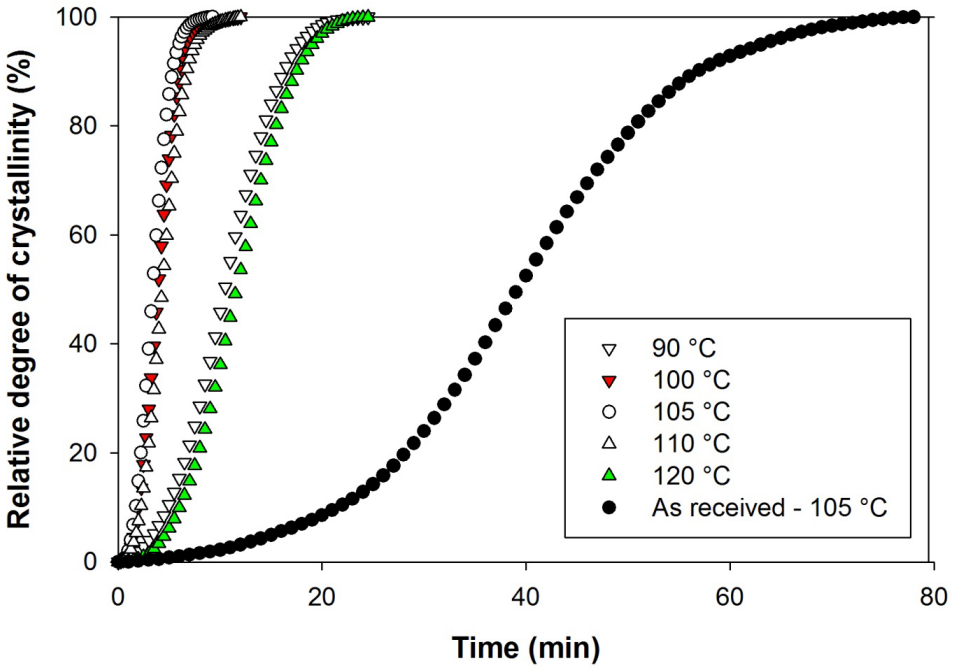

Figure 4.6: Relative degree of crystallinity as function of crystallization time for compounded PLA at different temperatures, and as-received PLA at 105 °C.

Figure 4.7 examines the effect of the fiber content on the relative degree of crystallinity at 90 °C for PLA-based composites. These samples exhibited a similar induction period of 3-4 min prior to a significant crystallinity growth. However, the subsequent crystalline development was clearly accelerated as the flax fiber content was increased. The crystallization half-time, $t_{1/2}$, decreased from 10.5 min for compounded PLA to 7 min for the 10 wt% flax fiber composite at 90 °C. This indicates that the flax fiber may play a nucleating role in the PLA crystallization. A similar behavior was observed in the overall temperature range investigated.

The isothermal crystallization kinetics of polymers during the crystalline growth rate stage (i.e. after induction and prior to secondary crystallization) is often described by the classical Avrami equation [48]:

$$X_c(t) = 1 - \exp(-Kt^n) \quad (4.1)$$

where X_c is the relative degree of crystallinity, K is a rate constant and n is the Avrami exponent that depends on the nature of nucleation and growth geometry of the crystals. Its value is typically between 2 and 4 for polymer crystallization.

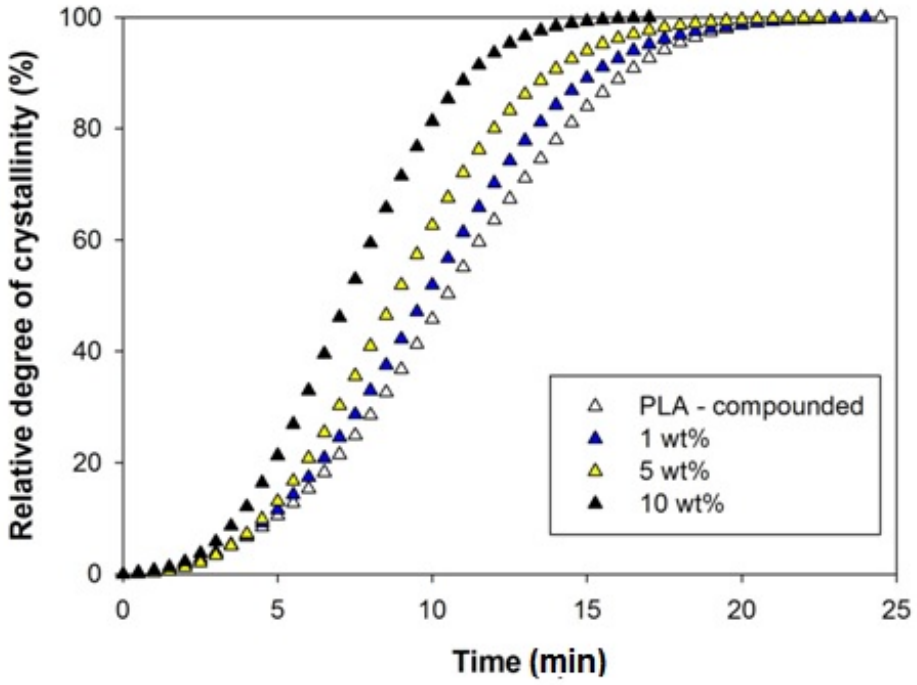

Figure 4.7: Relative degree of crystallinity as function of crystallization time at 90 °C for PLA-based composites and compounded PLA.

Figure 4.8 presents log (–ln(1 – $X_c(t)$)) against log t. This representation enables graphical evaluation of K and n from the graph ordinate and slope, respectively. For each composite, a series of straight lines were obtained showing that the crystallization kinetics followed a classical Avrami relationship. The values of n and K were obtained from the linear graph portion and are summarized in Table 4.1.

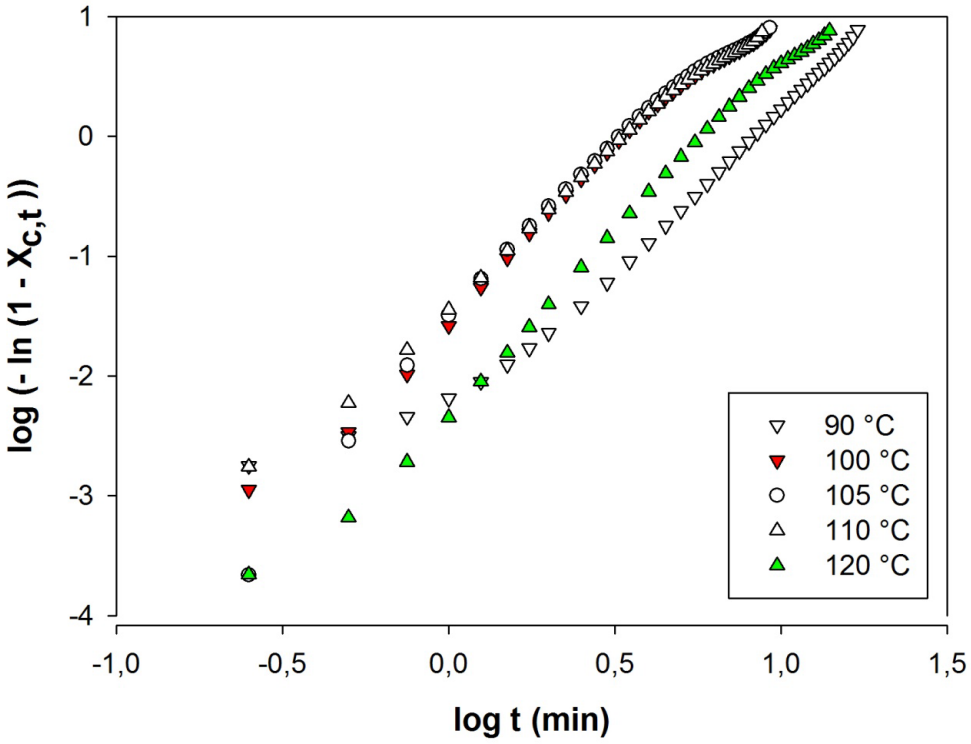

Figure 4.8: Avrami plots for the PLA – 10 wt% flax fiber composite at various crystallization temperatures.

Table 4.1: Kinetics parameters obtained from the Avrami analysis for flax fiber-reinforced PLA

Sample	***n*, *K* (min-n)**	**Tc (°C)**				
		90	**100**	**105**	**110**	**120**
PLA – as received	*n*	-	-	1.9	-	-
	K	-	-	3.51E-04	-	-
PLA - compounded	*n*	2.6	2.7	2.8	2.7	2.8
	K	1.56E-03	1.59E-02	2.03E-02	1.36E-02	6.86E-04
PLA - 1 wt%	*n*	2.5	3.1	2.8	2.9	3.0
	K	2.17E-03	1.48E-02	1.81E-02	1.26E-02	4.96E-04
PLA - 5 wt%	*n*	2.7	2.8	2.8	2.7	3.1
	K	2.07E-03	1.46E-02	1.63E-02	2.29E-02	1.54E-03
PLA - 10 wt%	*n*	2.6	2.8	3.0	2.6	3.0
	K	3.97E-03	2.90E-02	2.65E-02	3.86E-02	5.20E-03

It has been proposed that PLA predominantly exhibit homogeneous nucleation and two-dimensional crystal growth [10]. PLA-based composites, on the other hand, will undergo mostly

heterogeneous nucleation because of the presence of the fibers, with their growth dimensions being dependent on the filler geometry. Fiber-type fillers may promote an enhanced nucleation of spherulitic growth along fibers, and a columnar crystal morphology may be developed if the nucleation density is high [20]. Hence, the small difference in the Avrami exponent between compounded PLA and PLA composites may be explained by the development of two-dimensional crystal growth in both cases. Another explanation could be a low interaction between the fibers and the polymer chains; hence the geometry of the PLA crystals would not be modified much by the presence of the fibers.

The effect of crystallization temperature on crystallization half-time, $t_{1/2}$, is shown in Figure 4.9. All systems presented a "u" shape with a minimum $t_{1/2}$ in the 100-110 °C range. We can associate the "u" shape of the $t_{1/2}$ curve to two competing phenomena controlling the crystallization process: the nucleation rate and the chain mobility. The nucleation rate increases with the amount of undercooling, i.e. the difference between the melting temperature and the crystallization temperature. By contrast, the chain mobility is enhanced as the temperature increases. For the as-received PLA, the minimum half-time was around 39 min at 105 °C (not shown). The minimum half-time for compounded PLA and for 1 and 5 wt% flax fiber composites was significantly reduced, to around 3,5-4 min at the same temperature. With 10 and 20 wt% of flax fibers, the half-time was further decreased, below 3 min. Outside the 100-110 °C optimal crystallisation temperature range, the effect of fibre content was more significant with the highest flax concentrations leading to the lowest half-times. Some authors have suggested that the decrease in the induction time of semicrystalline polymers, in the presence of both synthetic and natural fibers, is due to the fact that surface roughness plays a key role in increasing crystal nucleus density [20, 23, 49]. Flax fibers may contribute to both phenomena, i.e. they may act as nucleation agents and improve local chain mobility, i.e. in the vicinity of the fibers. Further evidence of flax fibers nucleating ability and effect on local chain mobility is discussed below.

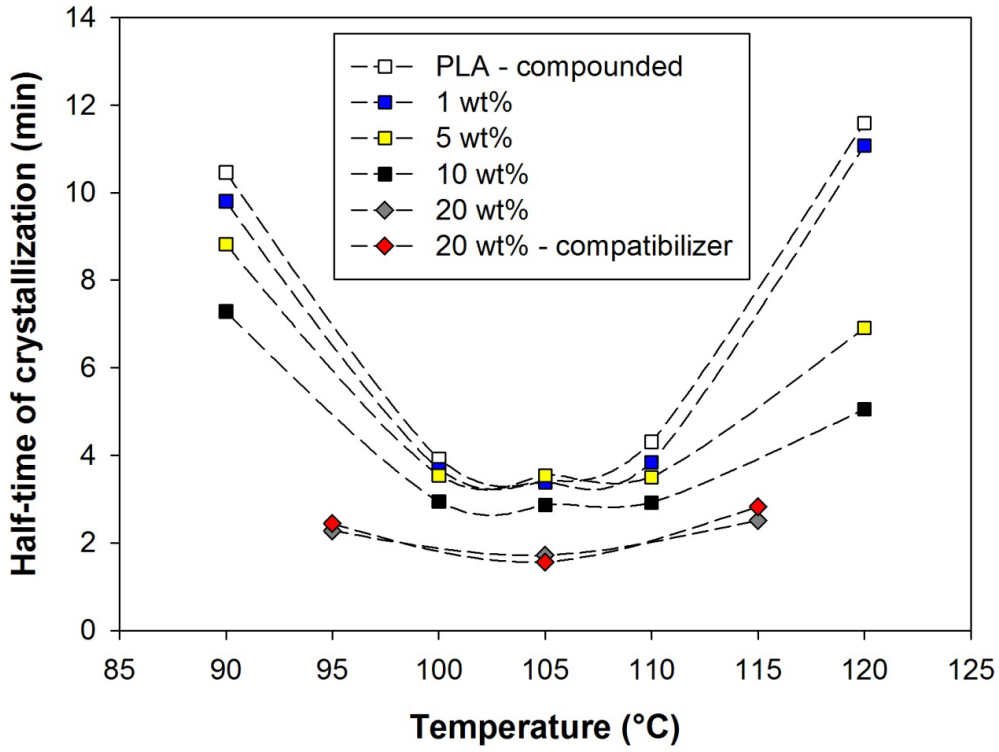

Figure 4.9: Isothermal crystallization half time as function of temperature for PLA-based composites and compounded PLA.

Figure 4.10 presents the DSC non-isothermal thermograms obtained for PLA (as-received and compounded), and PLA-based composites cooled at rates of 2, 5 and 10 °C/min. The glass transition temperature remained nearly constant for all composites and for PLA – compounded as well. According to the DSC thermograms (Fig. 4.10a, b and c) the T_g values are close to 60 °C in all cases. The crystallization and melting enthalpies obtained from the peak integration of the non-isothermal data (Fig. 4.10) are summarized in Figure 4.11. At 2 °C/min cooling (Figure 4.10a), the composites reached complete crystallization during the cooling stage, i.e. no crystallization peaks were formed upon reheating. As-received PLA did not crystallize under any cooling or heating stage. Compounded PLA exhibited a crystallization enthalpy of ~ 29 J/g which is equivalent to 31% of crystallinity (using 93,7 J/g as the theoretical value for the heat of fusion of PLA crystals [50]). The crystallinity developed upon cooling increased slightly as flax fiber content increased. At 10 wt% of fibers, the total crystallinity reached a value of 34%. At 5 °C/min cooling (Figure 4.10b), crystallization upon cooling was incomplete. It was completed via

cold crystallization on the subsequent reheating cycle. Upon cooling, the crystallization enthalpy grew from ~ 7 to ~ 28 J/g for flax fiber contents from 0 to 20 wt%, respectively. Maximum content of crystals reached during the cooling and second heating varied from 34% for compounded PLA, to 37% for 20 wt% flax fiber composites. Upon 5 °C/min cooling, PLA reached ~ 20% of its total crystallinity, while the composite at 10 wt% of flax fiber reached ~ 50% of its total crystallinity; at 20 wt% of flax fiber, about 80% of the total crystallinity was reached during the cooling stage. However, the total crystallinity achieved in all cases was between ~ 30% to ~ 37%. The crystallization peak upon cooling was shifted to higher temperatures as the fiber concentration increased, indicating that the crystallization started earlier under non-isothermal conditions. The cold crystallization peak followed the opposite tendency; it was displaced to lower temperatures for PLA-based composites, suggesting enhanced local mobility of polymer chains. Presence of fibers in the polymer matrix could be understood as "obstacles", going against the mobility and slippage of polymers chains; however, if these so-called obstacles locally multiply the number of crystal nucleus, it will be easier for the polymer chains to reach one nucleus, reducing the displacement and enhancing the local mobility.

At 10 °C/min cooling (Figure 4.10c), the crystallinity reached during cooling was negligible; only cold crystallization process took place in all samples. The crystallinity content built during cooling represented maximum ~ 8% of the total crystallinity of PLA-based composites. Total crystallinity values ranged from ~ 30% for compounded PLA to ~ 33% for PLA-20 wt% flax fiber composite.

If the crystallization initiates preferentially at the fiber surface, a transcrystalline morphology will be privileged, creating crystalline regions that could act as physical crosslink between matrix and filler [21]. This fact could most probably give a stronger fiber-matrix interphase, and consequently better mechanical performance. However the industrial processing of composites requires really fast cooling rates; it is still a challenge to develop PLA-based composites that crystallizes faster.

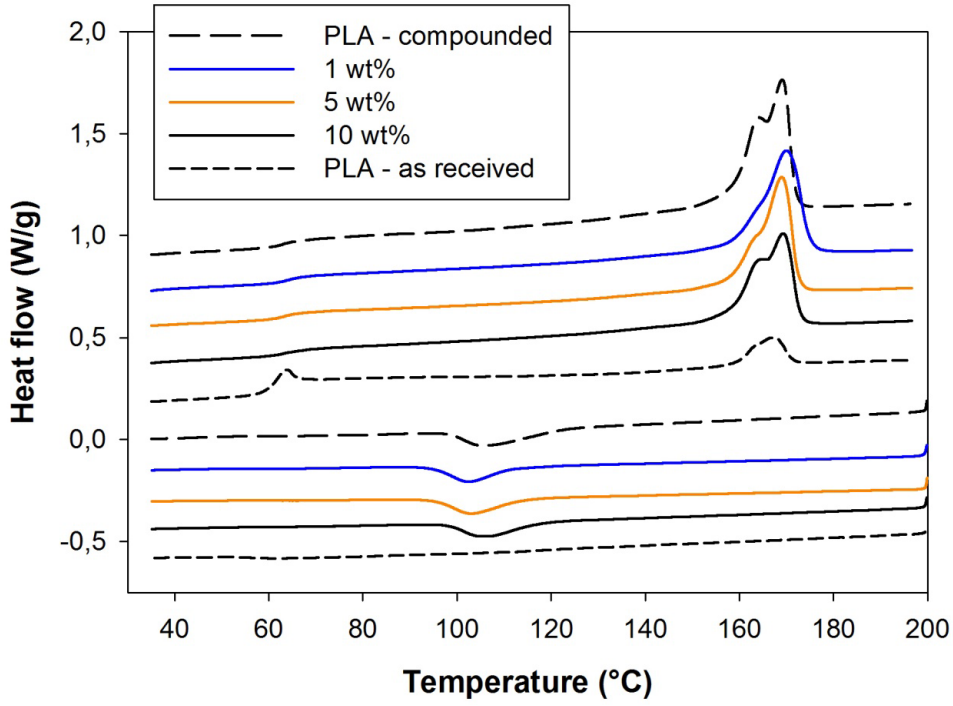
PLA - compounded
1 wt%
5 wt%
10 wt%
PLA - as received
Heat flow (W/g)
2,0
1,5
1,0
0,5
0,0
-0,5
40
60
80
100
120
140
160
180
200
Temperature (°C)

a)

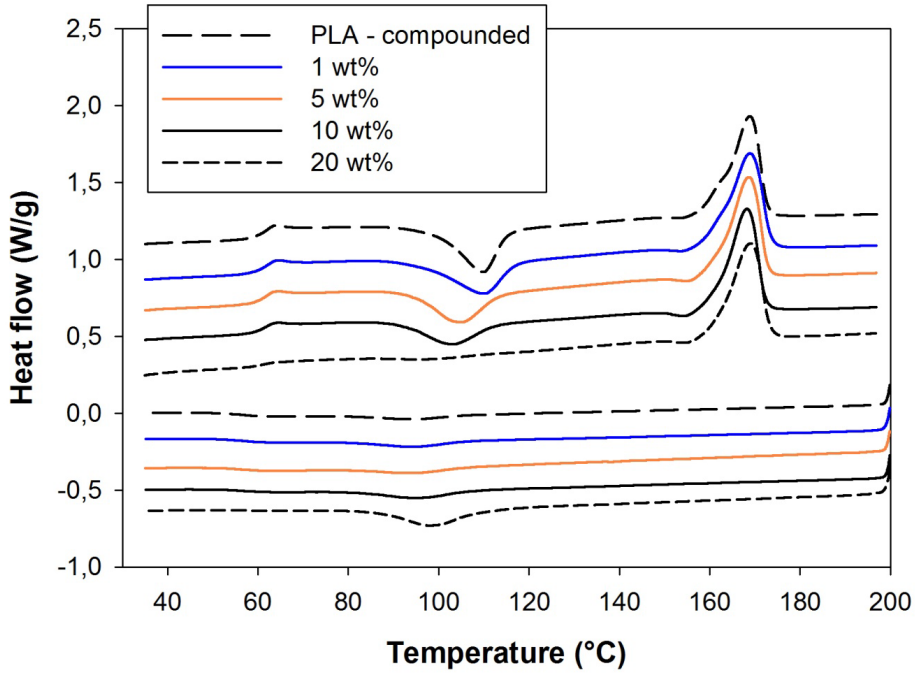
PLA - compounded
1 wt%
5 wt%
10 wt%
20 wt%
Heat flow (W/g)
2,5
2,0
1,5
1,0
0,5
0,0
-0,5
-1,0
40
60
80
100
120
140
160
180
200
Temperature (°C)

b)

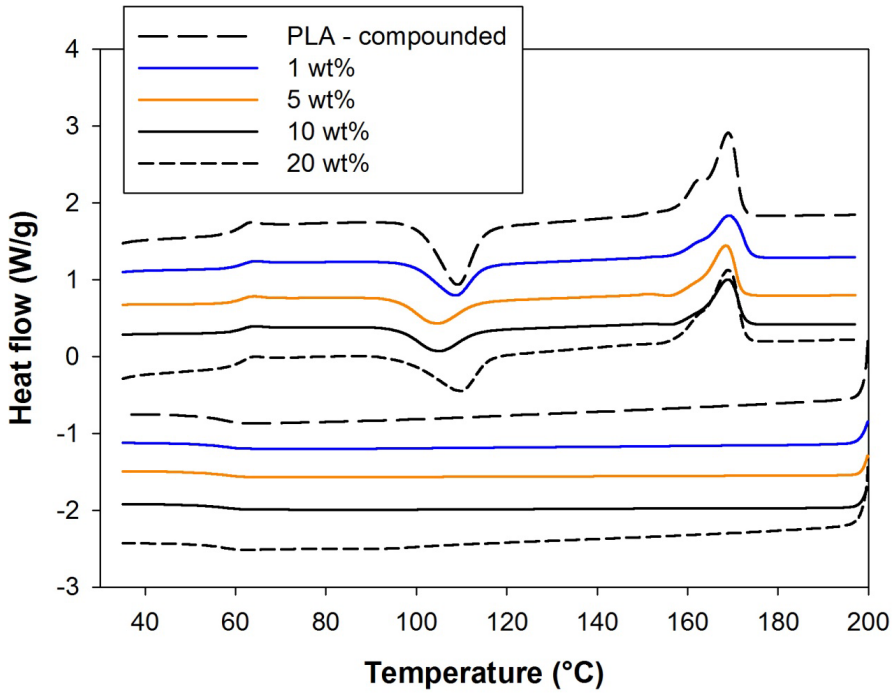

c)

Figure 4.10: DSC thermograms for PLA-based composites, compounded PLA and as-received PLA, cooling rates of: a) 2 °C/min, b) 5 °C/min and c) 10 °C/min.

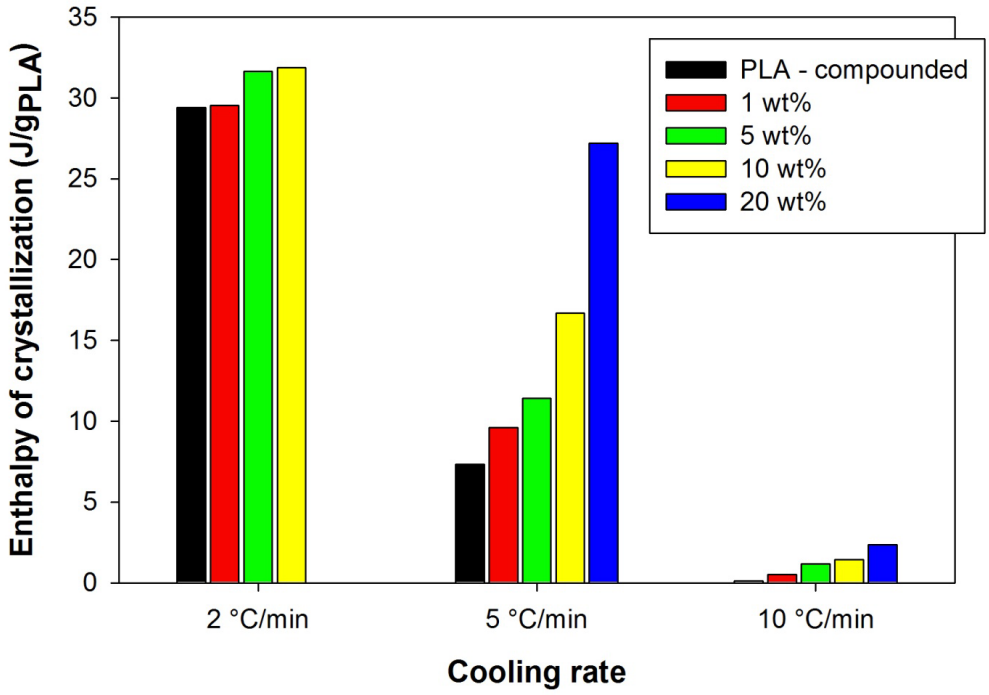

Figure 4.11: Enthalpy of crystallization during cooling for PLA-based composites and compounded PLA.

4.3.5 Thermo-mechanical properties

Figure 4.12 presents the dynamic storage modulus in dual cantilever bending mode, as a function of temperature and for compounded PLA and PLA-flax fiber composites. Maleic anhydride grafted polylactide, PLA-g-MA, was utilized as a compatibilizer in this analysis. The compounded PLA and PLA/PLA-g-MA blend showed a similar behavior: the storage modulus decreased dramatically at temperatures higher than ~ 70 °C, due to the softening of the composite when the glass transition temperature (T_g ~ 60 °C) is exceeded; the modulus started to increase after 100 °C recovering around 15% of the former reduction. This behavior may be explained by the cold crystallization process simultaneously taking place during the test. In fact, the partial organization of the polymer chains due to quiescent crystallization increases the resistance of the material to thermo-mechanical stresses. Similar results have been reported by Oksman et al. for PLA-flax fiber composites [30].

Figure 4.12 shows that the presence of 20 wt% of flax fibers has doubled the storage modulus of PLA at temperatures below ~ 70 °C, indicating the reinforcement effect of this filler. Compounded PLA exhibited a storage modulus of ~ 2200 MPa before softening; this parameter reached ~ 4000 MPa at 20 wt% of fiber content. During the softening process, PLA-flax fiber composites did not exhibit a recovery phenomenon, most probably because the crystallization has been completed upon previous cooling in these samples, due to the nucleating effect of the fibers. In addition, the storage modulus reduction was much smaller than for PLA and the PLA/PLA-g-MA blend above T_g, hence the fibers helped in retaining the mechanical properties at higher temperatures. This improvement is critical since one of the main drawbacks of PLA is its poor temperature resistance.

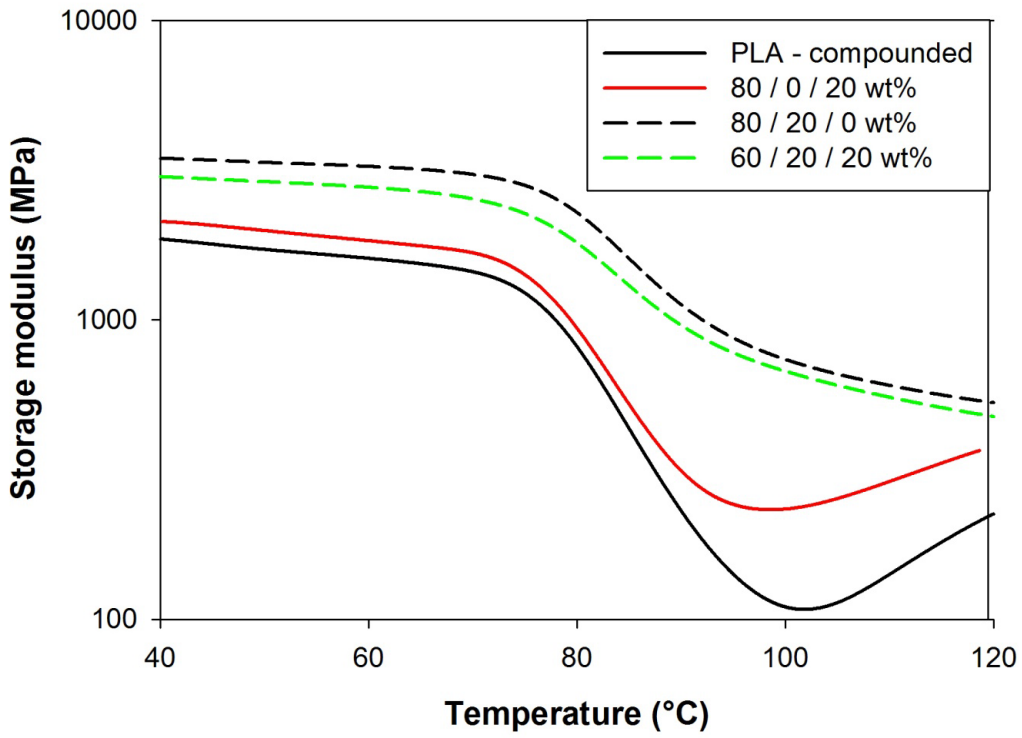

Figure 4.12: DMTA results for various PLA systems. The three numbers in the legend describe wt% of PLA, flax fiber and PLA-g-MA, respectively.

4.3.6 Tensile properties

The mechanical properties of PLA-20 wt% flax fiber composites in tensile testing were characterized and compared with those of the matrix. Three different formulations were compared. Figure 4.13 presents the relative Young modulus, tensile strength and elongation at break of various PLA systems. The relative properties are the composite properties divided by that of the compounded matrix. Compounded PLA had a tensile strength of 53 MPa, a modulus of 3.5 GPa and an elongation at break of 6%.

The addition of 20 wt% of flax fibers increased the Young modulus by approximately 50%, though the use of PLA-g-MA provided a slightly larger increase. The tensile strength is directly related to the ability of the materials to transfer stress from the matrix to the reinforcing fibers [51]. Tensile strength increased by 10% as flax fibers were added. The combination of 20 wt% PLA-g-MA and 20 wt% flax fiber resulted in the highest tensile strength and elastic modulus for all systems. This could suggest that the PLA-g-MA improved the fiber-matrix interfacial interaction. The elongation at break, however, decreased by about 50% for all systems, as

expected from the increased rigidity. Figure 4.13 also shows that the tensile strength of compounded neat PLA was slightly decreased (~ 10%) by the addition of the 20 wt% PLA-g-MA, possibly explained by the lower molecular weight of the PLA-g-MA.

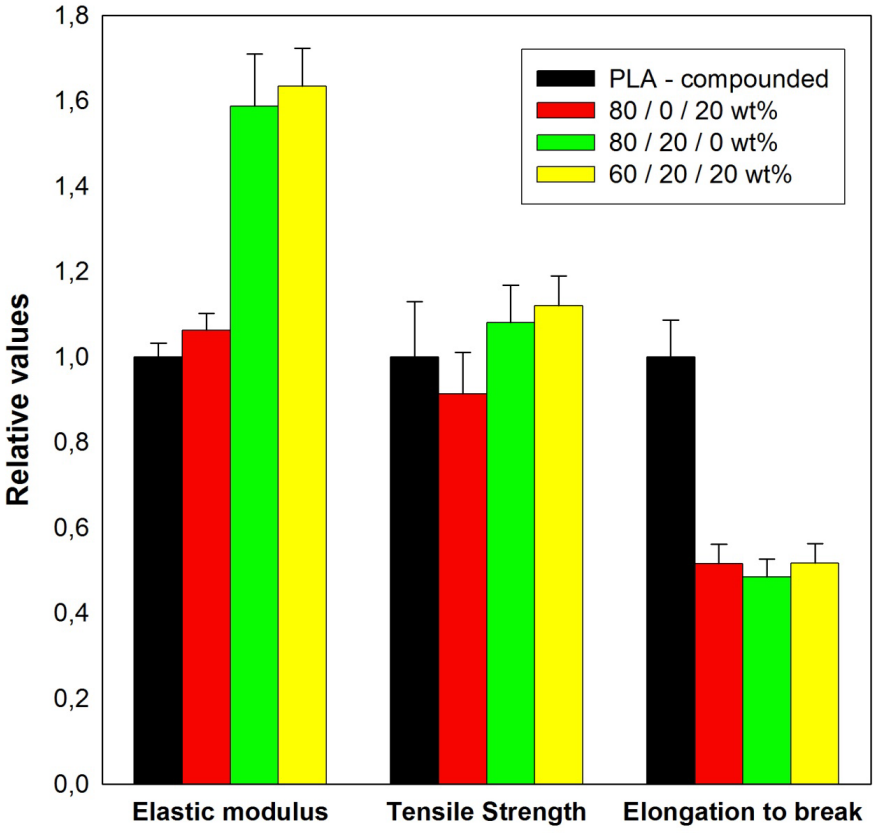

Figure 4.13: Tensile properties of various PLA systems. The three numbers in the legend describes wt% of PLA, flax fiber and PLA-g-MA, respectively.

In order to evaluate the level of reinforcement, an analytical homogenization model has been used to predict the effective reinforcement of randomly oriented fiber reinforced composites. The details of the model can be found in references: [52, 53]. Table 4.2 presents the parameters used for the modeling. The results showed that the theoretical Young modulus for a PLA biocomposite containing 18 vol% of flax fibers is 5.64, so the relative Young modulus is 1.6, which is in fact very close to the experimental value (Fig. 4.13) indicating that flax fiber effectively reinforced the matrix. Figure 4.14 presents an example of discretization of a random composite containing

150 fibers presenting an aspect ratio of 13. The volume fraction is 18% and the grid used was 128 x 128 x 128 voxels.

Table 4.2. Parameters used for modeling the Young modulus of PLA/flax fiber composites.

PLA 4032	Young Modulus (E) (GPa): 3.5 Poisson coefficient: 0.36
Flax fiber	Young Modulus (E) (GPa): 48 Concentration (%v/v): 18 Weighted mean ratio l/d (after compounding): 13 Poisson coefficient: 0.1

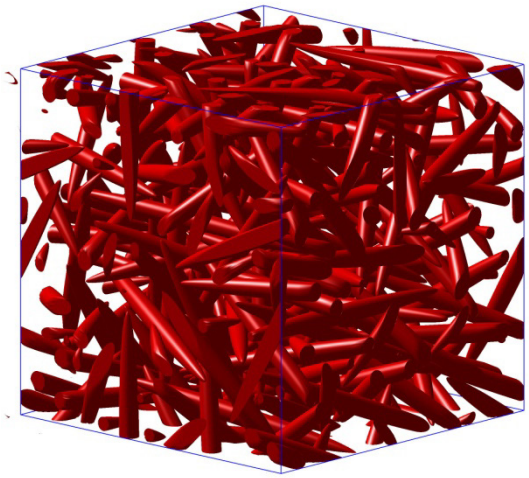

Figure 4.14. Discretization of a random microstructure on a grid of 128 x 128 x 128 voxels. The number of fibers is 150 and the volume fraction is 18%.

4.4 CONCLUSIONS

The goal of this study was to prepare flax-fiber reinforced PLA biocomposites by melt compounding, and to characterize their thermomechanical and crystallization behavior. Main findings can be summarized as follow: the mean flax fiber length was decreased by 75% from its initial length of 1 mm after compounding. In terms of diameter, most fiber bundles were broken up during compounding, with the fiber diameter reaching about 30 μm in the biocomposites, hence slightly larger than for a single fiber. Overall the aspect ratio decreased by about two times after compounding (from ~30 to ~15), and the distribution was much narrower. Rheological characterization showed that the complex viscosity of the composites was thermally unstable,

dropping by ~2% per minute at the highest concentration of fibers (10 wt%). The isothermal crystallization half-time of the composites showed a significant decrease as flax fiber content increased. Non-isothermal crystallization also exhibited an increase in the crystallization rate of biocomposites during cooling, as the flax fiber content increased; however total crystallinity remained nearly constant, around 36%. A significant rise in the Young modulus (~50%) was obtained in the presence of 20 wt% flax fibers, while tensile strength remained approximately constant and a decrease of 50% in the elongation at break was observed. Tensile properties indicate that flax fibers have a significant potential as reinforcement for the PLA matrix, however further investigation is needed to improve stress transfer from the matrix to the fiber during mechanical solicitation. The addition of PLA-g-MA to the composite also affected positively the mechanical performance. The PLA-flax fiber composite system is particularly interesting in a context of reduced environmental impact as it is entirely based on renewable resources, fully biodegradable, while exhibiting good thermomechanical properties.

4.5 ACKNOWLEDGMENTS

The authors gratefully acknowledge the Natural Sciences and Engineering Research Council of Canada (NSERC) for funding. They also thank Gilles Ausias from Laboratoire d'Ingénierie des Matériaux de Bretagne (LIMATB) for providing the flax fibers, and Cristina Kawano for her help with the optical microscopy measurements. Special thanks also go to Prof. Martin Lévesque from École Polytechnique de Montréal for his help for the simulation results.

4.6 REFERENCES

[1] J. K. Pandey, S. H. Ahn, C. S. Lee, A. K. Mohanty, and M. Misra, "Recent Advances in the Application of Natural Fiber Based Composites," *Macromolecular Materials and Engineering,* vol. 295, pp. 975-989, 2010.

[2] A. Bismarck, S. Mishra, and T. Lampke, "Plant Fibers as Reinforcement for Green Composites," in *Natrural Fibers, Biopolymers, and Biocomposites*, A. K. Mohanty, M. Misra, and L. T. Drzal, Eds., ed: CRC Press Taylor & Francis Group, 2005, pp. 37-108.

[3] M. J. John and R. D. Anandjiwala, "Recent Developments in Chemical Modification and Characterization of Natural Fiber-Reinforced Composites," *Polymer Composites,* vol. 29, pp. 187-207, 2008.

[4] X. Li, L. G. Tabil, and S. Panigrahi, "Chemical treatments of natural fiber for use in natural fiber-reinforced composites: A review," *Journal of Polymers and the Environment,* vol. 15, pp. 25-33, Jan 2007.

[5] M. N. G. Belgacem, Alessandro, "Surface Modification of Cellulose Fibres," in *Monomers, Polymers and Composites from Renewable Resources*, É. F. d. P. e. INPG, Ed., ed, 2008, pp. 385-400.

[6] M. Avella, G. Bogoeva-Gaceva, A. Bularovska, M. E. Errico, G. Gentile, and A. Grozdanov, "Poly(lactic acid)-based biocomposites reinforced with kenaf fibers," *Journal of Applied Polymer Science,* vol. 108, pp. 3542-3551, Jun 2008.

[7] D. Bondeson and K. Oksman, "Dispersion and characteristics of surfactant modified cellulose whiskers nanocomposites," *Composite Interfaces,* vol. 14, pp. 617-630, 2007.

[8] D. Garlotta, "A Litterature Review of Poly(Lactic Acid)," *Journal of Polymers and the Environment,* vol. 9, pp. 63-84, April, 2001 2001.

[9] R. Auras, B. Harte, and S. Selke, "An overview of polylactides as packaging materials," *Macromolecular Bioscience,* vol. 4, pp. 835-864, Sep 2004.

[10] H. W. Xiao, P. Li, X. Ren, T. Jiang, and J.-T. Yeh, "Isothermal Crystallization Kinetics and Crystal Structure of Poly(lactic acid): Effect of Triphenyl Phosphate and Talc," *Journal of Applied Polymer Science,* vol. 118, pp. 3558 - 3569, 2010.

[11] G. Perego, G. D. Cella, and C. Bastioli, "Effect of molecular weight and crystallinity on poly(lactic acid) mechanical properties," *Journal of Applied Polymer Science,* vol. 59, pp. 37-43, 1996.

[12] A. M. Harris and E. C. Lee, "Improving mechanical performance of injection molded PLA by controlling crystallinity," *Journal of Applied Polymer Science,* vol. 107, pp. 2246-2255, 2008.

[13] H. B. Li and M. A. Huneault, "Effect of nucleation and plasticization on the crystallization of poly(lactic acid)," *Polymer,* vol. 48, pp. 6855-6866, Nov 2007.

[14] Z. Qiu and Z. Li, "Effect of Orotic Acid on the Crystallization Kinetics and Morphology of Biodegradable Poly(L-lactide) as an Efficient Nucleating Agent," *Industrial & Engineering Chemistry Research,* vol. 50, pp. 12299-12303, 2011.

[15] J. Y. Nam, M. Okamoto, H. Okamoto, M. Nakano, A. Usuki, and M. Matsuda, "Morphology and crystallization kinetics in a mixture of low-molecular weight aliphatic amide and polylactide," *Polymer,* vol. 47, pp. 1340-1347, 2006.

[16] Y. Yuryev, P. Wood-Adams, M.-C. Heuzey, C. Dubois, and J. Brisson, "Crystallization of polylactide films: An atomic force microscopy study of the effects of temperature and blending," *Polymer,* vol. 49, pp. 2306-2320, 2008.

[17] M. L. Di Lorenzo, "Crystallization behavior of poly(L-lactic acid)," *European Polymer Journal,* vol. 41, pp. 569–575, 2005.

[18] J. Y. Nam, S. S. Ray, and M. Okamoto, "Crystallization Behavior and Morphology of Biodegradable Polylactide/Layered Silicate Nanocomposite," *Macromolecules,* vol. 36, pp. 7126–7131, 2003.

[19] H. Tsujia, Y. Tezukaa, S. K. Sahaa, M. Suzuki, and S. Itsunoc, "Spherulite growth of L-lactide copolymers: Effects of tacticity and comonomers," *Polymer,* vol. 46, pp. 4917-4927, 2005.

[20] C. Wang and C.-R. Liu, "Transcrystallization of polypropylene composites: nucleating ability of fibres," *Polymer,* vol. 40, pp. 289-298, 1999.

[21] A. P. Mathew, K. Oksman, and M. Sain, "The effect of morphology and chemical characteristics of cellulose reinforcements on the crystallinity of polylactic acid," *Journal of Applied Polymer Science,* vol. 101, pp. 300-310, 2006.

[22] R. A. Shanks, A. Hodzic, and D. Ridderhof, "Composites of poly(lactic acid) with flax fibers modified by interstitial polymerization," *Journal of Applied Polymer Science,* vol. 101, pp. 3620-3629, Sep 2006.

[23] N. E. Zafeiropoulos, C. A. Baillie, and F. L. Matthews, "A study of transcrystallinity and its effect on the interface in flax fibre reinforced composite materials," *Composites Part a-Applied Science and Manufacturing,* vol. 32, pp. 525-543, 2001.

[24] J. Biagiotti, D. Puglia, L. Torre, J. Kenny, A. Arbelaiz, G. Cantero*, et al.*, "A Systematic Investigation on the Influence of the Chemical Treatment of Natural Fibers on the Properties of Their Polymer Matrix Composites," *Polymer Composites,* vol. 25, pp. 470-479, 2004.

[25] M. Bengtsson, M. L. Baillif, and K. Oksman, "Extrusion and mechanical properties of highly filled cellulose fibre-polypropylene composites," *Composites Part A: Applied Science and Manufacturing,* vol. 38, pp. 1922-1931, 2007.

[26] A. Arbelaiz, B. Fernandez, G. Cantero, R. Llano-Ponte, A. Valea, and I. Mondragon, "Mechanical properties of flax fibre/polypropylene composites. Influence of fibre/matrix modification and glass fibre hybridization," *Composites Part a-Applied Science and Manufacturing,* vol. 36, pp. 1637-1644, 2005.

[27] M. Shibata, K. Ozawa, N. Teramoto, R. Yosomiya, and H. Takeishi, "Biocomposites made from short abaca fiber and biodegradable polyesters," *Macromolecular Materials and Engineering,* vol. 288, pp. 35-43, 2003.

[28] A. K. Bledzki, A. A. Mamun, and O. Faruk, "Abaca fibre reinforced PP composites and comparison with jute and flax fibre PP composites," *Express Polymer Letters,* vol. 1, pp. 755-762, 2007.

[29] A. P. Mathew, K. Oksman, and M. Sain, "Mechanical properties of biodegradable composites from poly lactic acid (PLA) and microcrystalline cellulose (MCC)," *Journal of Applied Polymer Science,* vol. 97, pp. 2014-2025, Sep 2005.

[30] K. Oksman, M. Skrifvars, and J. F. Selin, "Natural fibres as reinforcement in polylactic acid (PLA) composites," *Composites Science and Technology,* vol. 63, pp. 1317-1324, 2003.

[31] B. Bax and J. Mussig, "Impact and tensile properties of PLA/Cordenka and PLA/flax composites," *Composites Science and Technology,* vol. 68, pp. 1601-1607, Jun 2008.

[32] A. Le Duigou, I. Pillin, A. Bourmaud, P. Davies, and C. Baley, "Effect of recycling on mechanical behaviour of biocompostable flax/poly(L-lactide) composites," *Composites Part a-Applied Science and Manufacturing,* vol. 39, pp. 1471-1478, Sep 2008.

[33] E. Bodros, I. Pillin, N. Montrelay, and C. Baley, "Could biopolymers reinforced by randomly scattered flax fibre be used in structural applications?," *Composites Science and Technology,* vol. 67, pp. 462-470, Mar 2007.

[34] C. Baley, "Analysis of the flax fibres tensile behaviour and analysis of the tensile stiffness increase.," *Composites Part a-Applied Science and Manufacturing,* vol. 33, pp. 939-948, 2002.

[35] Y. Nabar, J. M. Raquez, P. Dubois, and R. Narayan, "Production of Starch Foams by Twin-Screw Extrusion: Effect of Maleated Poly(butylene adipate-co-terephthalate) as a Compatibilizer," *Biomacromolecules,* vol. 6, pp. 807-817, 2005.

[36] S. W. Hwang, S. B. Lee, C. K. Lee, J. Y. Lee, J. K. Shim, S. E. M. Selke*, et al.*, "Grafting of maleic anhydride on poly(L-lactic acid). Effects on physical and mechanical properties," *Polymer Testing,* vol. 31, pp. 333-344, 2012.

[37] J. George, E. T. J. Klompen, and T. Peijs, "Thermal degradation of green and upgraded flax fibres," *Advanced Composites Letters,* vol. 10, pp. 81-88, 2001.

[38] M. V. Ramiah, "Thermogravimetric and differential thermal analysis of cellulose, hemicellulose, and lignin," *Journal of Applied Polymer Science,* vol. 14, pp. 1323-1337, 1970.

[39] F. Shafizadeh and A. G. W. Bradbury, "Thermal degradation of cellulose in air and nitrogen at low temperatures," *Journal of Applied Polymer Science,* vol. 23, pp. 1431-1442, 1979.

[40] K. Van de Velde and E. Baetens, "Thermal and mechanical properties of flax fibres as potential composite reinforcement," *Macromolecular Materials and Engineering,* vol. 286, pp. 342-349, 2001.

[41] M. Le Troedec, D. Sedan, C. Peyratout, J. P. Bonnet, A. Smith, R. Guinebretiere*, et al.*, "Influence of various chemical treatments on the composition and structure of hemp fibres," *Composites: Part A Applied Science and Manufacturing,* vol. 39, pp. 514-522, 2008.

[42] K. Oksman, A. P. Mathew, R. Langstrom, B. Nystrom, and K. Joseph, "The influence of fibre microstructure on fibre breakage and mechanical properties of natural fibre reinforced polypropylene," *Composites Science and Technology,* vol. 69, pp. 1847-1853, Sep 2009.

[43] N. M. Barkoula, S. K. Garkhail, and T. Peijs, "Effect of Compounding and Injection Molding on the Mechanical Properties of Flax Fiber Polypropylene Composites," *Journal of Reinforced Plastics and Composites,* vol. 29, pp. 1366 - 1385, 2010.

[44] F. Alloin, D. A. Alessandra, A. Dufresne, N. El Kissi, and F. Bossard, "Poly(oxyethylene) and ramie whiskers based nanocomposites: influence of processing: extrusion and casting/evaporation," *Cellulose,* vol. 18, pp. 957-973, 2011.

[45] K. Madhavan Nampoothiri, N. Rajendran Nair, and R. Pappy John, "An Overview of the Recent Developments in Polylactide (PLA) Research," *Bioresource Technology,* vol. 101, pp. 8493-8501, 2010.

[46] O. Martin and L. Averous, "Poly(lactic acid): plasticization and properties of biodegradable multiphase systems," *Polymer,* vol. 42, pp. 6209-6219, Jun 2001.

[47] L. I. Palade, H. J. Lehermeier, and J. R. Dorgan, "Melt rheology of high L-content poly(lactic acid)," *Macromolecules,* vol. 34, pp. 1384-1390, 2001.

[48] M. Avrami, "Kinetics of Phase Change. I General Theory.," *Journal of Chemical Physics,* vol. 7, pp. 1103-1112, 1939.

[49] E. Hermida and V. Mega, "Transcrystallization kinetics at the poly(3-hydroxybutyrate-co-3-hydroxyvalerate)/hemp fibre interface," *Composites Part A: Applied Science and Manufacturing,* vol. 38, pp. 1387-1394, 2007.

[50] E. W. Fischer, H. J. Sterzel, and G. Wegner, "Investigation of the structure of solution grown crystals of lactide copolymers by means of chemical reactions," *Kolloid-Z. Z. Polym.,* vol. 251, pp. 980-990, 1973.

[51] B. D. Agarwal, L. J. Broutman, and K. Chandrashekhara, *Analysis and performance of fiber composites*, Third Edition ed.: Jhon Wiley & Sons, 2006.

[52] E. Ghossein and M. Lévesque, "A fully automated numerical tool for a comprehensive validation of homogenization models and its application to spherical particles reinforced composites," *International Journal of Solids and Structures,* vol. 49, pp. 1387-1398, 2012.

[53] E. Ghossein and M. Lévesque, "A comprehensive validation of analytical homogenization models: The case of ellipsoidal particles reinforced composites," *Mechanics of Materials,* vol. 75, pp. 135-150, 2014.

CHAPTER 5 ARTICLE 2 – RHEOLOGICAL STUDY OF CRYSTALLIZATION BEHAVIOR OF POLYLACTIDE AND ITS FLAX FIBER COMPOSITES[6]

Andrea Arias[1], Marie-Claude Heuzey[1], Michel A. Huneault[2], Paula Wood-Adams[3]*

1: Chemical Engineering, Research center for high performance polymer and composite systems – CREPEC, Polytechnique Montréal. Montréal, Canada

2: Chemical and Biotechnological Engineering Department, Université de Sherbrooke. Sherbrooke, Canada

3: Department of Mechanical and Industrial Engineering, Research center for high performance polymer and composite systems – CREPEC, Concordia University, Montréal, Canada

** Corresponding author: marie-claude.heuzey@polymtl.ca*

Abstract

In this work, the isothermal crystallization behavior of compounded polylactide (PLA) and polylactide-based flax fiber biocomposites was investigated by means of small amplitude oscillatory shear (SAOS) experiments. The rheological measurements were carried out in the parallel plate flow geometry at temperatures varying from 110 to 140 °C. In addition, the effect of pre-shearing flow on polylactide crystallization was studied by performing a shearing step prior to the SAOS tests that were performed at 140°C. Rheological measurements began one minute after reaching the set crystallization temperature. Time-temperature superposition and Arrhenius equation were used to predict the initial viscosity for all systems, and results were found to be in agreement with experimental values, particularly at lower crystallization rates. A simple empirical model was used to determine the crystallization induction time in a wide range

---

[6] *Submitted to Rheologica Acta journal.*

of supercooling conditions. Experimental issues associated to such studies were raised and key parameters ensuring reproducible and accurate measurements are discussed. The complete understanding of crystallization for PLA systems by means of rheometry for both, quiescent and flow-induced conditions, remains a challenge in the current state of the art.

Keywords: Quiescent crystallization, shear flow-induced crystallization, polylactide, induction time.

5.1 INTRODUCTION

Development of bio-based and biodegradable plastics and composites is a step toward the sustainable development of materials made from natural resources. Polylactide (PLA) has proven to be the most attractive biodegradable polyester due to its large-scale commercial availability and versatility in applications. PLA shows one of the fastest growth rates in the bio-based polymer market. Its commercial production has doubled since 2003 and it is forecasted to triple in the next 10 years [1]. Production of PLA at commercial scale is achieved by ring-opening polymerization of lactide, a dimer of lactic acid which can present three different sterochemical conformations, namely *L*-lactide, *D*-lactide or *meso*-lactide. Commercial PLA grades can be described as copolymers of *L*-lactide with small concentrations of *D*- or *meso*-lactide. At concentration higher than ~10% of *D*-lactide PLA is practically amorphous. The substitution of petroleum-based commodity polymers by PLA is somehow restricted by its slow crystallization, brittleness and low heating resistance in the amorphous state [2, 3]. The addition of nucleating agents accelerates crystallization and, in many cases, improves other properties such as oxygen barrier properties, thermal resistance and impact strength. It has been demonstrated that talc is an effective nucleating agent for PLA by several authors. For example the addition of 6 wt% of talc to PLA results in a reduction of the half-time of crystallization of ~80% at 110 °C, the optimal crystallization temperature [4, 5]. Cellulose fibers are often used as reinforcement for polymers; in addition to the enhancement of mechanical properties, it has been demonstrated that cellulose fibers can act as nucleation agents due to their surface heterogeneity and the release of “fiber particulates” produced by fiber breakage during melt compounding [6-8].

It is well known that quiescent crystallization from the molten state proceeds through a nucleation mechanism, which can be homogeneous, when the nucleus is made of the polymer

itself, or heterogeneous, which occurs when some particles different from the polymer act as nuclei. When the size of nuclei exceeds a critical size, the growth of crystallites becomes energetically favorable and primary crystallization takes place. Several techniques and experimental methods have been developed to study aspects such as induction time, crystallization rate, crystalline size and polymorph structures; differential scanning calorimetry (DSC) and X-ray diffraction (XRD) are among the most widespread techniques. During crystallization, the melt viscosity of the molten polymer is highly affected by the migration of polymer chains from the amorphous to the crystalline phase and by spherulitic growth. Rheometry has been proposed to monitor crystallization dynamics and therefore, several attempts to develop models correlating the transformed fraction of crystalline polymer with the rheological parameters have been reported in the literature. A simple equation assuming direct proportionally between the relative degree of crystallinity and the reduced storage modulus has been applied for polyolefins in a wide range of conditions [9-12]. However, DSC measurements have demonstrated that such proportionality only describes the beginning of the curves for a narrow interval of crystallization temperature:

$$\alpha(t) = \frac{G_t' - G_0'}{G_\infty' - G_0'} \qquad (5.1)$$

where α(t) is the relative degree of crystallinity, and G_0' and G_∞' are the elastic moduli at the beginning and at completion of crystallization. Carrot et al. have studied the isothermal crystallization of high density polyethylene (HDPE) using small amplitude oscillatory shear (SAOS) at 1 rad/s. The reduced storage modulus (*G'*), loss modulus (*G"*) and tangent delta (tan δ) raised to the powers of 1, -1/3 and -1/2 led to a single superposed curve with respect to time for each crystallization temperature. Such a curve was found to correlate with the evolution of the remaining crystallizable fraction obtained from DSC measurements at the same temperature [13]. Acierno et al. have shown that after a careful calibration of temperature sensors of DSC and rheometer equipments, the evolution of crystalline content obtained from both techniques was in a very good agreement. They worked with a copolymer of polypropylene and ethylene-polypropylene rubber phase [14]. The microstructure evolution of poly(1-butylene) at the early

stages of quiescent crystallization has been investigated by Coppola et al., who identified that the liquid-to-solid transition under isothermal conditions happened at surprisingly low degree of crystallinity, e.g. 1 to 1.5%. This finding is somehow contradictory with the assumption that spherulites act as solid particles suspended in the molten polymer and indicates that a more complex viscoelasticity evolution takes place at the very beginning of crystallization [15]. Boutahar et al. compared the dynamic properties of two polyolefins samples presenting very different morphologies during crystallization. The size of crystalline entities was found to control the viscoelastic behavior of the polymer upon crystallization; bigger spherulites sized of about 40 μm observed in the case of polypropylene led to a suspension behavior of spherical particles in a liquid matrix, whereas a colloid behavior was identified for spherulites about 10-20 times smaller, exhibited by high density polyethylene. [11]. Despite the efforts to develop accurate models, a unique expression can hardly take into account all the parameters controlling the evolution of rheological quantities due to crystallization phenomena. According to most of the authors, the mechanism through which the crystalline phase is developed and its effect on the viscoelastic transition requires further investigation; particularly a deep knowledge of the morphology evolution would contribute to a better understanding in this field. In addition, expressions remain specific to the studied polymer and conditions.

Obtaining induction time and kinetics of crystallization from rheological measurements have been reported with very limited success, mainly due (1) to the difficulty of determining a reliable onset of crystallization from rheological curves, and (2) the limited applicability of the equations relating the crystallized fraction and rheological properties such as complex viscosity or storage modulus. Several methods have been proposed for determining induction time from the rheological behavior of a crystallizing polymer. All of them are based on the sudden rise of rheological properties, seen at the early stage of the crystallization phenomenon. A popular approach for determining the crystallization induction time involves the intersection between two tangents from the normalized viscosity ($\eta_{(t)}/\eta_{(0)}$) or storage modulus ($G'_{(t)}/ G'_{(0)}$) [16, 17]. A second approach consists in the definition of the induction time as a specified increase of the complex viscosity. Hadinata et al. and Yu et al. defined the rheological induction time or onset of crystallization as the time at which the viscosity reaches twice the initial melt viscosity value [18, 19]. Recently, a precise determination of induction time was achieved using standardized residuals for quiescent crystallization of PLA. Experiments were carried out in a parallel-plate

flow geometry at temperatures varying from 140 to 155 °C. Induction times determined by rheology and DSC measurements showed close correlation [20].

During processing, molten polymers inevitably undergo strong deformations leading to preferred orientation of macromolecules, reducing the entropy of the system and leading to shear-induced or flow-induced crystallization from the melt [21]. In a general framework, the level of orientation of the macromolecular chains, achieved in the molten state due to flow, constitutes the driving force of this phenomenon. A change in morphology is usually involved, a low level of flow (or orientation) causes the production of oriented spherulites while a higher level of flow leads to fibrillar structures [22, 23]. This phenomenon has been relevant in controlling the microstructure and final properties of semi-crystalline polymers. The most staggering changes are associated with the transition from a relatively isotropic, spherulitic morphology to a highly oriented, shish-kebab morphology. For example, Langouche reported the evolution of the crystalline morphology of isotactic polypropylene (i-PP) subjected to shear rates up to 1000 s^{-1}. Spherulites evolved to uniform aligned and row nucleated lamellae with an average length of ~100 nm [24]. Somani et al. presented an extensive study on the formation mechanism of shish-kebab structures in ultra-high molecular weight polyethylene (UHMWPE) using *in situ* rheo-X-ray and *ex situ* microscopic examinations. They found that long chains are primarily responsible for the formation of the precursor structure under flow. They also identified that at shearing conditions of 60 s^{-1} for 5 s, the critical value for molecular weight of PE above which the level of orientation needed to produce a shish-kebab morphology could be obtained, and is about 250 kg/mol. [25].

A general identification of the different flow regimes associated to specific degrees of ordering of the polymer chains might contribute to the understanding of the physical processes governing flow-induced crystallization. For this purpose, the different flow regimes under which these experiments have been conducted were classified by van Merveeld et al. according to the dimensionless Deborah number, “De”, which is the ratio between the stress relaxation time and the characteristic time of the process. Low-level flow, which is characterized by De < 1-10, is responsible for an enhancement of the spherulitic formation rate. On the other hand, a higher level of flow (De >1-10) brings the development of different morphologies (rods, shish-kebab) [26]. The validity of this classification was confirmed by Zhong et al. working with PLA. They

also verified that, for a given shear rate, there is a critical shearing time above which no further acceleration of the crystallization process is observed [27].

The purpose of the current work is to study the crystallization of PLA and PLA-based natural fiber biocomposites by means of rheometry over a broad range of crystallization temperatures. Quiescent and shear-flow regimes are investigated using the same setup conditions. Such experimental data are rare for PLA in the literature because most crystallization studies are performed with other thermoplastics such as polypropylene, polyethylene and some polymer blends. In addition, the use of rheometry to characterize the crystallization of biocomposites has never been previously reported. This work also represents a validation and extension of the induction time determination technique presented previously [20]. The paper is organized as follows: First, the determination of optimum experimental conditions is described. Second, the time-temperature superposition for rheological properties of PLA and its flax fiber composites is presented. Third, the quiescent crystallization experiments and the calculation of induction times are discussed. Finally, the effect of shear flow on PLA crystallization is examined.

5.2 EXPERIMENTAL

The polylactide grade used in this work was PLA4032D from NatureWorks LCC. This is a semi-crystalline grade containing ~2% of *D*-lactide, its glass transition temperature is ~60 °C and melting point about 165 °C [6]. Previous work have reported a weight average molecular weight of 160 kg/mol as measured by gel permeation chromatography [27]. Flax fibers, cut to a nominal length of 1 mm, were supplied by LIMATB (Brittany, France), additional information concerning thermal stability and size distribution of these fibers is available elsewhere [6].

PLA-flax fiber (5 wt %) biocomposites were prepared through melt-compounding using an internal mixer (C.W. Brabender Plasticorder) under a nitrogen atmosphere. PLA pellets were added first to the chamber and flax fibers were combined subsequently to the molten polymer. The mixing cycle lasted 7 min at 60 rpm and 180 °C. Samples for rheological measurements were prepared by compression molding at the same temperature. A detailed description of the mixing conditions can be found in our previous work [6]. For comparison purposes, as-received PLA was also subjected to the same thermo-mechanical treatment.

The rheological measurements were carried out in a rotational rheometer MCR 301 from Anton-Paar GmbH, using a 25 mm parallel-plate flow geometry. A nitrogen atmosphere was used in all experiments. Quiescent and shear-induced crystallization studies were performed under small amplitude oscillatory shear. Crystallization is a complex phenomenon and rheometry is an unconventional technique for studying it; in order to identify the adequate measurement conditions, preliminary SAOS experiments were carried on PLA at 130 ºC. Shrinkage was encountered in this preliminary phase and it affected the outcome and reproducibility of the rheological tests. Normal force control was found to successfully offset the volume decrease of the sample, and guaranteed reliability of the tests. Several normal force profiles were examined; these results are explained in details in the first section of the paper. For all the SAOS tests, the strain amplitude was set at 1% and an angular frequency of 1 rad/s was used. All systems remained in the linear viscoelastic region in the absence of crystallinity.

Figure 5.1 shows the set of temperature profiles as a function of time for the quiescent (top) and shear-induced (bottom) crystallization experiments. Four crystallization temperatures were selected: 110, 120, 130 and 140 °C. The Peltier system was used as the heating device for all experiments because it can control and stabilize the temperature faster than a convection oven. Samples were molten at 180 °C and kept at this temperature for 3 min in order to erase any previous thermal history. Subsequently, the temperature was dropped at a cooling rate of 30 °C/min, until it reached the set crystallization temperature of the test. One minute of temperature stabilization was imposed before starting the SAOS experiment.

The thermal stability and rheological behavior of PLA and PLA-flax fiber systems were tested at three temperatures above the melting point, i.e. 180, 190 and 200 ºC, using the same rheometer mentioned above. Samples were shown to be nearly thermally stable over the measurement time at these temperatures: for PLA the average decrease was ~0.2% per minute, while the biocomposite presented a higher drop rate of ~1.0% per minute. The overall test duration was 10 min in the case of time sweeps and about 12 min for frequency sweeps.

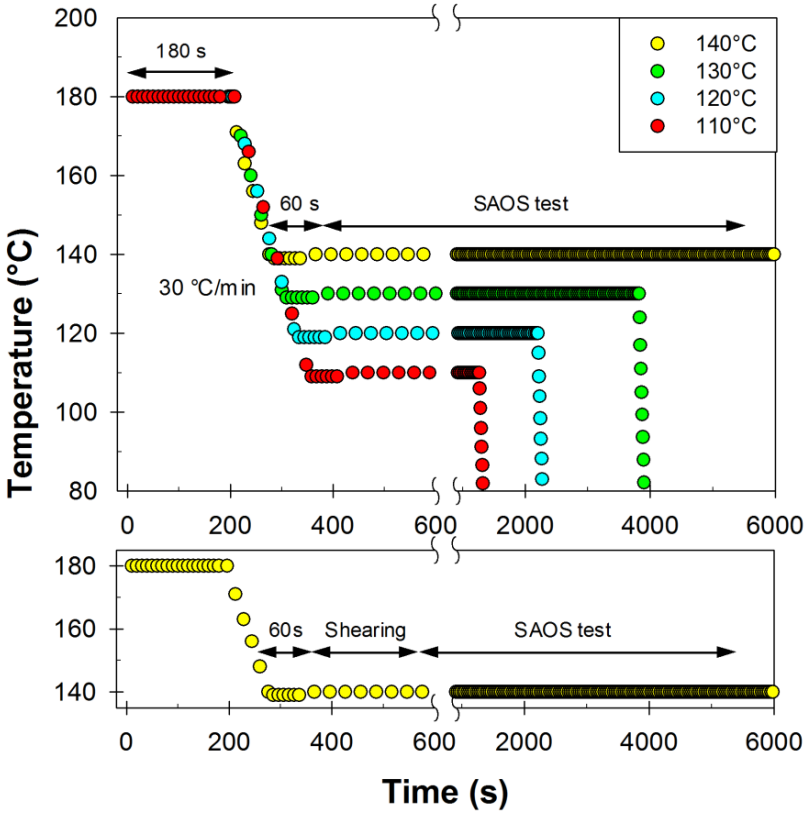

Figure 5.1: Temperature profiles of quiescent and shear flow-induced crystallization experiments.

In the case of shear-induced crystallization, a shearing step was performed prior to the SAOS measurements; all tests were performed at 140 ºC using only the PLA matrix. These tests were not performed with the PLA-flax fiber composites due to additional complication related to flax fiber orientation under flow. Two sets of experiments were considered, namely: (1) constant deformation and (2) constant shearing time. Table 5.1 provides the detailed conditions for both measurement sets.

Table 5.1: Shear rate, shearing time and deformation of shear-induced crystallization experiments.

Shear rate (s^{-1})	Set 1		Set 2	
	Shearing time (s)	**Deformation**	**Shearing time (s)**	**Deformation**
0.5	200	100	120	60
1.0	100	100	120	120
2.0	50	100	120	240
4.0	25	100	120	480

5.3 RESULTS AND DISCUSSION

5.3.1 Preliminary experiments

Shrinkage is a well-known phenomenon during polymer crystallization. Due to the organization of amorphous polymer chains into more compact crystalline structures, the volume of the sample decreases. The densities of purely amorphous and crystalline polylactide have been reported to be 1.25 and 1.36 g/cm^3 respectively; i.e. a reduction of ~8% in polymer volume [28].

Preliminary experiments were performed on PLA at 130 °C to evaluate the effect of shrinkage on the measurements and to determine the best experimental conditions for the following experiments. Three different sets of strain, angular frequency and normal force control for the SAOS measurements were investigated and the response of the storage (*G'*) and loss (*G"*) moduli, as well as the normal force and gap evolution, were monitored as functions of time. Figure 5.2 exhibits the evolution over time of *G'* and *G"*. Figure 5.3 shows the normal force and parallel plate gap for different conditions at a strain amplitude of 1%. The curves of *G'* and *G"* were first obtained without normal force control and at angular frequency ω, of 0.1 rad/s. Measurements were highly unstable and non-reproducible. Selected samples carefully removed from between the parallel plates after these tests revealed voids and a reduction of the sample thickness. These observations evidenced that polylactide shrunk throughout the experiment. A look at the normal force showed negative values from the moment that cooling began (Figure 5.3), indicating the loss of contact between the upper plate and the polymer sample due to volume

reduction. In order to counterbalance the shrinkage during cooling and preserve quiescent conditions, a constant normal force was imposed throughout the experiment still carried out at a frequency of 0.1 rad/s. This second set of conditions improved the stability but somehow still left issues with reproducibility. An increase in frequency from 0.1 to 1 rad/s led to a significant improvement of the stability and reproducibility of all curves, due to the stronger signal recorded by the rheometer as well as the shrinkage compensation. Samples recovered after these tests showed much fewer holes than the previous two sets. To that the measured moduli and complex viscosity were not normal force dependent, similar tests were carried out at initial normal forces of 0.5, 1 or 2N and with normal forces allowed to vary between 1 and 3N during the SAOS experiment. No significant effect of normal force level was found. However, the outcome in normal force was slightly more stable at starting values between 1 and 2N. The profile chosen for all subsequent tests consisted of an initial normal force of 1N, increasing to 2N during the SAOS stage. Some additional experiments were also performed using a rough parallel-plate flow geometry. Curves obtained from rough and smooth plates superposed each other, hence no evidence of slippage due to the sample hardening was encountered.

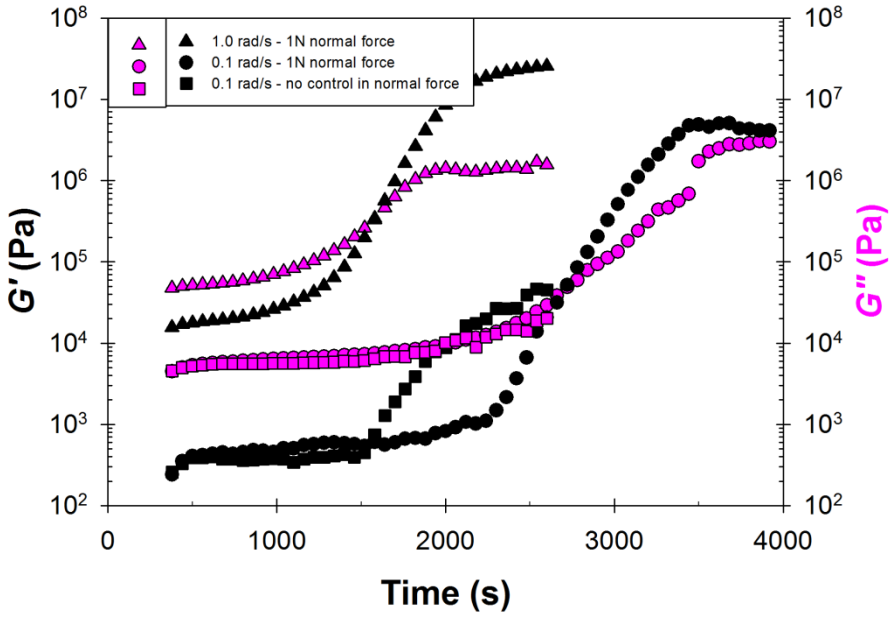

Figure 5.2: Evolution of storage (*G'*) and loss modulus (*G"*) of PLA at 130 °C in different preliminary conditions of normal force and angular frequency.

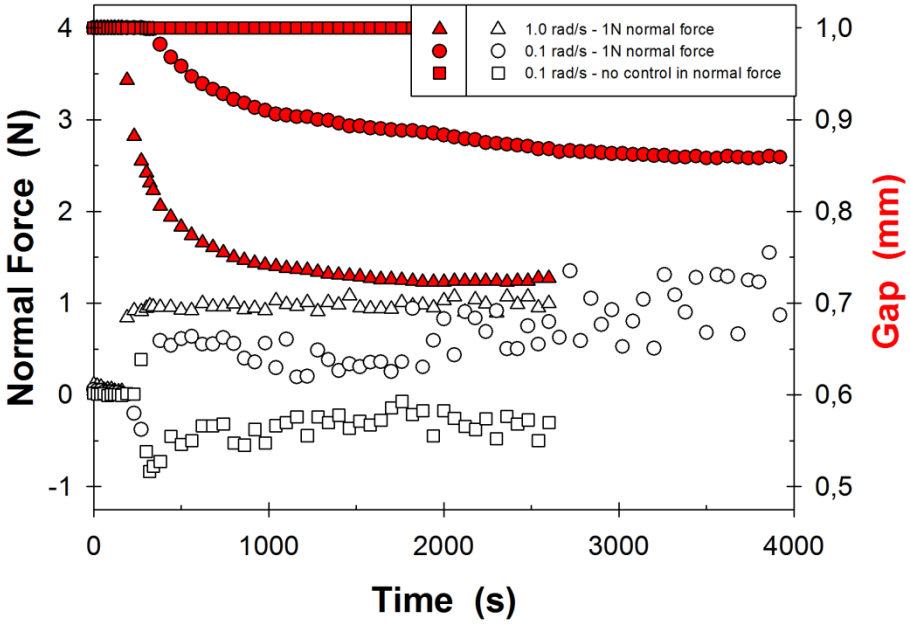

Figure 5.3: Evolution of normal force and gap in parallel plates for PLA at 130 °C, in the same experimental conditions used in Figure 5.2.

5.3.2 Melt rheology

The first minute of the isothermal crystallization tests was dedicated to temperature stabilization and thus no SAOS measurements were taken during that time lapse. This might be problematic at lower crystallization temperatures, close to the optimal PLA crystallization temperature of 105-110°C [6], since some crystallization may be initiated before the SAOS measurement during stabilization or even the cooling step. The half-time of crystallization of PLA at 110 °C measured by DSC has been reported to be ~4 min [6]. To make up for this loss of information, time-temperature superposition was used for estimating the initial complex viscosity of the investigated systems.

The dynamic properties as a function of angular frequency at 180, 190 and 200 °C were investigated for both systems. PLA and PLA-flax fiber composite exhibited a plateau complex viscosity at lower frequencies, followed by a shear-thinning behavior as frequency increased. At 180 °C, PLA exhibited a zero shear viscosity of about 3300 Pa.s. This value decreased by ~30% at 190 ºC and reached ~1400 Pa.s at 200 ºC, for a total reduction close to 60%. In the case of the

flax fiber composites, the zero shear viscosity at 180 ºC was ~4100 Pa.s, decreasing by ~40% at 190 °C and also by about 60% at 200 °C. The zero shear viscosity at this temperature was close to 1700 Pa.s. The complex viscosity of both systems at 180 °C was in the same range than in our previous work [6].

Storage and loss modulus of PLA are shown in Figure 5.4. They present the typical liquid-like behavior of molten polymers. The slopes of the terminal zones of the *G'* and *G"* curves are ~1.7 and 1.0, respectively. These values are in the same range as those reported for molten PLA at temperatures varying from 175 to 205 °C [29]. The deviation from the characteristic homopolymer-like behavior in the terminal zone, which is characterized by slopes of 2 and 1 for *G'* and *G"*, respectively, was more pronounced for the *G'* curve of the composite (results not shown). It presented a slope of ~1.45; however in the case of *G"*, the slope was ~0.98, hence close to 1. In the case of *G',* lower frequencies would be required to observe the typical terminal behavior, however these tests would take a longer time that would be unfavorable in terms of PLA degradation.

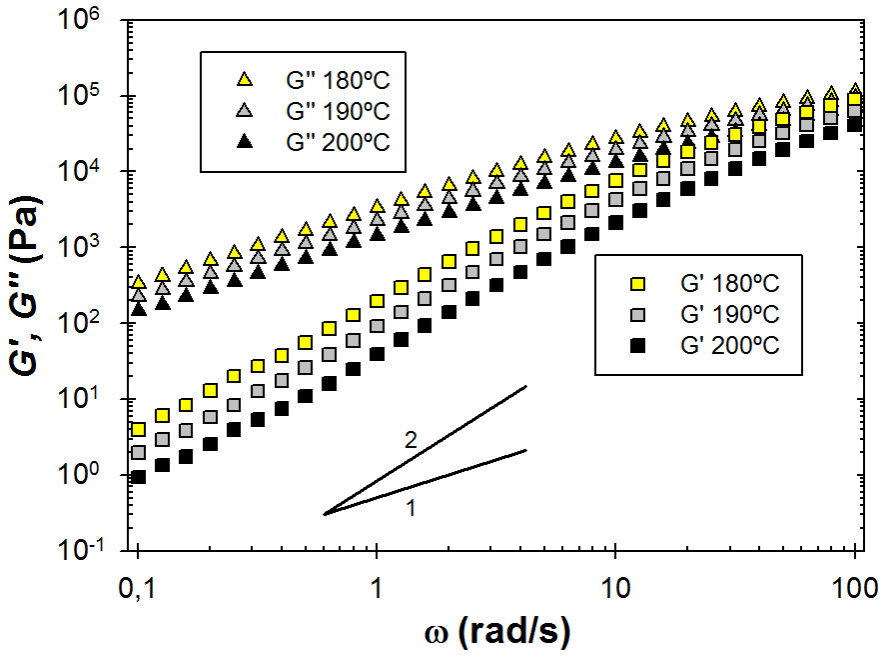

Figure 5.4: Storage (G') and loss modulus (G") as functions of angular frequency for PLA at 180, 190 and 200 °C.

For a thermorheologically simple material, all contributing retardation or relaxation mechanisms exhibit the same temperature dependence (Eq. 5.2). The double-logarithmic plot of viscoelastic functions versus time or angular frequency at different temperatures can be superposed on the same mastercurve by horizontal shifting by a constant distance identified as log a_T, and vertically by another constant identified as b_T (Eq. 5.3-5.4).

$$\lambda_i(T) = a_T\lambda_i(T_0) \qquad (5.2)$$

$$b_T G'(T, a_T\omega) = G'(T_0,\omega) \qquad (5.3)$$

$$b_T = T_0\rho_0/T\rho \qquad (5.4)$$

Considering that the melt rheological studies were performed in a narrow temperature interval ($T_0/T \cong 1.1$) and that changes in density are insignificant, the vertical shift factor, defined by Eq. 5.4, was considered equal to 1 in this study.

The horizontal shift factor has been determined using a trial and error graphic method. The curves of the complex modulus (G^*), which take into account the contribution of the storage and loss moduli (Eq. 5.5), were shifted using different values of a_T until they superposed the G^* curve at the reference temperature T_0 (200 °C). Since the SAOS experiments for crystallization at T_c were carried out at 1 rad/s, the success of the superposition method was ensured in the low frequency region. Figure 5.5 presents the master curve of the absolute value of the complex viscosity of PLA (top) and its composite (bottom). PLA showed perfectly superposed curves all over the angular frequency range, confirming its thermorheological simplicity. In the case of the 5 wt% flax fiber composite, a slight deviation from superposition was identified at $a_T\omega$ higher than 10 rad/s. This might be an artefact caused by the thermal degradation of the biocomposite, which is more important at higher temperatures.

$$|G^*| = [(G')^2 + (G'')^2]^{1/2} \qquad (5.5)$$

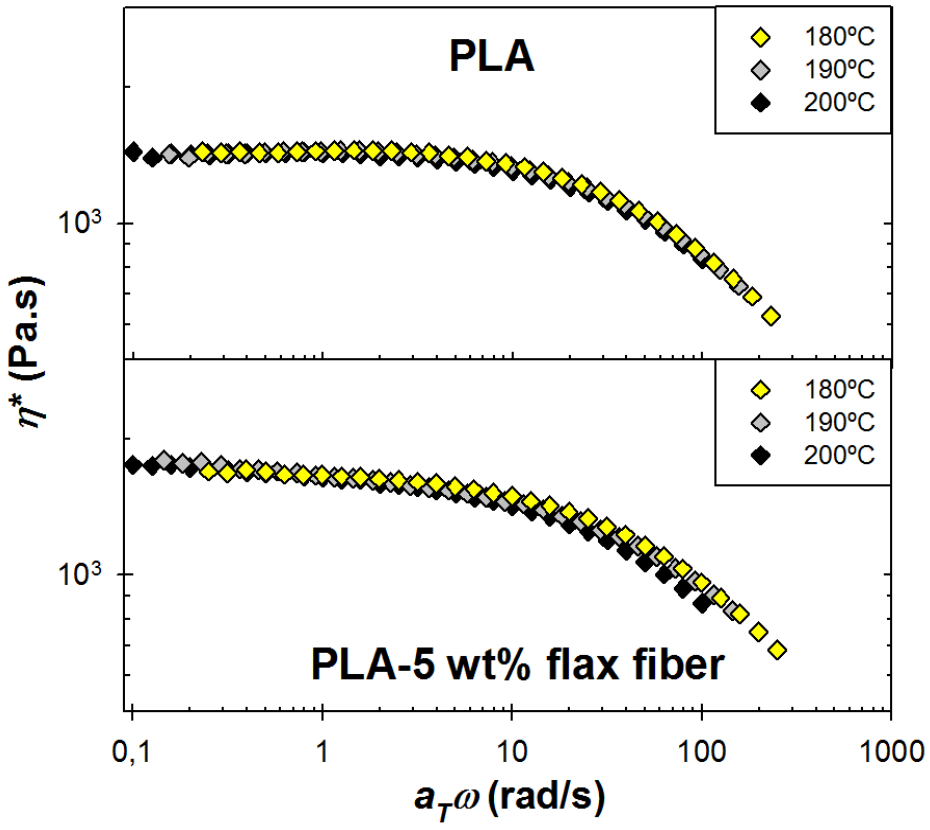

Figure 5.5: Master curves of the complex viscosity of PLA (top) and PLA-5 wt% flax fiber composite (bottom).

The dependence of a_T on temperature is usually fitted by two well-known empirical relationships. The Arrhenius equation (Eq. 5.6) has been found to fit well the data of linear polymers for temperatures at least 100 K above T_g. The constant E_a is the flow activation energy. On the other hand, the WLF (Williams, Landel, Ferry) equation offers reliable predictions for homopolymers at temperatures at most 100K above T_g.

$$a_T(T) = e^{\left[E_a/R(1/T - 1/T_0)\right]} \qquad (5.6)$$

Table 5.2 shows the values of a_T and E_a for both systems. The Arrhenius equation was found to fit the data with a high coefficient of determination (R^2), especially for neat PLA. Initial complex viscosity predictions at crystallization temperatures are displayed in Table 5.3. Despite the fact that the experiments were performed for temperatures considerably lower than the melting point, it will be shown in the next section that the predictions are highly accurate. This is important to provide a reliable value of the complex viscosity at the starting point of crystallization.

Table 5.2: Arrhenius fits for PLA and PLA-5 wt% flax fiber composite.

T (°C)	**PLA**	**PLA-5 wt%**
aT, 200°C	1.00	1.00
aT, 190°C	1.55	1.45
aT, 180°C	2.30	2.50
E_a (kJ/mol)	74.2	81.8
R^2	0.9982	0.9831

Table 5.3: Prediction of initial complex viscosity at crystallization temperatures for PLA and PLA-5 wt% flax fiber biocomposite.

T (°C)	140	130	120	110
η^*_{PLA} **(kPa.s)**	22,1	37,8	66,4	120
$\eta^*_{PLA\text{-}5\ wt\%}$ **(kPa.s)**	33,6	60,7	113	217

Regarding the flow activation energy of PLA, a wide range of values from about 40 to 180 kJ/mol is reported in the literature; molecular weight and stereochemical structure seem to have the most important effects on this parameter. For example, it has been reported that *L*-PLA and *D,L*-PLA with similar mass average molecular weight (M_w) showed E_a values of ~160 and ~120 kJ/mol, respectively. Wang et al. reported an E_a value of ~45 kJ/mol for commercial grades of PLA having M_w in the range of 100 kg/mol. In other study, PLA of M_w = 180 kg/mol and a polydispersity index of 1.7 exhibited a value 110 kJ/mol for the same parameter [30-32]. A recent investigation reported a E_a value of 80 kJ/mol for the PLA grade used in the present work. Our

estimation of E_a was particularly close (74 kJ/mol) to their result, indicating that our measurements are reasonable [27].

5.3.3 Quiescent crystallization

Quiescent crystallization experiments at 140, 130, 120 and 110 °C were carried out using the optimized conditions described previously. The rheological monitoring of crystallization requires the simultaneous examination of several variables. Beyond G', G'' and η^*, the shrinking and hardening of the sample as the test evolves requires the monitoring of the normal force, the torque and the gap. Figure 5.6 presents the complex viscosity, normal force and gap profiles as a function of time during the isothermal crystallization of PLA at 130 °C. The complex viscosity curve exhibited a sigmoidal shape very similar to the characteristic curves describing the degree of crystallinity of a polymer as a function of time. The normal force varied between 1 and 2N as the test progresses, following more or less a linear dependency. The torque remained low for the first half of the test; then it showed a sharp increase up to the rheometer limit (~200 mNm). At this point the rheological properties were not considered reliable anymore and in the following figures the rheological data were truncated at this point. As mentioned previously, the gap decreased (by ~25%) as a consequence of the normal force control. This reduction allows the equipment to compensate for sample shrinkage and keeps the normal force nearly constant. In the first 500 s of the experiment, the gap shows a marked drop of about 20%; afterwards, it decreased more slowly. It is worth mentioning that as the maximum torque is reached, the gap also becomes constant.

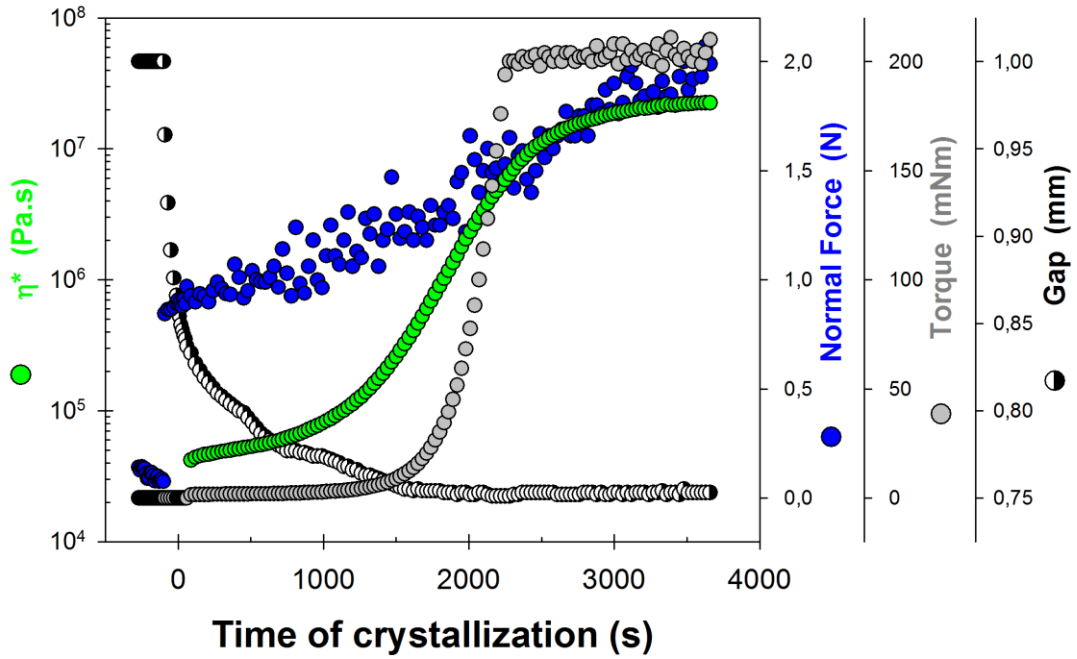

Figure 5.6: Evolution of complex viscosity of PLA at 130 °C. Right axes present the profiles of the normal force, torque and gap during the same experiment.

Trends observed in Figure 5.6 were representative of all experiments in the T_c interval explored in this study. Naturally, as temperature was decreased, crystallization occured faster, and then the duration of the test was reduced.

The evolution of the complex viscosity for both systems at all crystallization temperatures is shown in Figure 5.7. At 140 °C, the initial viscosity of PLA was ~23 kPa.s, which increased to ~42, ~115 and ~236 kPa.s as T_c decreased. These values were considerably higher in the case of the composite which exhibited viscosities of ~33, ~60, ~140 and ~317 kPa.s, respectively. PLA at 120 °C exhibited a short initial pseudo plateau which disappeared at 110 °C. The sigmoidal shape became sharper as temperature decreased probably due to crystallization initiation prior to SAOS measurements. At 140 °C, PLA crystallized extremely slowly and the test lasted for about 10 000 s. Regarding the composite, the faster evolution of the curves confirmed the crystallization rate increase due to the nucleation effect of the fibers. The plateau at the beginning of the experiments disappeared at all temperatures in the case of the composite. The effect of fiber on the complex viscosity is most evident at 140 °C. The maximum value of the complex

viscosity considered reliable was about the same for both systems at all temperatures, i.e. ~10^4 kPa.s. At that point, values were measured at a torque value close to the instrument limit.

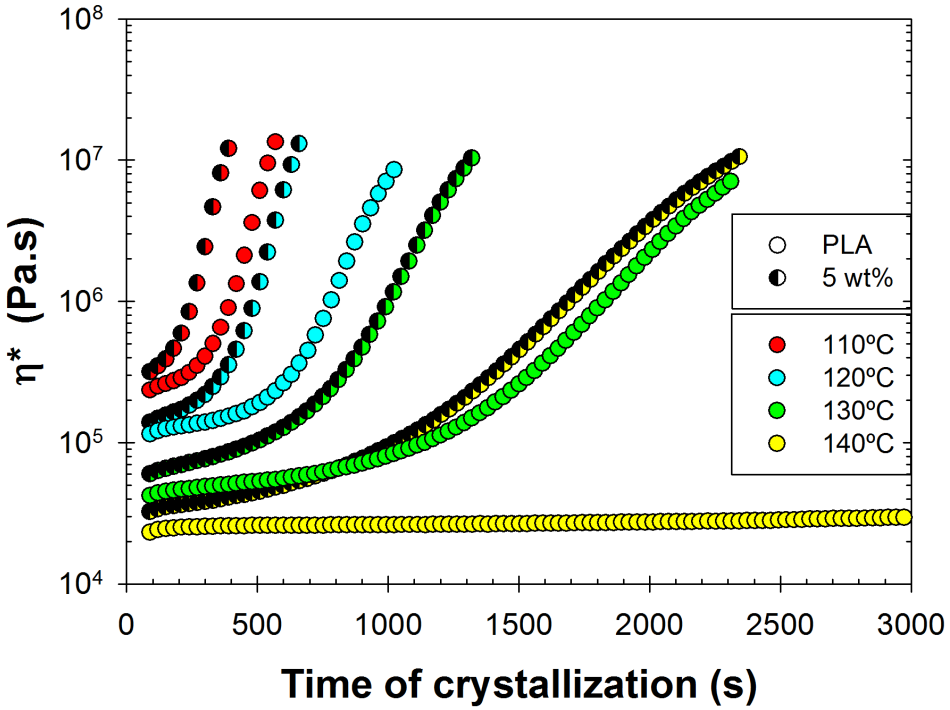

Figure 5.7: Evolution of complex viscosity at different crystallization temperatures for PLA and PLA-5 wt% flax fiber composite.

Figure 5.8 shows the predicted complex viscosity using the Arrhenius equation as a function of the experimental viscosity at a crystallization time of 90 s (the first measurement point of the rheometer). The predictions at 140 and 130 °C were in close agreement with the experimental data, both for PLA and for the PLA-based composites. At lower temperatures, i.e. 120 and 110 °C, a marked and increasing difference from the experimental values was observed. This fact strongly indicates that the nucleation and crystallization processes have already started when the first measurements of the complex viscosity were taken.

The time of crystallization was set to zero when T_c was reached upon cooling, i.e. when the stabilization temperature step started; this criterion was applied in all the following figures. From high to low temperatures, the duration of the test (from time zero up to maximum torque) was ~10 000, ~2 500, ~1 000 and ~600 s for PLA and, ~2 350, ~1 300, ~650 and ~400 s for the composites. Considering the PLA matrix as a reference point, this represented a reduction of 76, 43, 35 and 30% in the duration of the crystallization test due to the presence of 5 wt% of flax fibers.

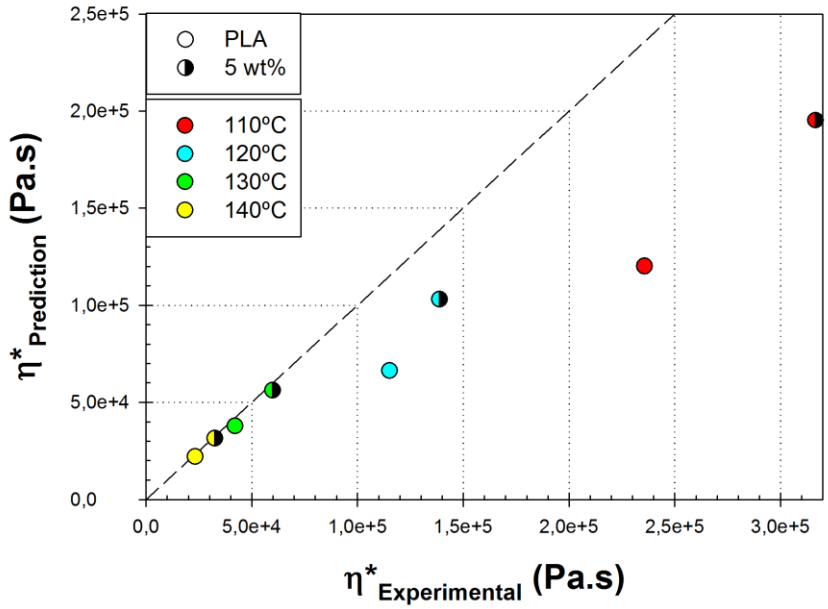

Figure 5.8: Comparison of complex viscosity predicted by the Arrhenius equation and initial complex viscosity from experiments (former curves of Fig. 5.7).

The induction time is an important parameter of the crystallization process. It represents the time necessary for the development of the nuclei before the crystallite growth begins. Despite the attempts done for relating crystallization rate and rheological functions, the challenge remains. Most of the methods reported in the literature are specific to the studied systems and, somehow, arbitrary. In the present study, we applied a method based on the standardized residuals technique (Eq. 5.7), which has been reported to effectively determine the induction time of homogeneous crystallization of PLA at low rates of crystallization [20]. In Eq. 5.7, e_i is the real residual and the

divider is the standard deviation of residuals. In this study, residuals were calculated as the difference between the measured complex viscosity and the prediction using the Arrhenius equation (Fig. 5.8). It was found that standardized residuals were a useful technique to determine the induction time due to the fact that they magnify the deviation of the experimental data with respect to the predicted value.

$$r_i = \frac{e_i}{\sqrt{\sigma^2}} = \frac{e_i}{\sqrt{\frac{1}{n-1}\sum_{i=1}^{i=n}(e_i - e)^2}} \qquad (5.7)$$

Standardized residuals of all systems are presented in Figure 5.9. Their initial values were close to zero for a certain time, after which a sharp rise was observed. The standardized residual took longer times to reach that sharp increase as the crystallization temperature was increased. In order to determine the induction time of crystallization, it was observed that a straight line could be drawn at the very early stage of crystallization. The time at which the curves diverge from this straight line was designated as the induction time. Figure 5.10 shows the graphical representation of the method described above and the results are plotted in Figure 5.11.

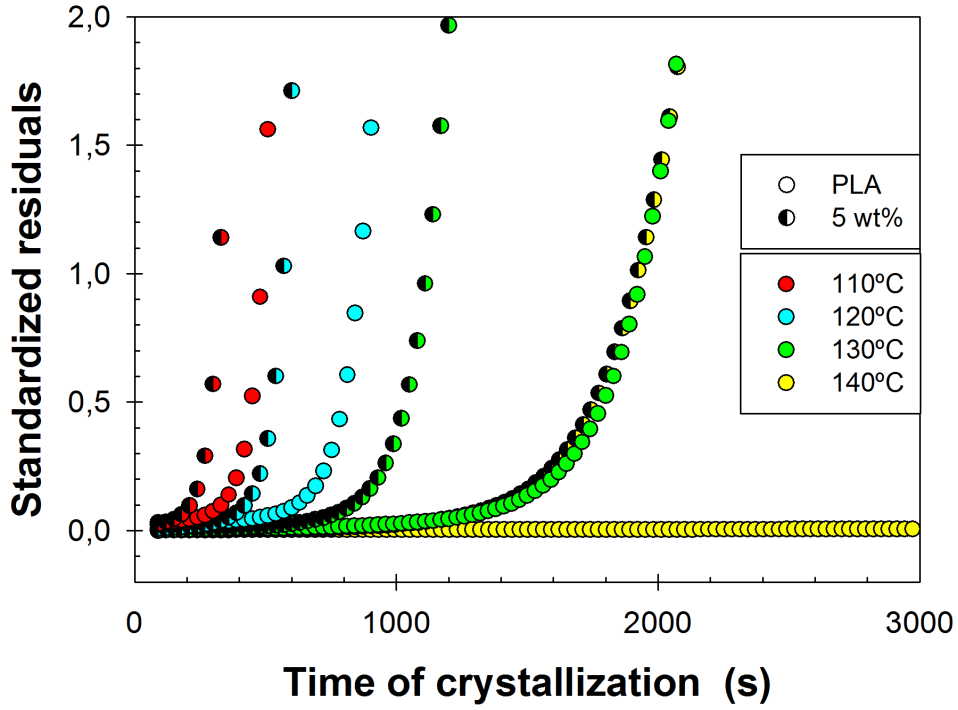

Figure 5.9: Standardized residuals of complex viscosity for PLA and PLA-5 wt% flax fiber composites at different crystallization temperatures.

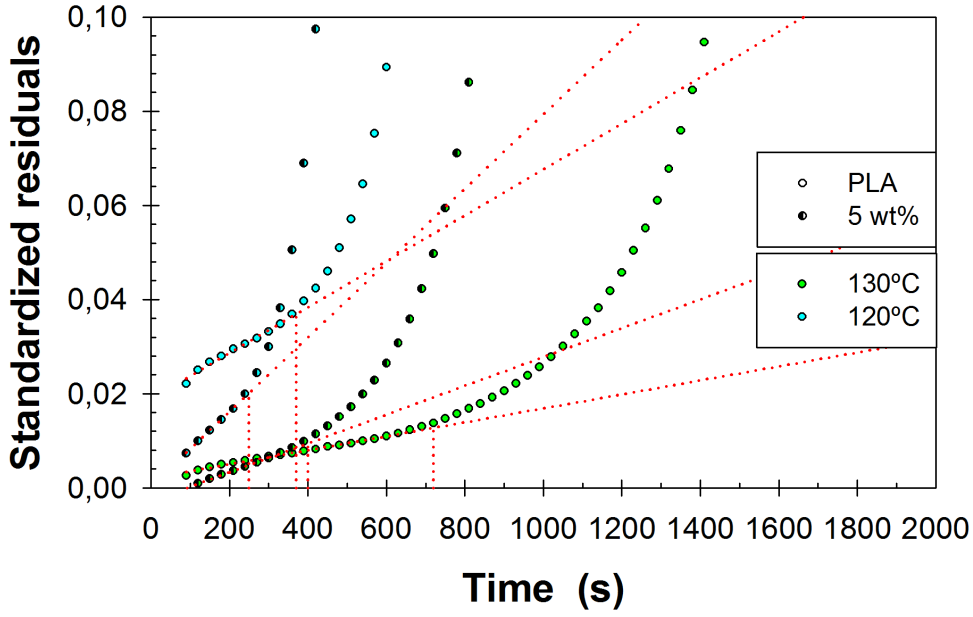

Figure 5.10: Determination of induction time of crystallization based on standardized residuals for PLA and PLA-5 wt% flax fiber composites at 120 and 130 °C.

The induction times of PLA increased with temperature presenting values of about 200 s at 110 ºC and about 2 300 s at 140 °C. The flax composite exhibited a linear relation between induction time and temperature. It also showed lower induction times than pure PLA, with a more significant difference at higher temperatures. For example, the induction time at 140 °C was close to 600 s, which represents only 25% of the value obtained for the neat matrix.

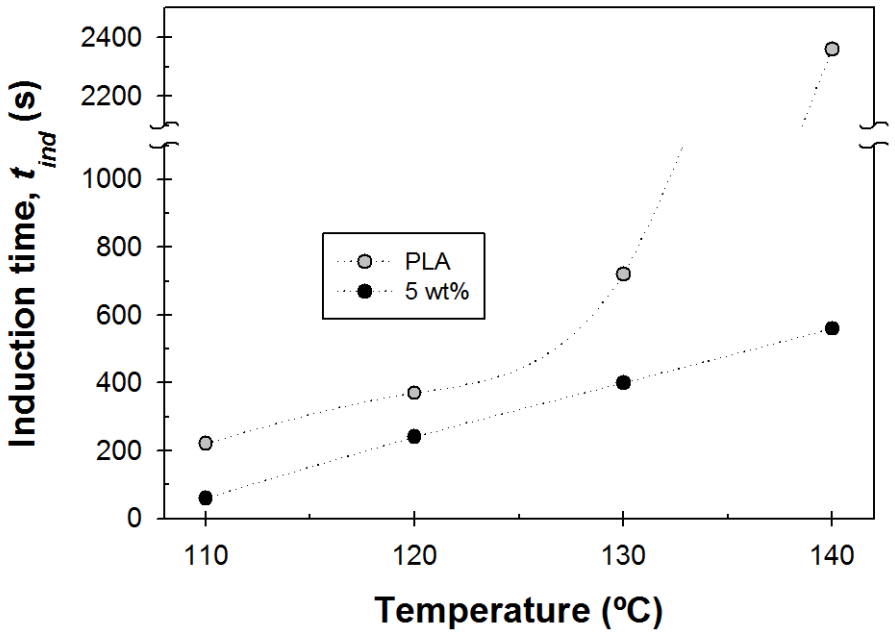

Figure 5.11: Induction time of crystallization based on standardized residuals for PLA and PLA-5 wt% flax fiber composite, at temperatures varying from 110 to 140 °C.

Table 5.4: Estimation of induction and half crystallization times for all systems

T (ºC)	t_{ind} (s) PLA	$t_{½}$ (s) PLA	t_{ind} (s) 5wt%	$t_{½}$ (s) 5wt%
110	220	260	< 60	210
120	370	700	240	670
130	720	1900	400	1280
140	2360	-	560	-

The crystallization half-time ($t_{½}$) of PLA and its composites has been reported in our previous work from differential scanning calorimetry (DSC) measurements [6]. It is clear that $t_{½}$ and t_{ind}

represent measurements at different stages of the crystallization process. The first depicts the time at which the relative degree of crystallization reaches 50%, meanwhile the second gives the time necessary for the nuclei formation. Nevertheless, a simple comparison of these values (Table 5.4) can provide an idea of the accuracy of the t_{ind} estimation using the standardized residual methods. For example, t_{ind} and $t_{½}$ for the PLA matrix at 110 °C were very similar, indicating that the t_{ind} was overestimated. At 120 °C the difference between these parameters increases and the t_{ind} was equivalent to 50% of the half-time, which probably indicates some level of overestimation since we expect the t_{ind} to be much smaller than the $t_{½}$. However, at 130 °C the gap between these two parameters became considerably important and at 140 °C, our estimation of t_{ind} for PLA was in very close agreement with the value reported by Yuryev et al., who have used a similar procedure for measuring the crystallization of PLA at temperatures between 140 and 155 °C. We believe that rheometry is an accurate technique for analyzing the crystallization behavior of polymers in a temperature range which presents low to very low crystallization rates, which is the case of PLA at T ≥ 130 °C. However, at high crystallization rates, the nucleation process takes place in a very short time, resulting in a fast development of crystallites, i.e. a rapid increase of the viscosity at the very beginning of the crystallization. It then becomes difficult to achieve accurate rheological measurements at this primary stage of crystallization, mostly due to the fact that samples for rheological experiments are about 50 times larger than DSC samples, leading to longer times for temperature stabilization.

5.3.4 Shear-induced crystallization

The effect of flow on the crystallization of PLA was also evaluated in this work using two different sets of shear conditions (Table 5.1). In the first set, the shearing time was adjusted to keep constant the total applied deformation at a value of 100 shear units. The second set was designed with the same shear rate interval but shearing time instead of deformation was kept constant. The gradual increase of the subsequently measured complex viscosity as a function of time for both sets of conditions is presented in Figures 5.12 and 5.13, respectively.

In general words, all curves plotted in Figures 5.12 and 5.13 exhibited a sigmoidal shape similar to those obtained under quiescent conditions. The increase in shear rate increased the crystallization rate of PLA, whether the parameter kept constant was the deformation or the shearing time, i.e. at higher shear rates the complex viscosity grew faster in both sets of shear

conditions. It is interesting to compare the evolution of complex viscosity after different shearing times for a constant value of shear rate (Fig. 5.13). At a constant shear rate, we expect a greater shearing time to result in a larger increase in crystallization rate. This kind of behavior was observed at shear rates of 0.5 and 1.0 s^{-1}. For 0.5 s^{-1}, crystallization after 200 s (Fig. 5.12) of shearing occurred faster than the one observed after 120 s of shearing (Fig.5.13). Similarly for 1 s^{-1}, crystallization after 120 s occurred faster than after the 100 s of shearing. Such behaviour confirms that the total deformation applied to the system is one of the parameters controlling the shear-flow induced crystallization phenomena (Fig. 5.13).

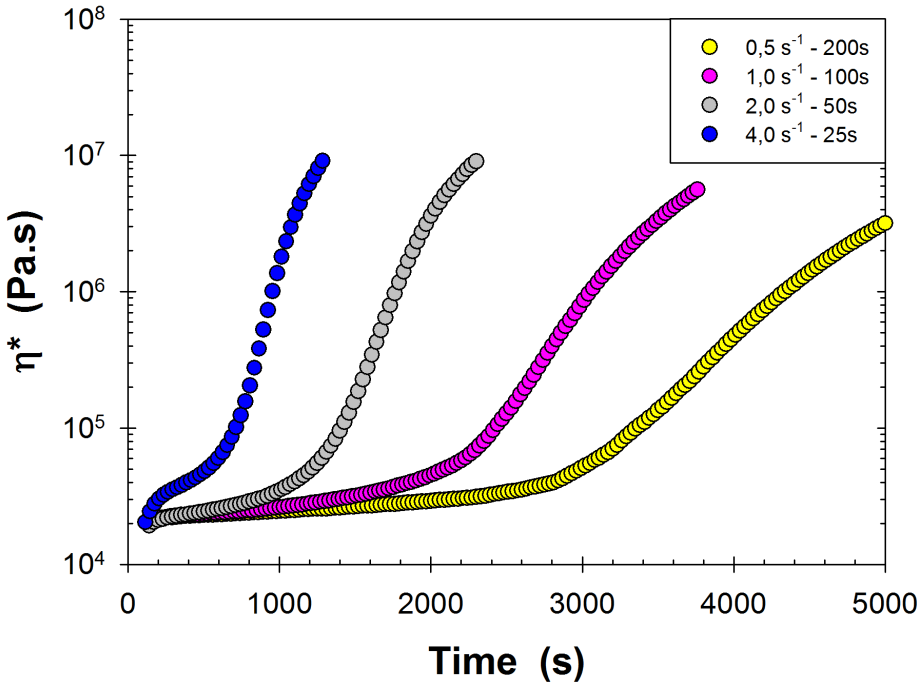

Figure 5.12: Evolution of complex viscosity of PLA at 140 °C for the set of conditions No.1 The deformation was constant in all cases.

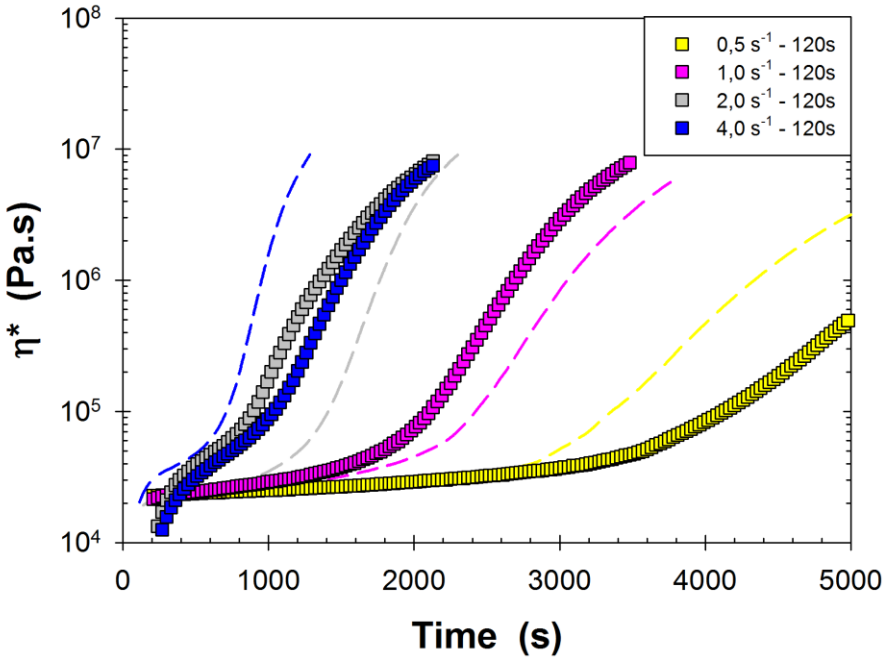

Figure 5.13: Evolution of complex viscosity of PLA at 140 °C for the set of conditions No. 2. The shearing time was constant in all cases. The dashed lines represent the former curves (Fig. 5.12).

At higher shear rates, i.e. 2.0 and 4.0 s^{-1} and constant shearing time, the resulting curves exhibited a modified shape for the first half of the experiment. Instead of a pseudo-plateau, the curves described two successive sharp increases; the first less intense than the second one. To our knowledge, this kind of shape of curves has not been reported in previous work related to flow-induced crystallization of polymers. We believe this behavior is related to a morphology transition, perhaps from unaligned spherulites to aligned spherulites, or from aligned spherulites to row nucleated lamellae. Further experimentation will be needed to clarify these specific results.

The investigations of flow-induced crystallization rarely correlate the morphological transitions undergone by the polymer with the evolution of rheological quantities. However, the identification of shearing conditions giving place to different morphology regimes has been achieved. For example, the effect of applied shear at 2.2 s^{-1} on the morphology of *i*-PP at 140 °C was substantial at shearing times higher than 30 s, when oriented crystals like cylinders and

strings of spherulites started to appear. Aligned structures were identified at a shearing time of 90 s [33]. Li et al. studied the morphology of PLLA under non-isothermal conditions at shear rates of 4, 5 and 6 s-1, the shearing time was kept at 60 s in all cases. At 5 s^{-1}, the intensity of shear led to the development of oriented nuclei which grew into cylindrical-like structures. The size and number of such structures was promoted by lowering the cooling rate of the experiments [34]. It was demonstrated that lower shear rates and longer shearing times, e.g. 1 s^{-1} during 480 s promoted the formation of similar cylindrical structures at T_c above 120 °C upon isothermal conditions [35]. Recently, Zhong et al. explored several shearing times in the range of 1 to 40 s at three different shear rates (1, 5, 10 s^{-1}) for a commercial grade of PLA. Despite the enhancement on nucleation density and crystallization rate, the morphological studies did not show the rod-like crystallites [27]. Taking into account the discussion above, it is clear that the shear flow conditions explored in the current study can alter the typical spherulitic structure developed under quiescent crystallization.

The determination of induction time for shear flow-induced crystallization followed the procedure based on the standardized residuals explained in the previous section (residuals are not shown for shear-induced crystallization experiments). Figure 5.14 shows t_{ind} as a function of shear rate, and compares the results between the two sets of conditions: (1) constant deformation and (2) constant shearing time. In both cases, t_{ind} decreases exponentially as shear rate increases. However, in the second case (constant shearing time), t_{ind} seems to reach a plateau value at shear rate of 2 s^{-1} or higher. It is worthy to note that the complex viscosity curves following shearing at 2 and 4 s-1 for 120 s are nearly superposed (Fig. 5.13); this indicates that the magnitude of impact on the nucleation is similar in both cases, although the deformation is different. We also note that the results obtained here are quite useful since no other report in the current literature is available for flow induced crystallization of this polymer.

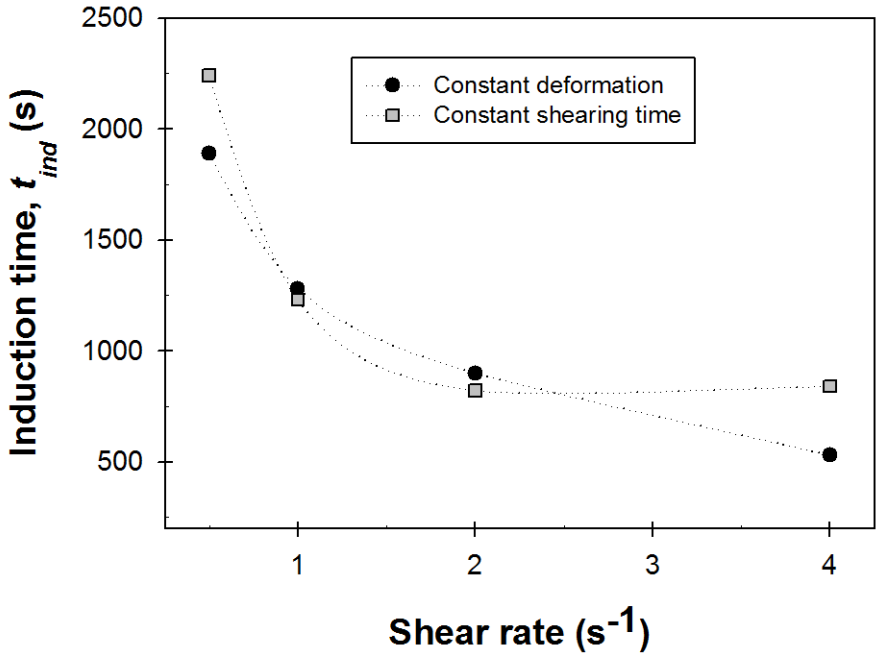

Figure 5.14: Comparison of induction times of crystallization of PLA as a function of shear rate at two different conditions: (1) constant deformation and (2) constant shearing time.

5.4 CONCLUSIONS

This work has explored the use of rheometry for the study of PLA crystallization in quiescent conditions and after a pre-shearing step. The main findings in this article can be listed as follows: first, polymer shrinkage which is a major consequence of high rates of crystallization was successfully compensated by the control of the normal force performed during the experiments. The experimental reproducibility was significantly improved through this approach, with uncertainties being reduced from 35 to 2%. Second, the evolution of the complex viscosity under quiescent conditions for a PLA-based flax-fiber composite indicated an enhancement of the rate of crystallization of PLA at the same temperature, due to the presence of cellulosic fibers. These results are in agreement with the previous studies of the same system performed by DSC. Third, the Arrhenius equation was found to predict well the initial viscosities of both neat PLA and its flax-fiber composite, at crystallization temperatures presenting low to very low crystallization rates. Under these conditions, the standardized residuals method allowed for an accurate estimation of the crystallization induction time. Finally, shear flow effectively accelerated the

crystallization of neat PLA at 140 °C. The induction time was decreased by about 75% at the maximum shear rate tested in the present study, i.e. 4 s^{-1}.

5.5 ACKNOWLEDGMENTS

Financial support from NSERC (Natural Sciences and Engineering Research Council of Canada) and FRQNT (Fonds québécois de la recherche sur la nature et les technologies) is gratefully acknowledged.

5.6 REFERENCES

[1] (2013, Market study on Bio-based Polymers in the World. Capacities, Production and Applications: Status Quo and Trends towards 2020.

[2] D. Garlotta, "A literature review of poly(lactic acid)," *Journal of Polymers and the Environment,* vol. 9, pp. 63-84, Apr 2001.

[3] A. P. Gupta and V. Kumar, "New emerging trends in synthetic biodegradable polymers - Polylactide: A critique," *European Polymer Journal,* vol. 43, pp. 4053-4074, Oct 2007.

[4] J. J. Kolstad, "Crystallization kinetics of poly(L-lactide-co-meso-lactide)," *Journal of Applied Polymer Science,* vol. 62, pp. 1079-1091, Nov 1996.

[5] H. Tsuji, H. Takai, N. Fukada, and H. Takikawa, "Non-isothermal crystallization behavior of poly(L-lactic acid) in the presence of various additives," *Macromolecular Materials and Engineering,* vol. 291, pp. 325-335, Apr 2006.

[6] A. Arias, M. C. Heuzey, and M. A. Huneault, "Thermomechanical and crystallization behavior of polylactide-based flax fiber biocomposites," *Cellulose,* vol. 20, pp. 439-452, Feb 2013.

[7] A. P. Mathew, K. Oksman, and M. Sain, "The effect of morphology and chemical characteristics of cellulose reinforcements on the crystallinity of polylactic acid," *Journal of Applied Polymer Science,* vol. 101, pp. 300-310, Jul 2006.

[8] A. Le Duigou, P. Davies, and C. Baley, "Macroscopic analysis of interfacial properties of flax/PLLA biocomposites," *Composites Science and Technology,* vol. 70, pp. 1612-1620, Oct 2010.

[9] Y. P. Khanna, "Rheological mechanism and overview of nucleated crystallization kinetics," *Macromolecules,* vol. 26, pp. 3639-3643, Jul 1993.

[10] J. W. Teh, H. P. Blom, and A. Rudin, "A study on the crystallization behavior of polypropylene, polyethylene and their blends by dynamic-mechanical and thermal methods," *Polymer,* vol. 35, pp. 1680-1687, 1994.

[11] K. Boutahar, C. Carrot, and J. Guillet, "Crystallization of polyolefins from rheological measurements - Relation between the transformed fraction and the dynamic moduli," *Macromolecules,* vol. 31, pp. 1921-1929, Mar 1998.

[12] A. Kelarakis, S. M. Mai, C. Booth, and A. J. Ryan, "Can rheometry measure crystallization kinetics? A comparative study using block copolymers," *Polymer,* vol. 46, pp. 2739-2747, Mar 2005.

[13] C. Carrot, J. Guillet, and K. Boutahar, "Rheological behavior of a semicrystalline polymer during isothermal crystallization," *Rheologica Acta,* vol. 32, pp. 566-574, Nov-Dec 1993.

[14] S. Acierno, R. Pasquino, and N. Grizzuti, "Rheological techniques for the determination of the crystallization kinetics of a polypropylene-EPR copolymer," *Journal of Thermal Analysis and Calorimetry,* vol. 98, pp. 639-644, Dec 2009.

[15] S. Coppola, S. Acierno, N. Grizzuti, and D. Vlassopoulos, "Viscoelastic behavior of semicrystalline thermoplastic polymers during the early stages of crystallization," *Macromolecules,* vol. 39, pp. 1507-1514, Feb 2006.

[16] S. Coppola, L. Balzano, E. Gioffredi, P. L. Maffettone, and N. Grizzuti, "Effects of the degree of undercooling on flow induced crystallization in polymer melts," *Polymer,* vol. 45, pp. 3249-3256, May 2004.

[17] A. Godara, D. Raabe, P. Van Puyvelde, and P. Moldenaers, "Influence of flow on the global crystallization kinetics of iso-tactic polypropylene," *Polymer Testing,* vol. 25, pp. 460-469, Jun 2006.

[18] F. Y. Yu, H. B. Zhang, R. G. Liao, H. Zheng, W. Yu, and C. X. Zhou, "Flow induced crystallization of long chain branched polypropylenes under weak shear flow," *European Polymer Journal,* vol. 45, pp. 2110-2118, Jul 2009.

[19] C. Hadinata, C. Gabriel, M. Ruellman, and H. M. Laun, "Comparison of shear-induced crystallization behavior of PB-1 samples with different molecular weight distribution," *Journal of Rheology,* vol. 49, pp. 327-349, Jan-Feb 2005.

[20] Y. Yuryev and P. Wood-Adams, "Rheological Properties of Crystallizing Polylactide: Detection of Induction Time and Modeling the Evolving Structure and Properties," *Journal of Polymer Science Part B-Polymer Physics,* vol. 48, pp. 812-822, Apr 2010.

[21] G. Kumaraswamy, "Crystallization of polymers from stressed melts," *Journal of Macromolecular Science-Polymer Reviews,* vol. C45, pp. 375-397, Oct-Dec 2005.

[22] H. Janeschitz-Kriegl and E. Ratajski, "Some fundamental aspects of the kinetics of flow-induced crystallization of polymers," *Colloid and Polymer Science,* vol. 288, pp. 1525-1537, Nov 2010.

[23] G. Lamberti, "Flow induced crystallisation of polymers," *Chemical Society Reviews,* vol. 43, pp. 2240-2252, 2014 2014.

[24] F. Langouche, "Orientation development during shear flow-induced crystallization of i-PP," *Macromolecules,* vol. 39, pp. 2568-2573, Apr 2006.

[25] R. H. Somani, L. Yang, L. Zhu, and B. S. Hsiao, "Flow-induced shish-kebab precursor structures in entangled polymer melts," *Polymer,* vol. 46, pp. 8587-8623, Sep 23 2005.

[26] J. van Meerveld, G. W. M. Peters, and M. Hutter, "Towards a rheological classification of flow induced crystallization experiments of polymer melts," *Rheologica Acta,* vol. 44, pp. 119-134, Dec 2004.

[27] Y. Zhong, H. G. Fang, Y. Q. Zhang, Z. K. Wang, J. J. Yang, and Z. G. Wang, "Rheologically Determined Critical Shear Rates for Shear-Induced Nucleation Rate Enhancements of Poly(lactic acid)," *Acs Sustainable Chemistry & Engineering,* vol. 1, pp. 663-672, Jun 2013.

[28] R. Auras, B. Harte, and S. Selke, "An overview of polylactides as packaging materials," *Macromolecular Bioscience,* vol. 4, pp. 835-864, Sep 2004.

[29] S. S. Ray and M. Okamoto, "New polylactide/layered silicate nanocomposites, 6 - Melt rheology and foam processing," *Macromolecular Materials and Engineering,* vol. 288, pp. 936-944, Dec 2003.

[30] Y. B. Wang, L. Yang, Y. H. Niu, Z. G. Wang, J. Zhang, F. Y. Yu*, et al.*, "Rheological and Topological Characterizations of Electron Beam Irradiation Prepared Long-Chain Branched Polylactic Acid," *Journal of Applied Polymer Science,* vol. 122, pp. 1857-1865, Nov 2011.

[31] D. H. S. Ramkumar and M. Bhattacharya, "Steady shear and dynamic properties of biodegradable polyesters," *Polymer Engineering and Science,* vol. 38, pp. 1426-1435, Sep 1998.

[32] S. Y. Gu, K. Zhang, J. Ren, and H. Zhan, "Melt rheology of polylactide/poly(butylene adipate-co-terephthalate) blends," *Carbohydrate Polymers,* vol. 74, pp. 79-85, Oct 2008.

[33] T. C. Sun, F. H. Chen, X. Dong, Y. Zhou, D. J. Wang, and C. C. Han, "Shear-induced orientation in the crystallization of an isotactic polypropylene nanocomposite," *Polymer,* vol. 50, pp. 2465-2471, May 2009.

[34] X. J. Li, G. J. Zhong, and Z. M. Li, "Non-isothermal crystallization of poly(L-lactide) (PLLA) under quiescent and steady shear conditions," *Chinese Journal of Polymer Science,* vol. 28, pp. 357-366, May 2010.

[35] X. J. Li, Z. M. Li, G. J. Zhong, and L. B. Li, "Steady-shear-induced isothermal crystallization of poly(L-lactide) (PLLA)," *Journal of Macromolecular Science Part B-Physics,* vol. 47, pp. 511-522, May-Jun 2008.

CHAPTER 6 ARTICLE 3 – ENHANCED DISPERSION OF CELLULOSE NANOCRYSTALS IN MELT-PROCESSED POLYLACTIDE-BASED NANOCOMPOSITES[7]

Andrea Arias[1], Marie-Claude Heuzey[1], Michel A. Huneault[2], Gilles Ausias[3], Abdelkader Bendahou[3]*

1: Chemical Engineering, Research center for high performance polymer and composite systems – CREPEC, Polytechnique Montréal. Montréal, Canada

2: Chemical and Biotechnological Engineering Department, Université de Sherbrooke. Sherbrooke, Canada

3: Laboratoire d'Ingénierie des MATériaux de Bretagne – LIMATB, Université de Bretagne Sud, Centre de Recherche Christiaan Huygens, Lorient, France

***** *Corresponding author:* marie-claude.heuzey@polymtl.ca

Abstract

Dispersion and distribution of cellulose nanocrystals (CNC) in a thermoplastic matrix is one of the most important issues in the development of CNC-based high performance composites. During melt processing, agglomeration of CNC is prone to occur due to poor polymer wetting on the hydrophilic CNC surface and to strong particle-particle interactions. Because of the high temperature and intensive mixing involved in melt-processing, degradation of the CNC is also possible. To avoid these problems, solvent mixing followed by solvent casting is the main processing route used in the majority of studies on polymer-CNC composites. In this work, we have explored a novel two-step process where solvent-mixing and melt-mixing were carried out sequentially to improve the overall dispersion of the CNC. The first step consisted in forming a

[7] *Submitted to Cellulose journal.*

CNC suspension into a polyethylene oxide (PEO) aqueous solution. In the second step, water was removed by freeze-drying to form a water-free well dispersed PEO/CNC mixture. The final step consisted in melt-mixing the PEO/CNC mixture into PLA for the preparation of the composites. PEO and PLA are known to be miscible in a certain molecular weight and composition range, thus leading to a composite where the CNC particles are well dispersed into a homogeneous mixture of PLA and PEO. Two different sources of CNC and two different PEO molecular weights were investigated in this study, and several formulations were compared under the same processing conditions. Direct blending of CNC and molten PLA was also attempted for comparison purposes. CNC particles tended to agglomerate during blending but the agglomerates were smaller and their number was considerably decreased when the PEO content increased in the formulation. At the highest PEO/CNC ratio, no agglomerates were observed. Thermomechanical and rheological properties of the PLA-based nanocomposites were also investigated.

Keywords: *Cellulose nanocrystals (CNC), dispersion, melt compounding, polyethylene oxide (PEO), polymer carrier.*

6.1 INTRODUCTION

Polylactide (PLA) is the most important synthetic polymer produced from a renewable feedstock. It has attracted considerable attention due to its bio-based nature and to the fact that it is biodegradable in an industrial composting environment. It can be extruded into films, injection-molded into different shapes or spun to obtain fibers. In recent years, PLA has also raised attention as a potential engineering material due to its high modulus and tensile strength. It suffers however from relatively low impact strength and from a low heat deflection temperature if not fully crystallized. In this context, it is interesting to use cellulosic materials as reinforcements in PLA to obtain composite materials with faster crystallization and enhanced properties, without affecting the overall bio-based content.

PLA is an aliphatic polyester synthesized by ring-opening polymerization of lactide (a cyclic dimer of lactic acid). Since lactic acid is stereoactive, it has *L*- and *D*- enantiomers. Commercially available bio-based PLA is typically produced from *L*-LA. The presence of *D*-LA units in the polymer chain acts as chain defects. Therefore, an increase in *D*-LA content tends to

decrease the melting temperature as well as the crystalline content, up to the point where the material becomes fully amorphous. Full reviews on the synthesis, properties and crystallization of PLA can be found elsewhere [1-4].

Cellulose is the most abundant polymer in nature. There has been a growing interest on the development of cellulose-based materials during the last decades. Among them, cellulose nanocrystals (CNC) have become widespread in the literature [5-8]. CNC are rod-shaped nanoparticles obtained from the acid hydrolysis of cellulose. They range approximately from 10 to 100 nm in diameter and from 100 to 1000 nm in length, depending on the cellulose source and the hydrolysis conditions. A wide range of aspect ratios is reported in the literature [9-11]. Because of the hydroxyl groups on the cellulose molecule, CNC strongly interact with water through hydrogen bonding. This strong interaction gives place to one important and specific characteristic of CNC aqueous suspensions: their ability to spatially self-assemble in different orientations depending on the concentration, going from isotropic to fully anisotropic phases. CNC was the first FDA approved nanoparticle, fully biosourced, biodegradable and renewable [12, 13]. CNC are also named nanocrystalline cellulose (NCC), cellulose nanowhiskers (CNW) or simply whiskers.

Incorporation of nano-sized cellulose particles into a polymer matrix may have several positive consequences. For example, well-dispersed nanoparticles are expected to improve mechanical performance through stress transfer from the matrix to the cellulose nanocrystals. Changes in polymer chain mobility as well as crystalline nucleation effect may also affect thermomechanical behavior and barrier properties. There are however two major challenges in the dispersion of CNC into a polymer matrix. The first one is that the CNC are produced in an aqueous media. The elimination of the suspending media through freeze-drying or spray-drying may therefore cause particle agglomeration. The second challenge is related to the highly hydrophilic character of cellulose nanocrystals, which may also cause their dispersion to be more difficult in non-polar polymer matrices. The first reports on polymer/CNC mixing focused on adding polymer latexes to CNC aqueous suspensions and evaporating the water to coagulate the polymer. For example, styrene-butylacrylate (poly(S-co-BuA)) [14-17] and polyvinyl acetate emulsions [18, 19] were mixed with CNC suspension to produce (after water-removal) CNC reinforced elastomers. A similar technique was used with water-soluble polymers, i.e. water-soluble polyvinyl alcohol

(PVOH) and polyethylene oxide (PEO) were respectively mixed with a CNC suspension and were casted to produce composite films [20-22]. Excellent dispersion of the CNC was found due to the highly hydrophilic nature of the polymer. Unfortunately, solution blending is not a viable mixing route for industrial production of reinforced thermoplastics.

An intermediate approach that was used to incorporate CNC was to solution blend the CNC with a carrier polymer and then, in a subsequent step, to melt-blend the CNC-carrier polymer mixture into the polymer matrix. Bondeson *et al.* have incorporated the CNC into polyvinyl alcohol by solution blending. They compared two incorporation methods into a PLA matrix using a twin-screw extruder. The first method was to pump the PVOH/CNC/water solution into the extruder and vent-off the water. In this case, the PLA was fed at the beginning of the extruder while the solution was fed into the molten PLA at the first third of the extruder. The second method was feed the dried PVOH/CNC along with PLA at the primary feed port of the extruder. The authors concluded that the CNC dispersion was better when liquid feeding was used [23]. Also, due to the immiscible nature of PVOH, the CNC tended to stay in the PVOH phases. A similar approach was used to incorporate CNC into polyethylene using PEO as the CNC carrier [24]. To alleviate the phase separation between the matrix polymer and the CNC carrier, Jiang *et al.* have investigated the use of a low molecular weight polyethylene oxide as a carrier for the CNC particulates. The CNC and PEO were solvent mixed in water and freeze dried. The dry PEO/CNC powders were then mixed with poly(3-hydroxybutyrate-co-3-hydroxyvalerate (PHBV) in a twin-screw extruder. However high agglomeration of CNC particles was found in the final blend, indicating that interfacial modification might be required to produce properly dispersed composites [25].

Direct mixing of freeze-dried CNC particulates using melt-processing have also been investigated. Pristine and chemically modified CNC in a dried state have been directly melt-blended up to 6 wt% in PLA using either a twin-screw microextruder or an internal mixer [26, 27]. Poor dispersion was found for freeze-dried pristine CNC composites. Improvements in nanoparticule dispersion were revealed by thermal and morphological characterization when using modified CNC; however, the presence of aggregates was still evidenced, indicating that nanolevel dispersion was not generalized. In addition, it is possible that the high shear rate used to promote dispersion of the CNC may have induced some degradation of the cellulose

nanocrystals. To improve the melt-mixing procedure, the use of a surfactant was investigated. Surfactant was solution blended to the CNC suspension, water was eliminated by freeze-drying of the surfactant/CNC system prior to melt-mixing in the PLA matrix. Dispersion was dramatically improved in the presence of a 5% surfactant content, but it promoted polymer chain degradation of the PLA matrix [28]. A hybrid approach was also considered: a master batch of PLA/CNC was first prepared by solution-blending in chloroform and then casted for solvent evaporation. PLA/CNC films were cut into small pieces and extruded with the PLA matrix. Pristine and chemically modified CNC were used in the same study. Authors claimed prevention of CNC degradation and excellent improvement in the nanofiller dispersion, due to the combination of both processing methods (solution-blending and melt extrusion) [29]. A similar approach has been reported for PLA-based cellulose nanofiber (CNF) composites [30]. Recently, it was shown that ring-opening polymerized PLA branches on the surface of CNC particles could improve the properties of PLA/CNC composites [31, 32]. Dispersion is not deeply commented by the authors but it can be assumed that the covalent bonding of PLA on the surface of the CNC resulted in improved compatibility between grafted-CNC and the PLA matrix. Crystallization, stiffness and heat deflection temperature (HDT) were also improved.

In the present work, the incorporation of CNC into PLA using a miscible carrier has been explored. A PEO/CNC blend was first produced by solvent mixing in water and then freeze-dried to produce a PEO/CNC dry powder. This material was directly melt compounded with PLA. In this ternary blend, the PEO is expected to form a miscible mixture with PLA. Miscibility of PLA/PEO blends in a wide range of molecular weights of PEO has been previously reported. PLA and PEO are miscible in the melt state over the complete concentration range [33] but will tend to phase separate when the temperature of the blend is reduced and that the PEO or PLA phases start to crystallize. This limits the room-temperature miscibility and it has been reported that for PEO molecular weight of 400 and 10000 g/mol, the miscibility limit was respectively 30 and 15%. [34, 35]. Two different PEO molecular weights were used and different PEO:CNC ratios were considered. The quality of CNC dispersion was evaluated by microscopy. Monitoring and analysis of crystallization, tensile properties and thermal transitions were carried out for various PLA nanocomposite formulations.

6.2 EXPERIMENTAL

6.2.1 Materials

Polylactide (PLA) grade 4032 from NatureWorks LLC was used as received. PLA 4032 is a semi-crystalline grade comprising around 2% *D*-lactide and has a melting point of ~165 °C. Spray-dried cellulose nanocrystals (CNC) in the form of powder were provided by FPInnovations. CNC were also extracted from flax fibers following the procedure reported by Bendahou *et al.* [36]. They will be referred to as CNC_{Flax}. Two polyethylene oxide (PEO) grades with $5x10^6$ g/mol and 1000 g/mol were supplied, respectively, by Polyscience Inc. and Merck Millipore. The high and low molecular weight PEO will be referred to H-PEO and L-PEO in the following text.

6.2.2 PEO/CNC blend preparation

Formulation of the PLA-based nanocomposites was carried out by first preparing a PEO/CNC blend, using a solvent mixing/freeze-drying method followed by a melt mixing step of the PEO/CNC into PLA. When using low molecular weight PEO (L-PEO), the CNC was directly incorporated to the L-PEO aqueous solutions. In the case of H-PEO, the high viscosity of the PEO solutions required to separately prepare a CNC aqueous suspension and then to mix it with the H-PEO aqueous solution. The high molecular weight PEO (H-PEO) was dissolved in de-ionized water at 2 wt% concentration. Overnight stirring and filtration followed. A suspension containing 3 wt% CNC was prepared by mixing the CNC powder in de-ionized water under magnetic stirring overnight. The aqueous CNC suspension also underwent sonication in an ice bath using a Vibra Cell 75185 sonicator. Sonication conditions were set at 130 W, 20 Hz and 40% amplitude. A series of 10 min cycles were performed until getting a translucent suspension without visible agglomerates. The suspension was then filtered to eliminate impurities. The CNC suspension was slowly poured into the H-PEO solution followed by stirring and sonication to form a CNC suspension in the PEO solution. For both types of PEO/CNC suspensions, water was subsequently removed by freezing of the suspension followed by freeze-drying until full sublimation of water. After freeze drying, all samples were ground to obtain powders.

The various PEO/CNC binary blends are listed in Table 6.1. The blends differ in terms of molecular weight of PEO and PEO:CNC ratio. Binary blends BB4 and BB5 have a similar composition but the latter is made from the CNC extracted from flax.

Table 6.1: PEO/CNC binary blends.

Formulation	CNC (wt%)	PEO (wt%)		Ratio PEO:CNC
		H-PEO	L-PEO	
BB1	80.0	20.0	--	0.25
BB2	50.0	50.0	--	1.0
BB3	45.5	--	55.5	1.25
BB4	7.4	--	92.6	12.5
BB5	7.4 (CNC_{Flax})	--	92.6	12.5

6.2.3 Melt compounding

The melt-compounded formulations are listed in Table 6.2. The first series is composed of the blends prepared by the hybrid solution/melt mixing method (blends #1 to #5). In this method, the CNC were introduced into the PLA matrix by melt-blending PLA with the PEO/CNC binary blends described above. We will refer to this method as the hybrid preparation method. The second series of blends were prepared by direct melt-mixing of the CNC powder, H-PEO and PLA in the internal mixer (blends #6 to #9). In all cases, the blends were melt-mixed for 7 minutes at 190 ^{o}C using an internal mixer operated at a screw rotational speed of 50 rpm and under a nitrogen atmosphere. The compounded materials were removed from the chamber and compression molded into ~1 mm thick sheets using a hot-press at 180 ºC and a force increasing slowly from 0 to 30 kN for about 5 min. The resulting sheets were left in air to cool down to room temperature. To prepare samples for mechanical testing, the sheets from selected samples were heated up with a hot air gun, and dumbbell-shaped and rectangular samples were punched using the appropriate cutting-die.

A PLA/CNC nanocomposite containing 3 wt% of CNC was also provided by CelluForce (Canada) and was used for comparison purposes. In this material, the CNC was grafted with PLA branches using a proprietary *in situ* polymerization process [37]. The grafted CNC were dispersed by direct melt-mixing in NatureWorks's PLA 3251 grade. This PLA has a significantly lower viscosity (hence molecular weight) than PLA grade 4032 and has a *D*-lactide content of 1.5%. We will refer to this material as the interface-modified melt-mixed composite (PLA-g-CNC/PLA). The two neat PLA grades and interface-modified melt-mixed PLA/CNC samples were processed in the same conditions to allow comparison under the same thermal history.

Table 6.2: Formulations prepared by melt compounding.

No.	Mixing method	CNC source	PEO (MW)	PLA (wt%)	CNC (wt%)	PEO (wt%)	Ratio PEO:CNC
1	Hybrid method	BB1	H	96.25	3.0	0.75	0.25
2		BB2	H	94.0	3.0	3.0	1.0
3		BB3	L	97.75	1.0	1.25	1.25
4		BB4	L	86.5	1.0	12.5	12.5
5		BB5	L	86.5	1.0	12.5	12.5
6	Melt-mixing	Spray dried	H	96.25	3.0	0.75	0.25
7		Spray dried	H	94.0	3.0	3.0	1.0
8		Spray dried	n/a	97.0	3.0	0.0	n/a
9		Spray dried	n/a	94.0	6.0	0.0	n/a

6.2.4 Characterization techniques

Thermal gravimetric analysis – TGA

Thermal stability was characterized with a Seratam TG-DTA 92-10 thermal analyzer under a nitrogen atmosphere at a flow rate of 80 mL/min. Two different profiles were established: freeze-dried products underwent heating at 2 ºC/min from 25 to 300 ºC, and of 5 ºC/min from 300 until 600 ºC. In the case of the neat resins and nanocomposites, the heating rate was kept constant at 5

ºC/min until 600 ºC. The samples weight was approximately 20 mg. At least three samples of each formulation were tested.

Microscopy

Micrographs of cellulose nanocrystals (CNC) were obtained under ambient conditions using light tapping mode on a Nanoscope IIIA atomic force microscope (AFM) from Digital Instruments. CNC dimensions were measured using the section analysis software of the microscope. A micro-drop of a diluted CNC suspension was disposed onto a ~1 cm^2 freshly cleaved mica surface and then it was placed into a SPIN150 spin processor from SPS Europe for about 60 s at 2500 rpm. The mica sheet was then attached to an AFM specimen holder for observation.

Nanocomposite samples were microtomed using a Leica RM2165 microtome equipped with a liquid nitrogen cooling system. Selected microtomed surfaces underwent selective solvent etching with ethanol at 35 ºC. Ethanol etches preferentially PEO without affecting PLA. Prior to SEM observations, the samples were kept overnight in a vacuum oven at 30 ºC and then coated with a gold-palladium alloy for 15 s. Micrographs were obtained using a SEM-FEG JEOL JSM6500 at 2 kV and 6-8 A in scanning electron image (SEI) and low electron image (LEI) modes. Two different samples of each formulation were analyzed.

Differential Scanning Calorimeter – DSC

The crystallization behavior of PLA and PLA-based nanocomposites was evaluated using a DSC882 from Mettler-Toledo under a helium atmosphere. Samples of about 10 mg were sealed in aluminium pans and underwent a first heating from room temperature to 200 ºC at 10 ºC/min to erase their previous thermal history. The non-isothermal crystallization was examined by cooling the samples from 200 down to 30 ºC using cooling rates of 1, 5 and 10 ºC/min. For isothermal crystallization, samples were cooled at a rate of 50 ºC/min from 200 ºC to various crystallization temperatures T_c: 100, 110 and 120 °C and maintained at T_c until the crystallization was completed. Afterwards, all samples underwent a second heating at 10 ºC/min up to 200 ºC to verify the final crystalline content. The results reported are the average of at least two tests for each formulation.

Rheology

The dynamic rheological behavior of PLA and PLA-based nanocomposites was investigated using a MCR 301 rheometer from Anton-Paar GmbH using a 25 mm parallel-plate flow geometry. Measurements were performed in oscillatory mode in the linear viscoelastic regime. A thermal soak time of 4 min was used prior to the oscillatory measurements. Thermal stability was monitored with time sweep tests at a frequency of 0.628 rad/s for about 10 min. Frequency sweeps were performed in the linear viscoelastic regime, from low to high and high to low frequencies ranging from 0.1 to 100 rad/s, for an overall duration of 12 min. At least two specimens of each formulation were characterized.

Dynamic Mechanical Analysis – DMA

Dynamic mechanical analysis was performed on a DMA50N from Acoem Group. Measurements were carried out in tension film mode from room temperature to 160 ºC at a heating rate of 2 ºC/min and frequency of 6.28 Hz. Rectangular specimens were ~1 mm thick, ~10 mm wide and 20 mm long. Two different samples of each formulation underwent the DMA testing.

Tensile Testing

Uniaxial tensile tests were performed following the ASTM D638 standard for tensile properties of plastics. Standard type V dumbbell-shaped samples were tested using a cell load of 1 or 10 kN and a crosshead speed of 1 or 10 mm/min, depending on the blend. The reported results are the average of at least 6 specimens for each formulation.

6.3 RESULTS AND DISCUSSION

6.3.1 Morphology of cellulose nanocrystals

AFM micrographs of diluted aqueous suspensions of cellulose nanocrystals (CNC) are presented in Figure 6.1. Figure 6.1a shows individual and well distributed nanowhiskers from the spray-dried CNC suspensions. They are rodlike particles approximately 160 nm long and ~30 nm diameter. In the case of CNC extracted from flax fiber (Figure 6.1b), nanowhiskers are ~230 nm long and ~40 nm thick. They exhibit a similar shape but are less uniform in length than the spray-dried powder.

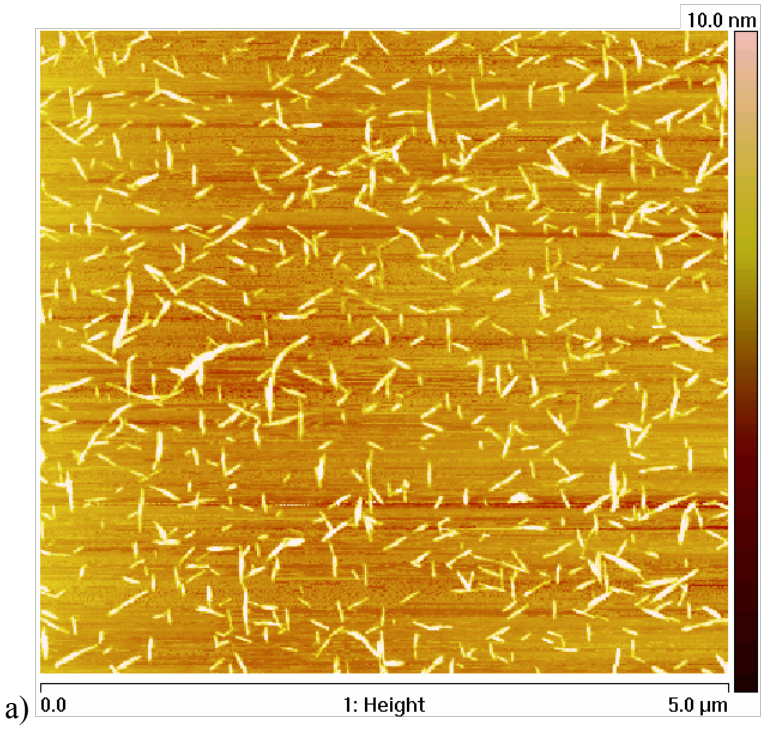

Figure 6.1: AFM micrographs of aqueous diluted suspensions of a) spray-dried CNC and b) CNC extracted from flax fibers. The scanned surface is 25 μm^2 in both cases.

6.3.2 Thermal stability

Thermogravimetric analysis was performed on the CNC powder and on all freeze-dried PEO/CNC products in order to assess their thermal stability. Figure 6.2a presents the relative weight drop as a function of temperature. All curves exhibited three important weight losses over the investigated temperature range. The first one occurred between room temperature and ~100 ºC and was associated with the evaporation of residual moisture. This weight loss represented about 5 wt% of the total sample weight. The second one took place from 250 to about 300 ºC, and corresponds to the depolymerisation temperature of cellulose. The last one occurred above 350 ºC and is related to the degradation of PEO. The thermogram of the CNC powder showed the first and second weight losses, but still exhibited ~20 wt% at high temperature. This residue is due to the flame retardant effect of sulfate groups present on the nanocrystal surfaces [38]. It is worth mentioning that the degradation of the CNC powder starts at about 250 ºC, which is similar to the degradation of natural cellulosic fibers [39].

Figure 6.2b presents the corresponding first derivative of the weight drop as a function of temperature. The peaks related to cellulose depolymerisation are evidenced between 250 ºC and 310 ºC. The peaks are superposed, except for sample BB3, which exhibited an earlier depolymerisation by about 20 ºC. Sample BB4 which comprises 92.6% PEO showed a delayed degradation, starting at about 300 ºC due to the high PEO content. Since the CNC degrades faster than the PEO, the intensity of the second (i.e. CNC weight loss) and third peaks (i.e PEO weight loss) in Figure 6.2b are directly related to the PEO:CNC ratio. Similar TGA tests were performed for the polymer resins used in this work: H-PEO, L-PEO, PLA 4032 and PLA 3251 (results not shown). All polymer resins were stable up to 300 ºC and presented one straight weight drop accounting for 100% of the initial sample weight above this critical temperature.

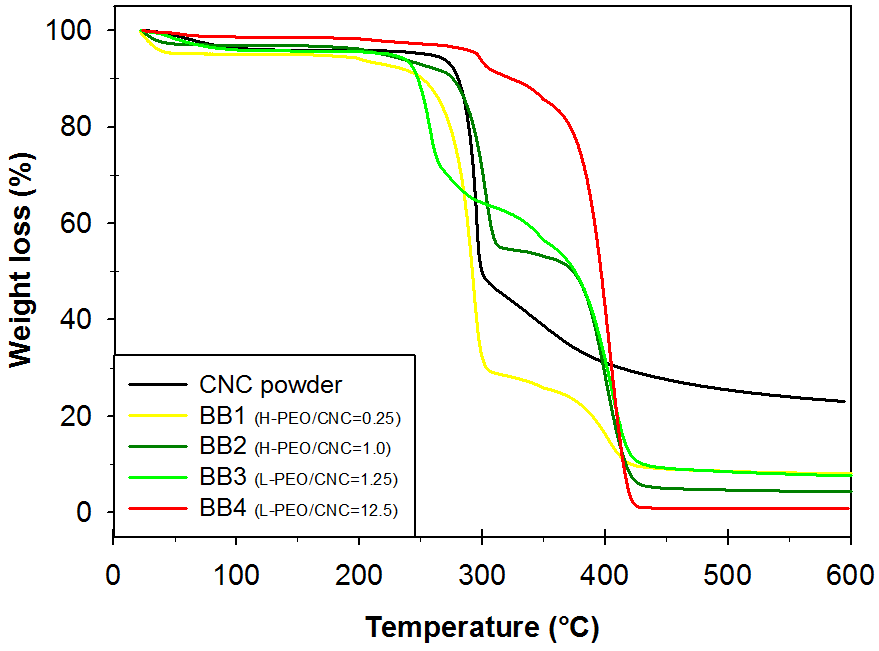

a)

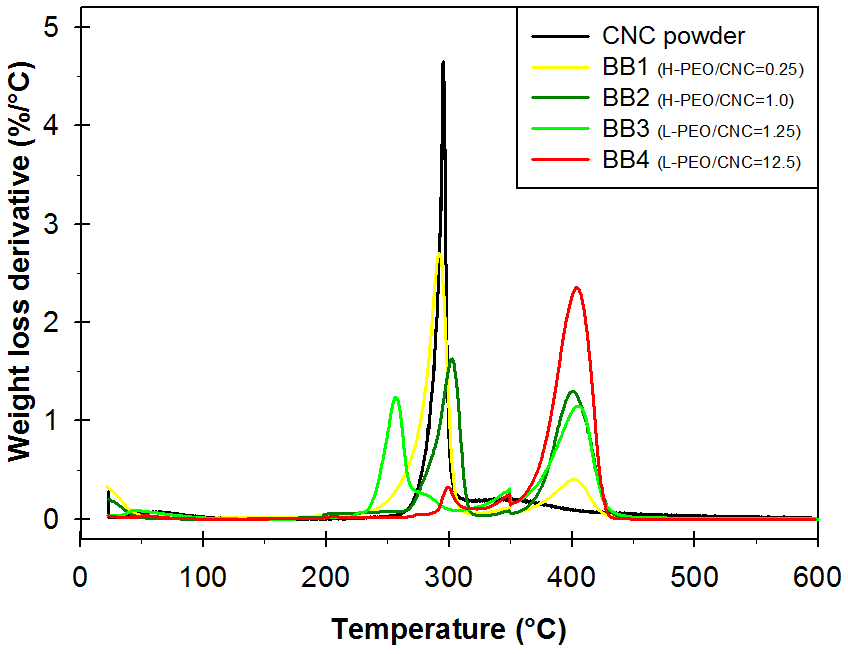

b)

Figure 6.2: Thermogravimetric curves of spray-dried CNC and binary blends, a) weight loss and b) weight loss derivative.

6.3.3 Morphology

Morphology characterization was carried out to evaluate the level of nanoparticle dispersion and the effectiveness of the different mixing approaches. Scanning electron micrographs are reported in Figures 6.3-6.5. Figure 6.3 compares the neat PLA reference to composites prepared by direct melt-mixing and interface-modified PLA/CNC nanocomposites. Figure 6.4 and 6.5 present micrographs of formulations prepared with the hybrid solution/melt mixing procedure.

As expected, the PLA reference (Figure 6.3a) showed a flat and homogeneous surface; the straight and parallel lines are marks left by the glass knife during the microtoming step. The melt-mixed blend with 3 wt% CNC (blend #8, Fig. 6.3b) exhibited large agglomerates with sizes varying from ~2 to ~10 µm, similar to the original dried-CNC powder agglomerates prior to blending [40]. Therefore, no evidence of agglomerates break-up or of individually dispersed nanocrystals was found. A different morphology was encountered in the interface-modified melt-mixed samples. Figure 6.3c and 6.3d present the latter at two different magnifications. At low magnification, lighter circular areas (see dotted line) that can be associated to CNC-rich clusters coming from the *in situ* grafting can be observed. Good adhesion of these clusters with the rest of the material can be observed however, in contrast with the unmodified blend where the agglomerate clearly separate from the matrix. In addition, an interconnected network of particles that spreads entirely over the polymer matrix can be seen. Some agglomerates can be observed from which filaments emerge in all directions.

a)

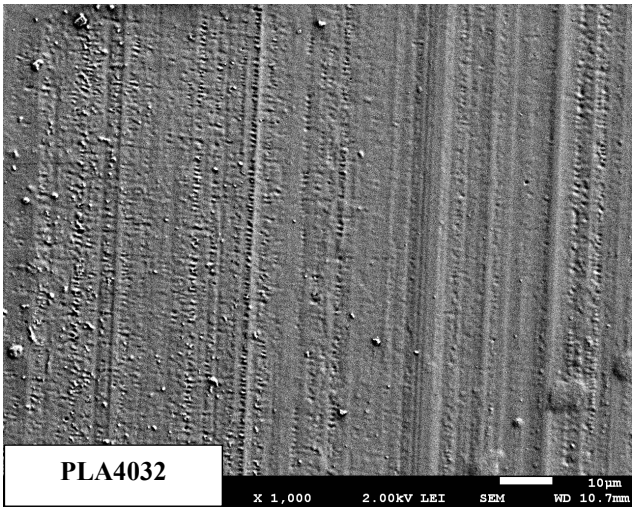
PLA4032
X 1,000
2.00kV LEI
SEM
10µm
WD 10.7mm

b)

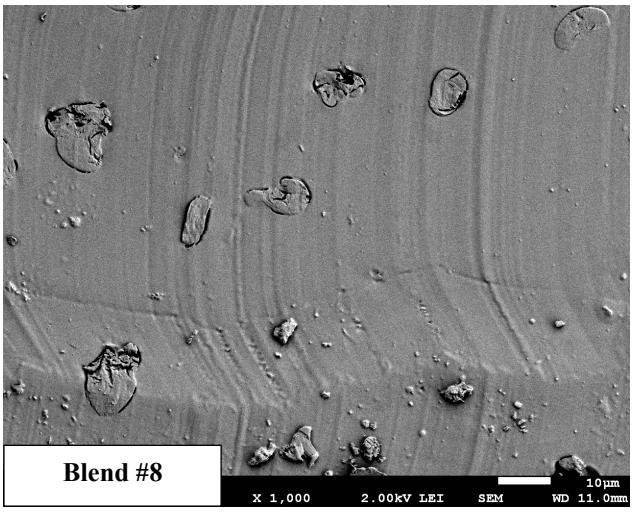
Blend #8
X 1,000
2.00kV LEI
SEM
10µm
WD 11.0mm

c)

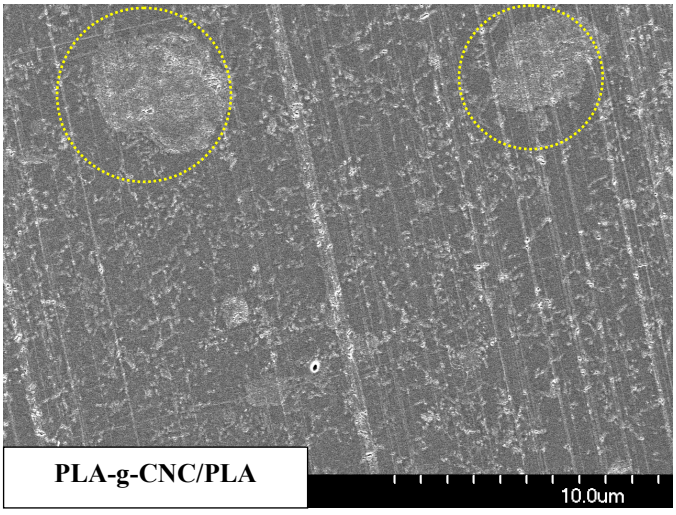
PLA-g-CNC/PLA
10.0um

d) 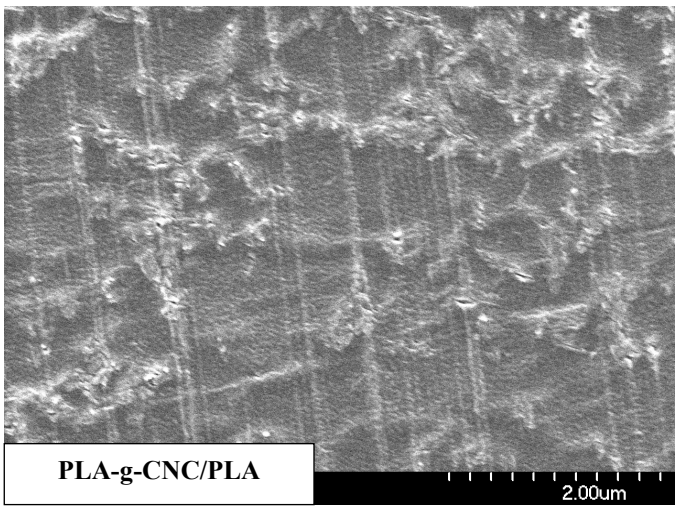

Figure 6.3:.Morphology of a) neat PLA matrix and nanocomposites prepared by b) direct melt-mixing and c, d) interface-modified melt-mixing PLA/CNC. Scale bars represent 10, 10, 10 and 2 μm, respectively.

Figure 6.4 presents micrographs of formulations prepared with the hybrid solvent/melt mixing method, using the high molecular weight PEO and comprising 3 wt% CNC. Figure 6.4a is a low magnification micrograph showing ~10 to ~20 μm agglomerates observed in blend #1 (H-PEO and PEO:CNC ratio of 0.25). This illustrates that the binary PEO/CNC blends made with H-PEO are difficult to redisperse in the PLA matrix due to their high viscosity especially, with the 0.25 PEO:CNC ratio. To probe the internal structure of an agglomerate, a high magnification micrograph was taken after a selective dissolution of the PEO phase using ethanol (Fig. 6.4c). The CNC fibrils are clearly present in the extracted agglomerate and the micrograph also shows that, even though PEO and PLA are known to be thermodynamically miscible, the blending step has not enabled full dissolution of the PEO phase into the PLA matrix, especially at this high molecular weight. It is also noteworthy that even if large agglomerates are present, higher magnification micrographs of the same blend showed the presence of disintegrating agglomerates (Fig 6.4b). At the H-PEO:CNC ratio of 1.0 (blend #2, Fig. 6.4d), no large agglomerates were observed but interestingly a large number of regularly distributed sub-micron agglomerates were found. The size reduction of agglomerates, evidenced when the H-PEO:CNC ratio increased from 0.25 to 1.0, indicates that H-PEO promoted the interactions between the nanocrystals and the PLA matrix.

As a mean to improve dispersion, the CNC content was lowered from 3 to 1 wt% and the lower molecular weight L-PEO was used. A ratio of PEO:CNC of 1.25 (blend #3) and a higher ratio of 12.5 (blend #4) were also investigated. Figure 6.5 presents the morphologies obtained when using the L-PEO. In Figure 6.5a, the PEO:CNC ratio is similar to the one in Fig. 6.4d with H-PEO. In Figure 6.5a, lowering of the PEO molecular weight led to similarly sized agglomerates compared to the corresponding H-PEO analog (blend #2). The number of agglomerates was however reduced; suggesting that part of the CNC has been dispersed as primary particles difficult to observe by SEM. On the other hand, when using the high L-PEO:CNC ratio the agglomerates completely disappeared, indicating a much finer dispersion level (blend #4 and #5, Fig. 6.5b-c). Dispersion of CNC_{Flax} (blend #5) appeared to be quite similar to blend #4, no significant differences between these two blends were revealed by SEM micrographs. Similar observations were made on samples subjected to ethanol extraction to see if a distinct PEO phase could be revealed. No droplet-matrix morphology was observed, indicating that the PEO and PLA form a homogeneous miscible mixture. These observations confirmed that the hybrid mixing method proposed in this study can provide a novel and simple mean to develop well-dispersed PLA nanocomposites.

a)

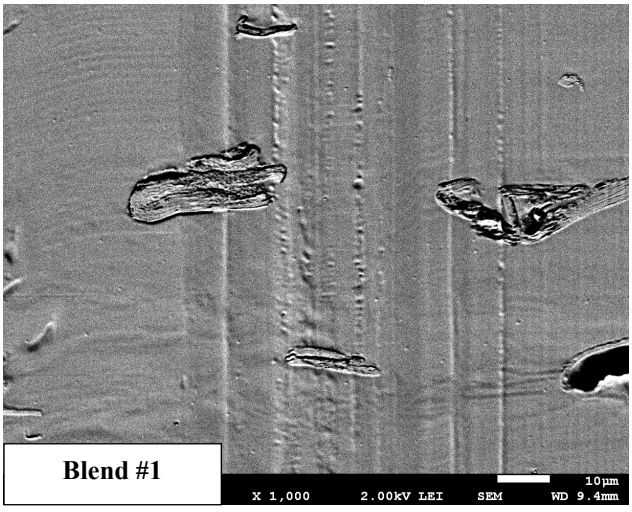

b)

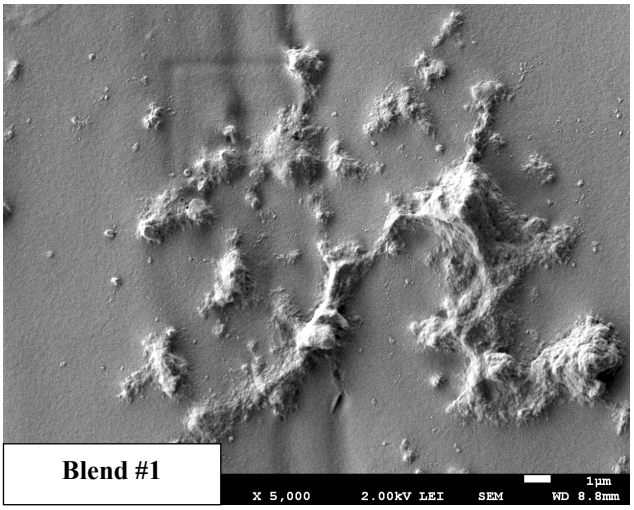

c)

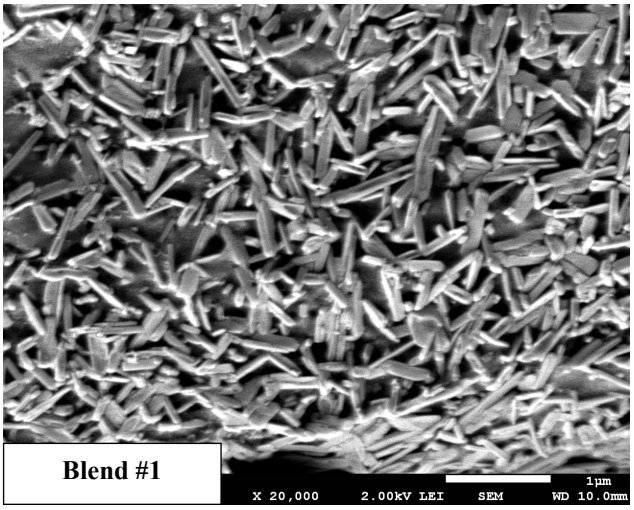

d)

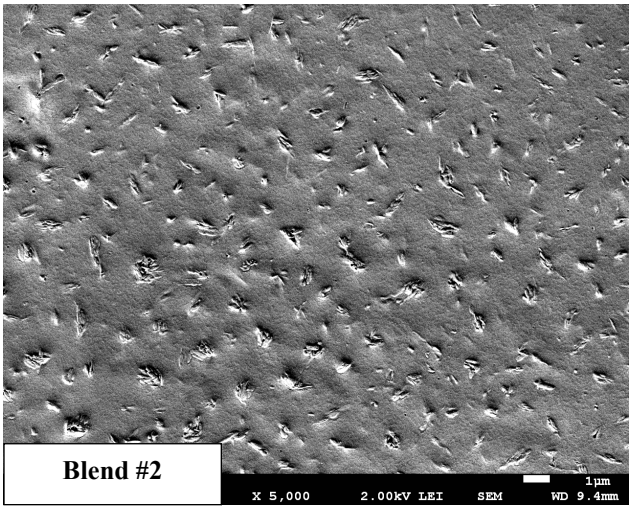

Figure 6.4: Effect of H-PEO on the dispersion of PLA/CNC nanocomposites prepared by the hybrid solution/melt mixing procedure. Micrographs show a, b) blend #1 (H-PEO/CNC = 0.25);

c) blend #1 after ethanol extraction and d) blend #2 (H-PEO/CNC = 1.0). Scale bars represent 10, 1, 1 and 1 μm, respectively.

a)

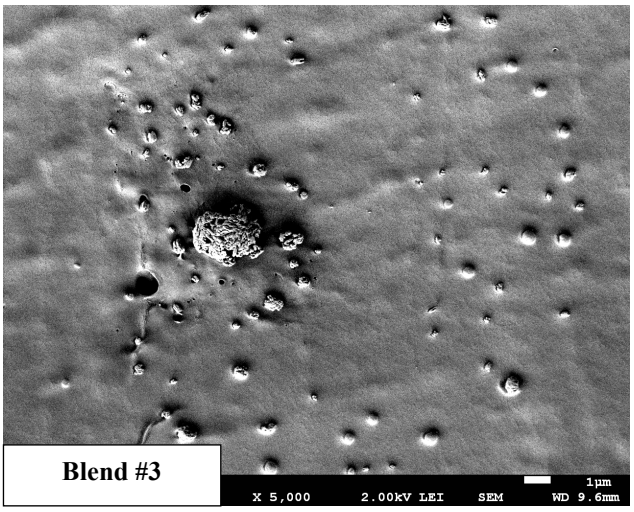

b)

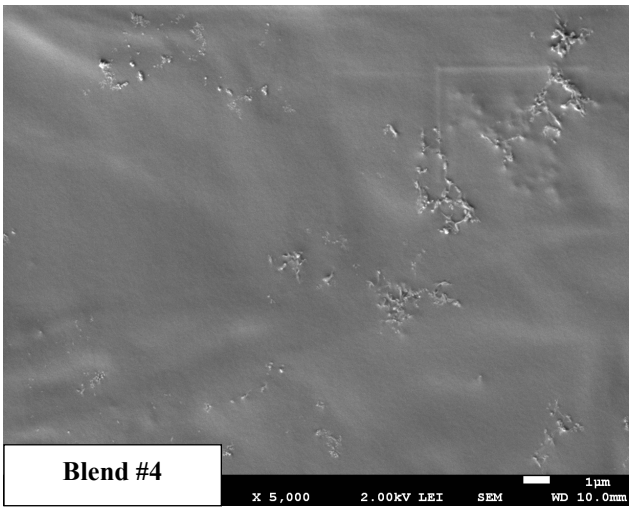

c) 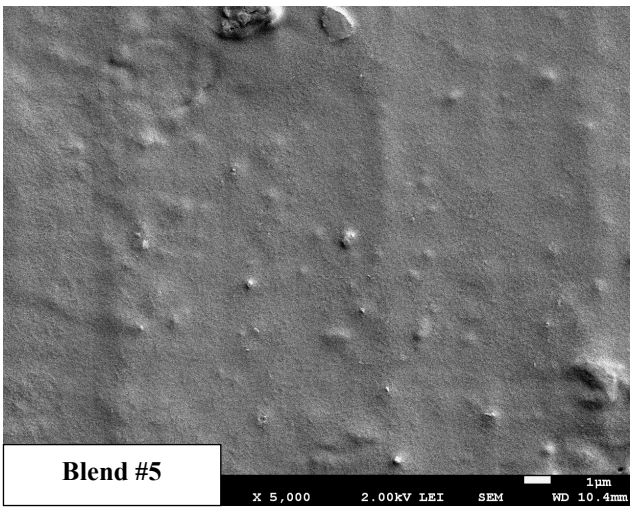

Figure 6.5: Effect of L-PEO on the dispersion of PLA/CNC nanocomposites prepared by the hybrid solution/melt mixing procedure. Micrographs show a) blend #3 (L-PEO/CNC = 1.25); b) blend #4 (L-PEO/CNC = 12.5) and c) blend #5 (L-PEO/CNC_{Flax} = 12.5). All scale bars represent 1 μm.

6.3.4 Crystallization

All formulations have been analyzed by differential scanning calorimetry (DSC) for determining the nucleating ability of CNC on the crystallization of PLA nanocomposites. Figure 6.6 compares the non-isothermal crystallization behavior of selected formulations prepared by direct (blend #8), hybrid (blend #3, #4 and #5) and interface-modified (PLA-g-CNC/PLA) melt-mixing procedures. Neat PLA is also shown for comparison purposes. Cooling scans are presented in Figure 6.6a. Blend #8 did not crystallize upon cooling. Blend #3 (L-PEO:CNC = 1.25; 1.0 wt%CNC) exhibited a wide crystallization peak starting at ~110 ºC with a maximum at about 88 ºC; blend #4 (L-PEO:CNC = 12.5; 1.0 wt% CNC) started crystallization at the same temperature, presenting a shifted peak at 96 ºC due to a faster crystallization rate. Blend #5, prepared with CNC_{Flax} and similar composition than blend #4, exhibited comparable crystallization to blend #4, with a maximum at 92 ºC. Figure 6.6b presents the second heating scans of the same cycle. Nanocomposites based on the binary blends did not exhibit any sign of cold crystallization, indicating that materials were fully crystallized upon the cooling stage. The interface-modified melt-mixing sample (PLA-g-CNC/PLA) started crystallizing upon cooling and also exhibited

cold crystallization during the heating step. Melting peaks of direct and hybrid melt-mixed nanocomposites showed up between 165-170 ºC in all cases, which corresponds to the typical melting range of the neat PLA matrix.

It is surprising that blend #3 reached full crystallization upon cooling, while it contained only 1.25 wt% of L-PEO. Sungsanit et al. have investigated the effect of L-PEO content up to 20 wt% on the crystallization of PLA/PEO blends prepared by melt-compounding. PLA and PEO grades were similar to those proposed in the present study. They reported that full crystallization upon cooling at 10 ºC/min is attained when PEO concentration is higher than 15 wt%; this is mostly explained by the increase in polymer chain mobility due to the plasticization effect of PEO [41]. This fact supports the idea that PEO and CNC have a synergistic effect on the crystallization process of PLA/CNC nanocomposites. PEO might play a double role, acting as a plasticizer of the matrix and, at the same time, contributing to the dispersion of the nanocrystals. On the other hand, CNC act as a nucleating agent for the plasticized PLA, as indicated by the enhanced crystallization. Similar synergistic effects between plasticization and nucleation agents have been reported for PLA-based blends plasticized with acetyl tributyl citrate (ATBC) and low molecular weight PEO in the presence of 1 wt% talc. The best results in terms of acceleration of crystallization were observed for PLA/PEO/talc blends [42].

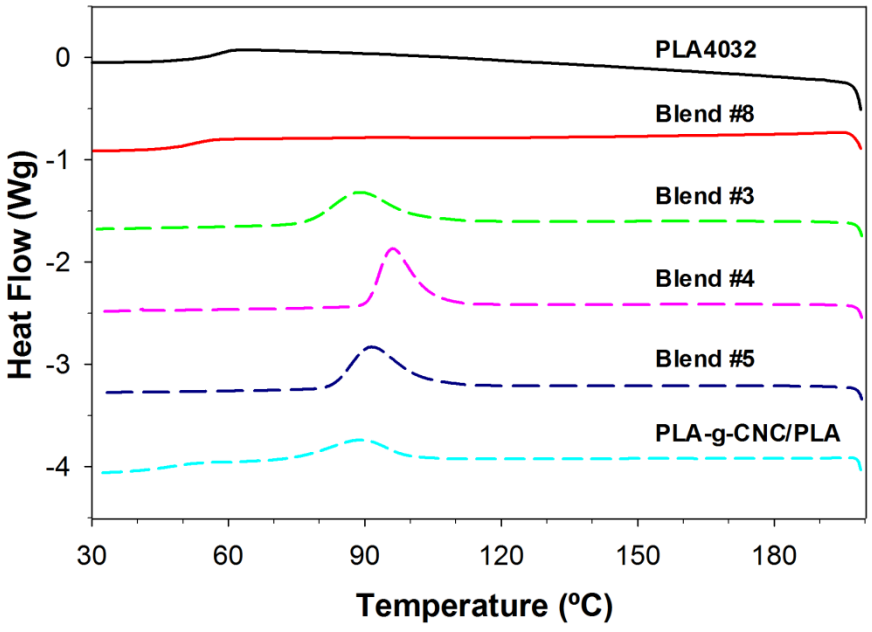

a)

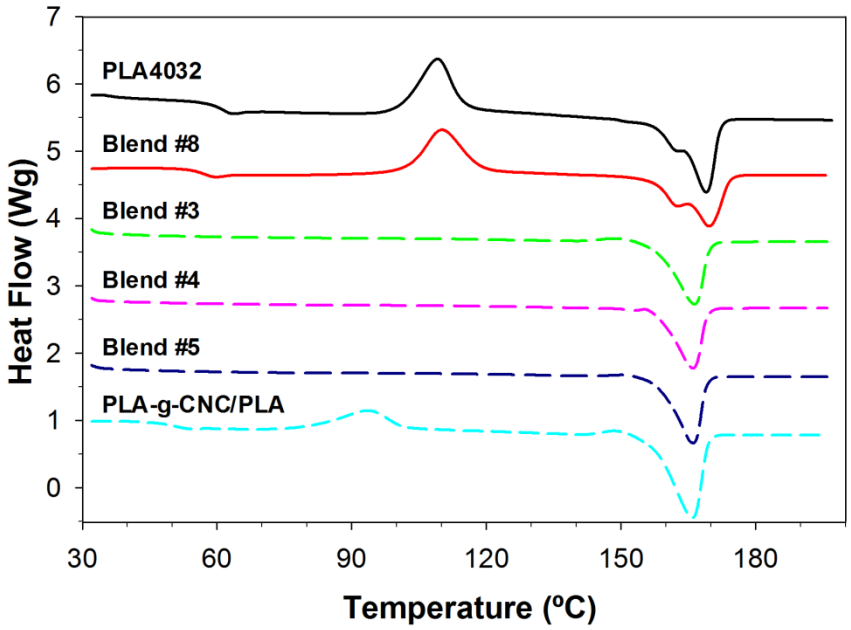

b)

Figure 6.6: Non-isothermal DSC scans for various PLA/CNC nanocomposites: a) cooling step, b) second heating step. Temperature rate = 10 ºC/min in both cases.

Table 6.3 summarizes the glass transition (T_g), crystallization (T_c), cold crystallization (T_{cc}), recrystallization (T_{rc}) and melting temperatures (T_m) as well as the respective enthalpies for the selected nanocomposites. Direct melt-mixed nanocomposites (blend #8) presented very similar transition temperatures and enthalpies to the neat PLA matrix. Formulations containing L-PEO and prepared by the hybrid procedure (blends # 3, 4 and 5) exhibited a reduction in T_g of about 15 ºC, due to the plasticization effect. Regarding the melting point, these nanocomposites exhibited a single and narrower melting peak. This fact is most probably related to the high homogeneity of the crystal sizes. The melt enthalpies of the various formulations were all in the same range of values, except in the case of the interface-modified melt-mixing material (PLA-g-CNC/PLA) which presented a melt enthalpy ~15% higher than other nanocomposites.

Table 6.3: Transition temperatures, crystallization and melting enthalpies for various PLA/CNC nanocomposites.

Sample	T_g (ºC)	T_c (ºC)	T_{cc} (ºC)	T_{rc} (ºC)	T_{m1} (ºC)	T_{m2} (ºC)	ΔH_c (J/g)	ΔH_{cc} (J/g)	ΔH_{rc} (J/g)	ΔH_m (J/g)
PLA4032	60.0	-	109	-	162	169	-	33.1	-	34.5
Blend #8	57.6	-	110	-	162	169	-	35.0	-	37.2
Blend #3	44.6	88.5	-	-	166	-	36.1	-	-	37.6
Blend #4	45.4	96.2	-	-	166	-	36.6	-	-	37.4
Blend #5	45.4	91.6	-	-	166	-	35.3	-	-	36.8
PLA-g-CNC/PLA	62.5	89.3	95.1	149	165	-	17.0	20.3	2.80	42.5

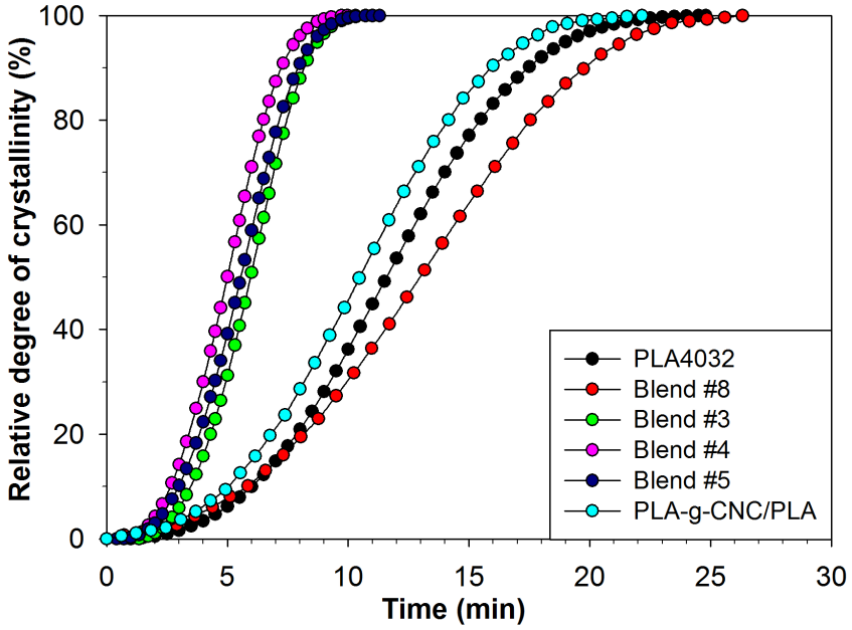

Figure 6.7: Relative degree of crystallization as a function of time at 120 ºC for various PLA/CNC nanocomposites.

Isothermal crystallization tests have also been performed at 120 ºC. Typical sigmoid curves plotting the degree of crystallization as a function of time are presented in Figure 6.7. Curves of selected hybrid solution/melt mixing materials (blends #3, 4 and 5), containing all 1 wt% of CNC, are practically superposed. The differences between these three curves are much less

pronounced than in the non-isothermal scans (Fig. 6.6a). The fact that the L-PEO concentration is 10 times higher in blends #4 and 5 seems to have a marginal effect in isothermal crystallization at 120 ºC. This might suggest that the nucleation is mostly controlled by CNC (constant concentration in the three blends) at temperatures higher than the optimal T_c (i.e. the temperature for which the polymer exhibits the highest crystallization rate), such as 120 ºC. The half-time of crystallization ($t_{1/2}$) of hybrid mixing materials is about 5 min, which is comparable with the $t_{1/2}$ of PLA-based flax fiber composites charged at 10 wt% [43]. This represents an improvement of about 60% in comparison with the $t_{1/2}$ of 12 min for the neat PLA matrix. Regarding direct melt-mixing of the PLA/3 wt% CNC material, it was superposed with the neat PLA curve at the beginning stage of crystallization and slightly slower after ~8 min, with a $t_{1/2}$ of ~13 min. This confirms that the direct melt-mixing route does not allow the dispersion at the nanolevel scale of spray-dried CNC, as previsously observed by SEM (Fig. 6.3b). As for the PLA-g-CNC/PLA nanocomposite, it crystallized slightly faster than PLA4032.

6.3.5 Rheology

Thermal stability of all blends was tested by rheological measurements at the processing temperature (results not shown). All materials exhibited stable rheological curves over the duration of the test (~10 min). The loss in complex viscosity was less than 1% per minute for all formulations, except for blends #4 and 5, which reached a decrease of 1.5% per minute.

Complex viscosity as a function of frequency of selected blends is shown in Fig. 6.8. The same group sorting can be observed in this figure. With the exception of the interface-modified melt-mixing sample (PLA-g-CNC/PLA), all formulations exhibited a non-Newtonian behavior characterized by a plateau viscosity at low frequency, up to ~10 rad/s, followed by a power-law drop at higher frequencies. Considering the PLA4032 as a reference point, direct melt-mixing materials containing 3 and 6 wt% CNC (blends #8 and #9) accounted decreases of ~10 and 30% in complex viscosity. For hybrid solution/melt mixed nanocomposites containing low concentrations of PEO (i.e. blends #1 and #3), the decrease in complex viscosity was of the same order than the direct melt-mixing sample. For higher PEO contents, blends #4 and #5 (only the #4 is shown) complex viscosity was diminished about 10 times due to plasticization effect.

Interface modified melt-mixing nanocomposite (PLA-g-CNC/PLA) exhibited a solid-like behavior at low frequencies characterized by a continuous increase of complex viscosity as frequency decreases, indicating the presence of a CNC network structure that gives the material a better resistance against the applied deformation at low frequency. This network-like behavior is coherent with the SEM observation (Fig. 6.3c-d). Goffin et al. studied the viscoelastic properties of poly(ε-caprolactona) (PCL)/CNC nanocomposites prepared by direct and interface-modified melt-mixing procedures, observing no effect in the direct melt-mixed PCL/CNC materials whereas PCL-g-CNC/PCL induced a solid-like behavior beyond 8 wt% [44]. This behavior was due to the formation of a physical CNC network promoted by entanglements between the PCL matrix and the grafted-PCL chains. Following a similar nanocomposite preparation procedure, Bitinis et al. identified that the percolation threshold for the formation of a particle network occurred between 3 and 5 wt% CNC in PLA/natural rubber/PLA-g-CNC blends [29].

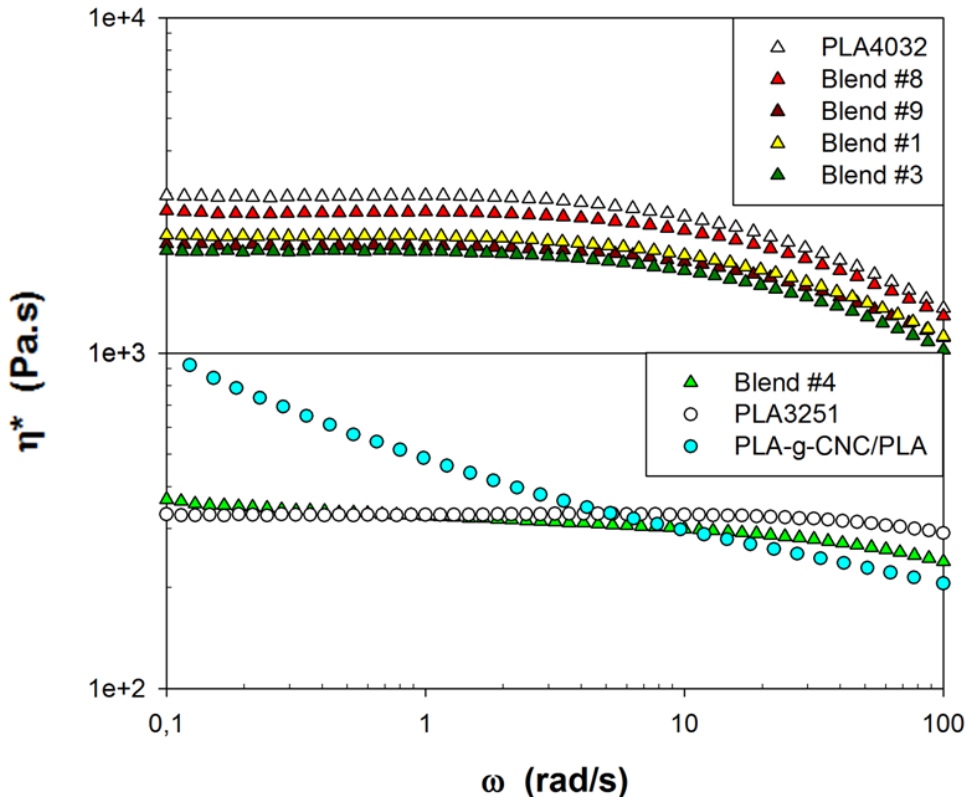

Figure 6.8: Frequency sweeps for various PLA/CNC nanocomposites at 180 ºC and 1% strain.

6.3.6 Mechanical behaviour

Dynamic Mechanical Analysis – DMA

Thermomechanical characterization was performed in order to evaluate the effect of cellulose nanocrystals and compare the different blending methods proposed. Figure 6.9a presents the storage modulus of the polymer resins and of the melt-mixed blends as a function of temperature, while Figure 6.9b presents the same results obtained for the formulations prepared with the hybrid approach. In all cases, the storage modulus was stable up to the glass transition temperature, went through a sharp decrease due to the transition from the glass to the rubbery state and increased again at temperatures where the PLA can complete its crystallization; such behavior has been also reported in our previous work [43]. The main differences between the various formulations were the onset temperature of the sharp loss and recovery process and the extent of the loss. For melt-mixed materials (Fig. 6.9a), the initial storage moduli was about 2 GPa. As temperature went above T_g, the PLA4032-based formulations presented an overlap during the whole loss and recovery process. This suggests that neither the dynamic mechanical behavior nor cold crystallization were influenced by the addition of CNC under direct melt mixing. The interface-modified melt-mixed composites exhibited faster crystallization and thus exhibited the modulus recovery about 10 ºC earlier than melt-mixed samples. This, however, may be related to the different PLA grade used in the two materials (lower *D*-lactide content). The effect of the PEO present in the materials prepared using the hybrid mixing method is important since dissolving PEO can promote crystallization of PLA. We observe that the low molecular weight PEO decreases the transition temperature and increases the rate of crystallization of the PLA matrix. Previous studies have reported a decrease of about 15 ºC in PLA/PEG blends containing 10 wt% of PEG of molecular weights from 1000 to 20 000 g/mol [34, 41]. In all cases, the storage modulus values after recovery were similar (about 0.1 GPa) and the net loss (difference between final and initial value) in the storage modulus was about 1 decade.

Figure 6.9b shows the storage modulus as a function of temperature for materials prepared by the hybrid mixing procedure. PLA is added for comparison. Blends containing H-PEO exhibited a behavior similar to that of the neat matrix. Remarkable differences were found in the three formulations containing the L-PEO. Initial values of the storage modulus were about 1 GPa, followed by a drop of around 2 decades extended from 40 to 50 ºC. At this point, the curves

reached a pseudo-steady value for the next 20 °C. At about 70 ºC, the storage moduli recovered quickly, again due to cold crystallization, and attained values close to 0.1 GPa.

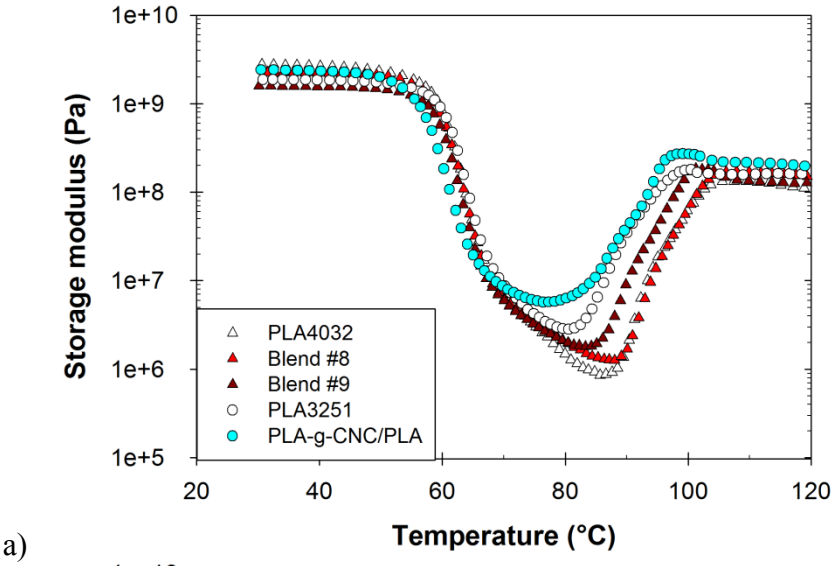

a)

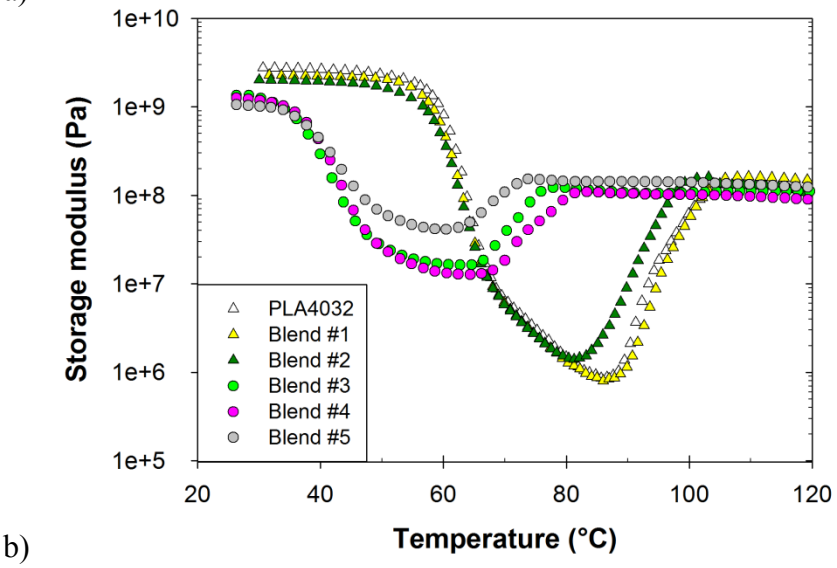

b)

Figure 6.9:. Storage modulus as a function of temperature for various PLA/CNC nanocomposites at frequency of 6.28 rad/s.

Figures 6.10a-b show the tan δ of the formulations presented in Figures 6.9a-b. The tan δ peaks of direct melt-mixing formulations were superposed to the PLA4032. The peak of PLA-g-CNC/PLA was slightly shifted to lower temperatures. Formulations prepared by the hybrid procedure containing L-PEO showed narrower peaks than blends containing H-PEO. They were

clearly shifted to lower temperatures in comparison with the tan δ peak of the neat matrix. This fact indicated that the rubbery transition begins at lower temperatures, which is a clear sign of plasticization of the neat PLA. Therefore these nanocomposites will exhibit higher flexibility and ductility as compared to the matrix, which may be interesting for further applications.

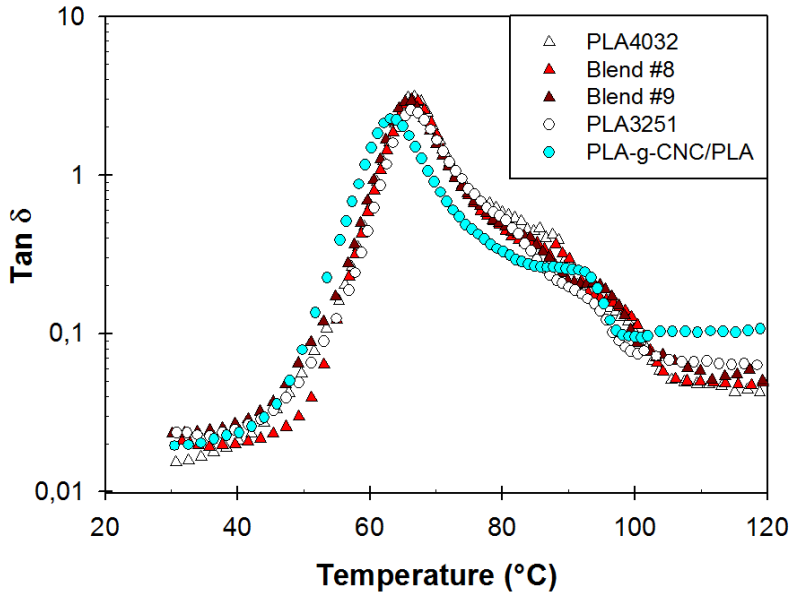

a)

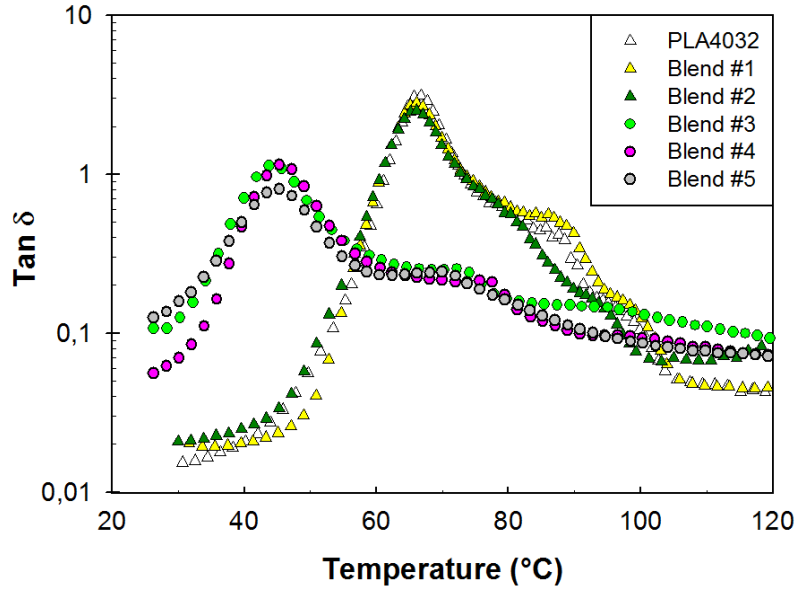

b)

Figure 6.10: Tan δ as a function of temperature for various PLA/CNC nanocomposites at a frequency of 6.28 rad/s.

Tensile properties

Mechanical properties under uniaxial tension were evaluated for all blends. Figure 6.11 presents the stress-strain curves. The tensile modulus, tensile strength and elongation at break obtained from the tensile testing are reported in Tables 6.4 and 6.5. Figure 6.11a presents the results for the materials prepared by direct melt-mixing and the interface-modified melt-mixing materials. They presented a similar behavior to the respective PLA matrices, i.e. a high tensile modulus and no yielding. PLA exhibited a Young's modulus of ~3.4 GPa, a tensile strength of 60 MPa and a strain at break of 2%. The tensile modulus was slightly increased in the presence of directly mixed 3 and 6 wt% CNC, increasing to about 3.8 and 3.6, GPa, respectively. PLA-grafted CNC based nanocomposites exhibited a tensile modulus in the same range. The tensile strength however was severely decreased by the presence of the PLA-grafted CNC, dropping from 54 MPa for neat PLA3251 to 35 MPa. The tensile strength for the unmodified 3 wt% CNC blend was nearly unchanged compared to neat PLA.

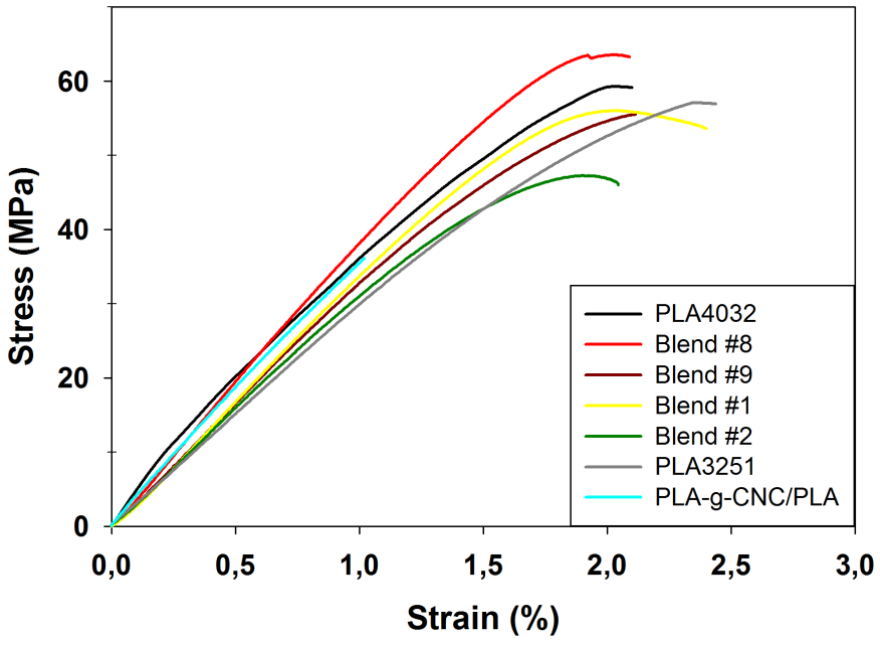

a)

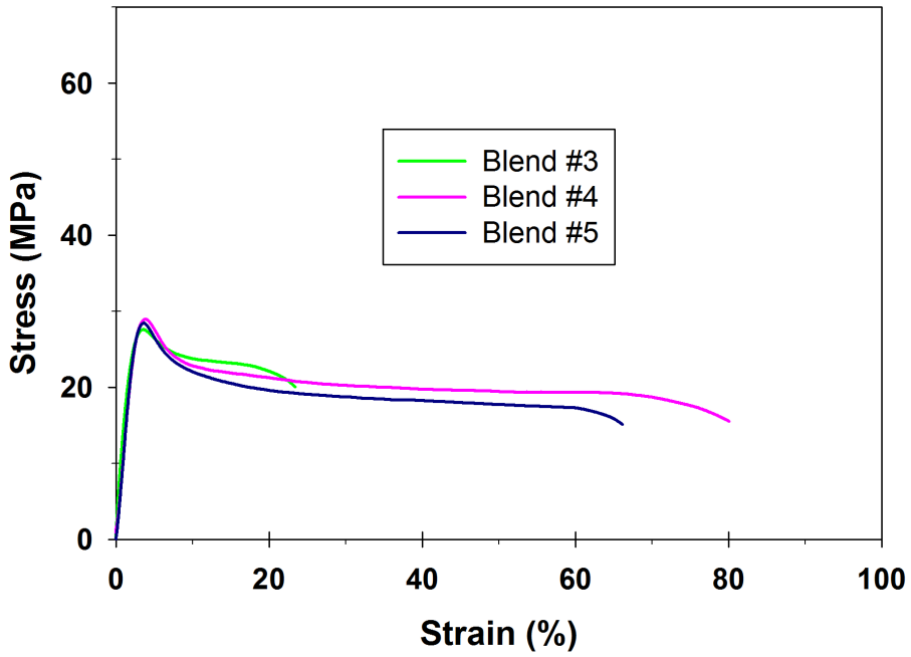

b)

Figure 6.11: Typical stress-strain curves for various PLA/CNC nanocomposites.

Table 6.4: Tensile properties of various PLA/CNC nanocomposites

No.	Mixing method	CNC source	Ratio PEO:CNC	E (GPa)	σ_{max} (MPa)	ε_{break} (%)
1	Hybrid method	BB1	0.25	3.6 ± 0.2	53 ± 4	2.5 ± 0.4
2		BB2	1.0	3.3 ± 0.2	47 ± 2	2.4 ± 0.4
3		BB3	1.25	1.5 ± 0.2	26 ± 3	28 ± 13
4		BB4	12.5	1.3 ± 0.2	30 ± 1	80 ± 5
5		BB5	12.5	1.0 ± 0.2	28 ± 2	51 ± 16
6	Melt-mixing	Spray dried	0.25	3.5 ± 0.2	60 ± 2	2.3 ± 0.3
7		Spray dried	1.0	3.5 ± 0.1	54 ± 2	2.0 ± 0.2
8		Spray dried	n/a	3.8 ± 0.1	63 ± 1	2.2 ± 0.1
9		Spray dried	n/a	3.6 ± 0.3	54 ± 4	2.0 ± 0.3

Table 6.5: Tensile properties of neat PLA matrices and interface modified PLA/CNC nanocomposites

Samples	E (GPa)	σ_{max} (MPa)	ε_{break} (%)
PLA 4032	3.4 ± 1.7	61 ± 1.2	2.7 ± 0.5
PLA3251	2.9 ± 0.6	54 ± 3.6	2.4 ± 0.4
PLA-g-CNC/PLA	3.7 ± 1.7	38 ± 2.4	1.1 ± 0.2

The materials prepared by the hybrid mixing procedure all incorporate a fraction of PEO. Those prepared with H-PEO (blends #1 and #2) exhibited a superposed behavior to the neat PLA matrix (Figure 6.11a), meanwhile the L-PEO present in the blends #3, #4 and #5 plasticized the nanocomposites and resulted in a much more ductile behavior with a yield stress and an extensive deformation before break (Figure 6.11b). The elongation at break attained values ~10 times larger than the neat PLA matrix for the PEO/CNC ratio of 1.25 (i.e. 1.25 wt% PEO) and more than 20 times for the ratio of 12.5. Accordingly tensile modulus and tensile strength were decreased due to plasticization, reaching values about 1.5 GPa and 30 MPa, respectively.

It is worth to note that the improvement of the tensile modulus and tensile strength does not necessarily mean well-dispersed nanocrystals. For example, it was shown in the morphology section that the interface-modified melt-mixing route exhibited better nanoparticule dispersion than the direct-melt mixed route; however the former material presented an important decrease in tensile strength. A similar situation was found in the nanocomposites prepared by the hybrid mixing route. No significant improvement or decrease was noticed in the tensile behavior of the blends containing H-PEO, however they exhibited big agglomerates of the PEO/CNC freeze-dried product after melt-mixing (Fig. 6.4a). Blends based on L-PEO exhibited an exceptional CNC dispersion, however the plasticization controlled the tensile behavior and the concentration of cellulose nanocrystals (1 wt%) was too low to allow a noticeable improvement of the mechanical behavior.

6.4 CONCLUSION

In this work the preparation of PLA-based cellulose nanocrystal (CNC) nanocomposites via a novel two-step process for improving the nanolevel dispersion of CNC was successfully achieved. The first step consisted in the encapsulation of the nanocrystals using polyethylene oxide (PEO) as a polymer carrier via a solution-mixed procedure, followed by freeze-drying. In a second step, the binary blend formed by PEO and CNC was melt-mixed in the PLA matrix. High and low molecular weights PEO were chosen and four PEO/CNC ratios were evaluated (two for each MW). Morphology of nanocomposite microtomed surfaces showed that the number of agglomerates was reduced as the H-PEO/CNC ratio raised from 0.25 to 1.0, suggesting that part of the CNC had been dispersed as primary particles difficult to observe in SEM, due to the presence of PEO. When using the L-PEO and higher ratios (i.e. 1.25 and 12.5) the agglomerates completely disappeared, indicating a much finer dispersion of CNC. Nanocomposites based on L-PEO/CNC binary blends reached full crystallization upon cooling, demonstrating a clear synergic effect between the plasticization of PLA due to the presence of L-PEO and the nucleation effect of the well-dispersed cellulose crystals. Evolution of the storage modulus as a function of temperature exhibited a surprising recovery, mainly explained by the faster cold crystallization taking place in the material. Mechanical properties under uniaxial tension showed that the brittle behavior of PLA could be transformed to ductile as the L-PEO content increased. L-PEO exhibited very good performance as a carrier and dispersing agent for CNC, leading to the formation of well-dispersed PLA/PEO/CNC nanocomposites. Synergistic effects between plasticization and reinforcement at higher contents of CNC might represent an interesting way to improve further the properties of these largely bio-based materials.

6.5 ACKNOWLEDGMENTS

The authors kindly thank the funding program for international internships provided by FQRNT (Fonds de Recherche Nature et Technologie du Québec) which made possible the collaboration between LIMATB (Lorient, France) and Polytechnique (Montréal, Canada) for this study. Funding from NSERC (Natural Sciences and Engineering Research Council of Canada) is also greatly acknowledged.

6.6 REFERENCES

[1] D. Garlotta, "A literature review of poly(lactic acid)," *Journal of Polymers and the Environment,* vol. 9, pp. 63-84, Apr 2001.

[2] R. Auras, B. Harte, and S. Selke, "An overview of polylactides as packaging materials," *Macromolecular Bioscience,* vol. 4, pp. 835-864, Sep 2004.

[3] S. Saeidlou, M. A. Huneault, H. B. Li, and C. B. Park, "Poly(lactic acid) crystallization," *Progress in Polymer Science,* vol. 37, pp. 1657-1677, Dec 2012.

[4] A. P. Gupta and V. Kumar, "New emerging trends in synthetic biodegradable polymers - Polylactide: A critique," *European Polymer Journal,* vol. 43, pp. 4053-4074, Oct 2007.

[5] N. Lin, J. Huang, and A. Dufresne, "Preparation, properties and applications of polysaccharide nanocrystals in advanced functional nanomaterials: a review," *Nanoscale,* vol. 4, pp. 3274-3294, 2012.

[6] S. Kalia, A. Dufresne, B. M. Cherian, B. S. Kaith, L. Averous, J. Njuguna*, et al.*, "Cellulose-based bio- and nanocomposites: A review," *International Journal of Polymer Science,* p. 837875 (15 pp.), / 2011.

[7] G. Siqueira, J. Bras, and A. Dufresne, "Cellulosic Bionanocomposites: A Review of Preparation, Properties and Applications," *Polymers,* vol. 2, pp. 728-765, Dec 2010.

[8] M. Samir, F. Alloin, and A. Dufresne, "Review of recent research into cellulosic whiskers, their properties and their application in nanocomposite field," *Biomacromolecules,* vol. 6, pp. 612-626, Mar-Apr 2005.

[9] J. F. Sassi and H. Chanzy, "Ultrastructural aspects of the acetylation of cellulose," *Cellulose,* vol. 2, pp. 111-127, Jun 1995.

[10] S. Elazzouzi-Hafraoui, Y. Nishiyama, J. L. Putaux, L. Heux, F. Dubreuil, and C. Rochas, "The shape and size distribution of crystalline nanoparticles prepared by acid hydrolysis of native cellulose," *Biomacromolecules,* vol. 9, pp. 57-65, Jan 2008.

[11] I. Kvien, B. S. Tanem, and K. Oksman, "Characterization of cellulose whiskers and their nanocomposites by atomic force and electron microscopy," *Biomacromolecules,* vol. 6, pp. 3160-3165, Nov-Dec 2005.

[12] Y. Habibi, L. A. Lucia, and O. J. Rojas, "Cellulose Nanocrystals: Chemistry, Self-Assembly, and Applications," *Chemical Reviews,* vol. 110, pp. 3479-3500, Jun 2010.

[13] S. J. Eichhorn, "Cellulose nanowhiskers: promising materials for advanced applications," *Soft Matter,* vol. 7, pp. 303-315, 2011.

[14] V. Favier, H. Chanzy, and J. Y. Cavaille, "Polymer nanocomposites reinforced by cellulose whiskers," *Macromolecules,* vol. 28, pp. 6365-6367, Aug 1995.

[15] V. Favier, G. R. Canova, J. Y. Cavaille, H. Chanzy, A. Dufresne, and C. Gauthier, "Nanocomposites materials from latex and cellulose whiskers," *Polymers for Advanced Technologies,* vol. 6, pp. 351-355, May 1995.

[16] W. Helbert, J. Y. Cavaille, and A. Dufresne, "Thermoplastic nanocomposites filled with wheat straw cellulose whiskers .1. Processing and mechanical behavior," *Polymer Composites,* vol. 17, pp. 604-611, Aug 1996.

[17] A. Dufresne, J. Y. Cavaille, and W. Helbert, "Thermoplastic nanocomposites filled with wheat straw cellulose whiskers .2. Effect of processing and modeling," *Polymer Composites,* vol. 18, pp. 198-210, Apr 1997.

[18] N. L. G. de Rodriguez, W. Thielemans, and A. Dufresne, "Sisal cellulose whiskers reinforced polyvinyl acetate nanocomposites," *Cellulose,* vol. 13, pp. 261-270, Jun 2006.

[19] G. Chauve, L. Heux, R. Arouini, and K. Mazeau, "Cellulose poly(ethylene-co-vinyl acetate) nanocomposites studied by molecular modeling and mechanical spectroscopy," *Biomacromolecules,* vol. 6, pp. 2025-2031, Jul-Aug 2005.

[20] M. Samir, F. Alloin, J. Y. Sanchez, and A. Dufresne, "Cellulose nanocrystals reinforced poly(oxyethylene)," *Polymer,* vol. 45, pp. 4149-4157, May 2004.

[21] M. Roohani, Y. Habibi, N. M. Belgacem, G. Ebrahim, A. N. Karimi, and A. Dufresne, "Cellulose whiskers reinforced polyvinyl alcohol copolymers nanocomposites," *European Polymer Journal,* vol. 44, pp. 2489-2498, Aug 2008.

[22] I. Kvien and K. Oksman, "Orientation of cellulose nanowhiskers in polyvinyl alcohol," *Applied Physics a-Materials Science & Processing,* vol. 87, pp. 641-643, Jun 2007.

[23] D. Bondeson and K. Oksman, "Polylactic acid/cellulose whisker nanocomposites modified by polyvinyl alcohol," *Composites Part a-Applied Science and Manufacturing,* vol. 38, pp. 2486-2492, 2007.

[24] K. Ben Azouz, E. C. Ramires, W. Van den Fonteyne, N. El Kissi, and A. Dufresne, "Simple Method for the Melt Extrusion of a Cellulose Nanocrystal Reinforced Hydrophobic Polymer," *Acs Macro Letters,* vol. 1, pp. 236-240, Jan 2012.

[25] L. Jiang, E. Morelius, J. W. Zhang, M. Wolcott, and J. Holbery, "Study of the Poly(3-hydroxybutyrate-co-3-hydroxyvalerate)/Cellulose Nanowhisker Composites Prepared by Solution Casting and Melt Processing," *Journal of Composite Materials,* vol. 42, pp. 2629-2645, Dec 2008.

[26] E. E. M. Ahmad and A. S. Luyt, "Morphology, thermal, and dynamic mechanical properties of poly(lactic acid)/sisal whisker nanocomposites," *Polymer Composites,* vol. 33, pp. 1025-1032, 2012.

[27] J. M. Raquez, Y. Murena, A. L. Goffin, Y. Habibi, B. Ruelle, F. DeBuyl*, et al.*, "Surface-modification of cellulose nanowhiskers and their use as nanoreinforcers into polylactide: A sustainably-integrated approach," *Composites Science and Technology,* vol. 72, pp. 544-549, Mar 2012.

[28] D. Bondeson and K. Oksman, "Dispersion and characteristics of surfactant modified cellulose whiskers nanocomposites," *Composite Interfaces,* vol. 14, pp. 617-630, 2007.

[29] N. Bitinis, R. Verdejo, J. Bras, E. Fortunati, J. M. Kenny, L. Torre*, et al.*, "Poly(lactic acid)/natural rubber/cellulose nanocrystal bionanocomposites Part I. Processing and morphology," *Carbohydrate Polymers,* vol. 96, pp. 611-620, 2013.

[30] M. Jonoobi, J. Harun, A. P. Mathew, and K. Oksman, "Mechanical properties of cellulose nanofiber (CNF) reinforced polylactic acid (PLA) prepared by twin screw extrusion," *Composites Science and Technology,* vol. 70, pp. 1742-1747, Oct 2010.

[31] B. Braun, J. R. Dorgan, and L. O. Hollingsworth, "Supra-Molecular EcoBioNanocomposites Based on Polylactide and Cellulosic Nanowhiskers: Synthesis and Properties," *Biomacromolecules,* vol. 13, pp. 2013-2019, Jul 2012.

[32] A. L. Goffin, J. M. Raquez, E. Duquesne, G. Siqueira, Y. Habibi, A. Dufresne*, et al.*, "From Interfacial Ring-Opening Polymerization to Melt Processing of Cellulose Nanowhisker-Filled Polylactide-Based Nanocomposites," *Biomacromolecules,* vol. 12, pp. 2456-2465, Jul 2011.

[33] S. Buddhiranon, N. Kim, and T. Kyu, "Morphology Development in Relation to the Ternary Phase Diagram of Biodegradable PDLLA/PCL/PEO Blends," *Macromolecular Chemistry and Physics,* vol. 212, pp. 1379-1391, Jul 2011.

[34] M. Sheth, R. A. Kumar, V. Dave, R. A. Gross, and S. P. McCarthy, "Biodegradable polymer blends of poly(lactic acid) and poly(ethylene glycol)," *Journal of Applied Polymer Science,* vol. 66, pp. 1495-1505, Nov 1997.

[35] M. Baiardo, G. Frisoni, M. Scandola, M. Rimelen, D. Lips, K. Ruffieux*, et al.*, "Thermal and mechanical properties of plasticized poly(L-lactic acid)," *Journal of Applied Polymer Science,* vol. 90, pp. 1731-1738, Sep 2003.

[36] A. Bendahou, Y. Habibi, H. Kaddami, and A. Dufresne, "Physico-Chemical Characterization of Palm from Phoenix Dactylifera-L, Preparation of Cellulose Whiskers and Natural Rubber-Based Nanocomposites," *Journal of Biobased Materials and Bioenergy,* vol. 3, pp. 81-90, Mar 2009.

[37] W. Y. Hamad and C. Miao, "Nanocomposite biomaterials of nanocrystalline cellulose (NCC) and polylactic acid (PLA)," ed: Google Patents, 2011.

[38] M. Roman and W. T. Winter, "Effect of sulfate groups from sulfuric acid hydrolysis on the thermal degradation behavior of bacterial cellulose," *Biomacromolecules,* vol. 5, pp. 1671-1677, Sep-Oct 2004.

[39] R. J. Li, J. M. Fei, Y. R. Cai, Y. F. Li, J. Q. Feng, and J. M. Yao, "Cellulose whiskers extracted from mulberry: A novel biomass production," *Carbohydrate Polymers,* vol. 76, pp. 94-99, Mar 2009.

[40] Y. C. Peng, D. J. Gardner, and Y. S. Han, "Drying cellulose nanofibrils: in search of a suitable method," *Cellulose,* vol. 19, pp. 91-102, Feb 2012.

[41] K. Sungsanit, N. Kao, and S. N. Bhattacharya, "Properties of linear poly(lactic acid)/polyethylene glycol blends," *Polymer Engineering and Science,* vol. 52, pp. 108-116, Jan 2012.

[42] C. Courgneau, V. Ducruet, L. Averous, J. Grenet, and S. Domenek, "Nonisothermal crystallization kinetics of poly(lactide)effect of plasticizers and nucleating agent," *Polymer Engineering and Science,* vol. 53, pp. 1085-1098, May 2013.

[43] A. Arias, M. C. Heuzey, and M. A. Huneault, "Thermomechanical and crystallization behavior of polylactide-based flax fiber biocomposites," *Cellulose,* vol. 20, pp. 439-452, Feb 2013.

[44] A. L. Goffin, J. M. Raquez, E. Duquesne, G. Siqueira, Y. Habibi, A. Dufresne*, et al.*, "Poly(epsilon-caprolactone) based nanocomposites reinforced by surface-grafted cellulose nanowhiskers via extrusion processing: Morphology, rheology, and thermo-mechanical properties," *Polymer,* vol. 52, pp. 1532-1538, Mar 2011.

CHAPTER 7 GENERAL DISCUSSION

This chapter contains complementary analysis to the discussion presented in the three articles summarizing the main results of this project.

Availability of flax fibers

Availability of natural fibers for composite applications was a major difficulty identified at the very beginning of this project. Traditional applications of flax and hemp fibers are dedicated to the production of different types of woven fabrics for the textile industry. Europe is the largest producer of flax fiber accounting for about two thirds of the world production for textile applications. The high quality of flax fiber produced in Europe is the result of the combination of suitable soils, favorable climatic conditions and experienced farmers. The emerging market of biocomposites has promoted the adaptation of extraction methods and treatments for producing low cost natural fibers with homogenous dimensions and high specific mechanical properties, but their market is still in development.

Canada is among the larger producers and exporters of flax seeds in the world. Although the widespread flax and hemp plantations in this country, few suppliers of natural high-strength fibers exist. To our knowledge, BioFibre Industries Ltd. (Saskatchewan) and Stemergy (before called Hempline, Ontario) have been the first companies getting involved in the production of flax and hemp short fibers for composite applications. However, the samples provided by these two companies were not suitable for research purposes since they exhibited high dispersion in size and shape, and residues from the extraction process were still present.

Short flax fiber samples from France were also obtained, thanks to the collaboration with the research center LIMATB (Laboratoire d'Ingénierie de MATériaux) from the Université de Bretagne Sud). Preliminary optical microscope observations allowed confirming the rod-like shape of these fibers, which had a monodisperse length of ~1mm. These fibers were chosen as reinforcements for the subsequent phases of the project.

Fiber/matrix interactions

Fiber/matrix interactions play a key role in the development of reinforced polymer composites, it has been pointed out for most of the researchers working in this field that poor fiber wettability is the main reason for explaining the low improvement of properties. In this project, the compatibilizer PLA-g-MA was studied in a large range of concentrations. It was encountered that PLA-g-MA is extremely brittle, which is not suitable for PLA biocomposites. Extensive morphological analysis by means of SEM of non-compatibilized and compatibilized formulations led to conclude that PLA and flax fiber exhibited a medium level of intrinsic interactions at the molecular scale, even in the absence of a compatibilizer. Fibers partially covered by polymer and fiber breakage during tensile test instead of pull out were often encountered in the case of non-compatibilized samples. Great similarities in the surface fractures for both systems (compatibilized and non-compatibilized) were found. Based on these results, it was established that PLA-g-MA did not play a significant role as a compatibilizer for reinforced PLA systems, and that it detrimentally contributed to the brittleness of the biocomposites.

Regarding the vast variety of physicochemical treatments proposed in the literature for improving the hydrophilic/lipophilic balance at the fiber surface; the chemical grafting of an aminosilane compound (3-aminopropyl triethoxysilane, APTES) to the surface of as-received flax fibers was performed. SEM micrographs of as-received and silane-modified fibers are shown in Figure 7.1. After modification smoother and cleaner surfaces were encountered. Subsequent compounding and tensile testing indicated that no significant improvements on mechanical properties were obtained by the chemically-modified reinforcement. Finally, the as-received fibers were chosen for the following phases of this project, and inherent interactions between flax and PLA were investigated through monitoring of crystallization and characterization of mechanical and thermomechanical properties.

a)

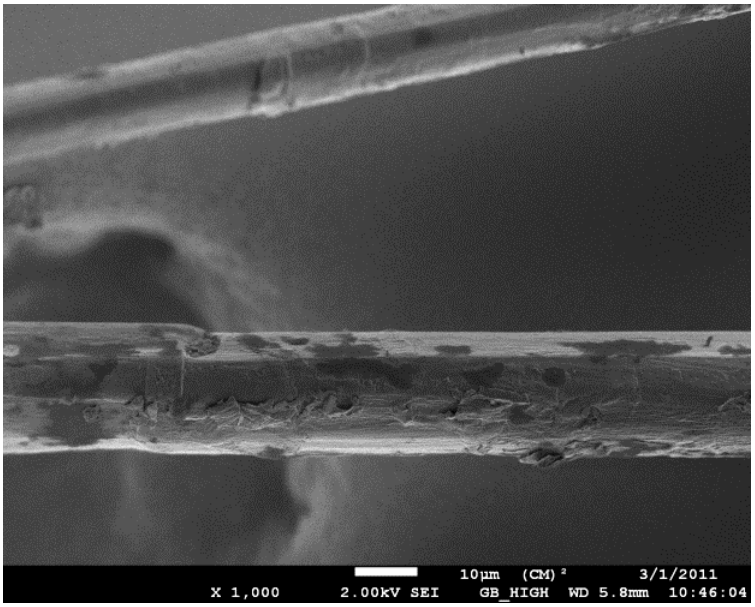

b)

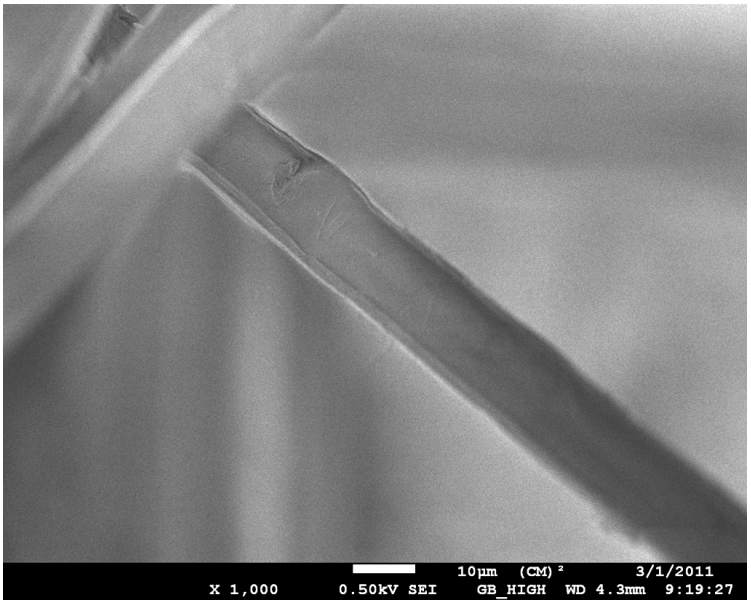

Figure 7.1: SEM micrographs of a) as-received and b) silane-modified flax fibers.

Polymer crystallization is one of the most significant phenomena in polymer science; each polymer exhibits more or less a particular crystallization behavior depending on its intrinsic characteristic e.g., chemical structure and molecular weight, but also external conditions such as thermal history, cooling or heating rates, shear or elongation flow and the presence of additives or

other polymer phases. Therefore, understanding the mechanism of crystallization may allow its control and further applications.

In order to understand the factors promoting the important reductions observed in the half-time of crystallization as the fiber loading rose in biocomposites, the development of crystalline structures of selected systems upon isothermal conditions was examined by means of optical microscopy. An Axioskop 40 from Carl Zeiss, equipped for polarized microscopy, was used to observed films ~60 μm thick prepared by compression molding. Films were placed between two glass slides and were melted at 180 °C in a Linkam hot stage connected to a temperature controller. The temperature was decreased slowly until reaching the set T_c.

These measurements evidenced that, in the presence of fibers, the nucleation density was increased in the bulk polymer and slight improvements in the spherulitic growth rate were identified. However, morphological studies did not evidence the preferential crystallization around the flax fibers. Transcrystalline structures, which have been clearly observed for PP-based flax fiber composites, were rarely evidenced in the case of PLA biocomposites. Fig. 7.1 compares two micrographs of compounded PLA (Fig. 7.1a) and 5 wt% flax fiber composites (Fig. 7.1b) after 400s of isothermal crystallization at 120 °C. Nuclei were equally generated in the bulk polymer than on the fiber surface. However, the spherulitic growth rate was found to be accelerated for biocomposites.

It was demonstrated that during compounding, flax fibers underwent important reductions in diameter and length. This fact has two main consequences: (1) the enlargement of the free fiber surface which may lead to higher fiber/matrix interactions and, (2) during fiber breakage, fine particles which may be called “fiber powder” will be liberated. These effects may explain the higher density of nuclei and therefore, the improvements on the crystallization rate observed by DSC measurements.

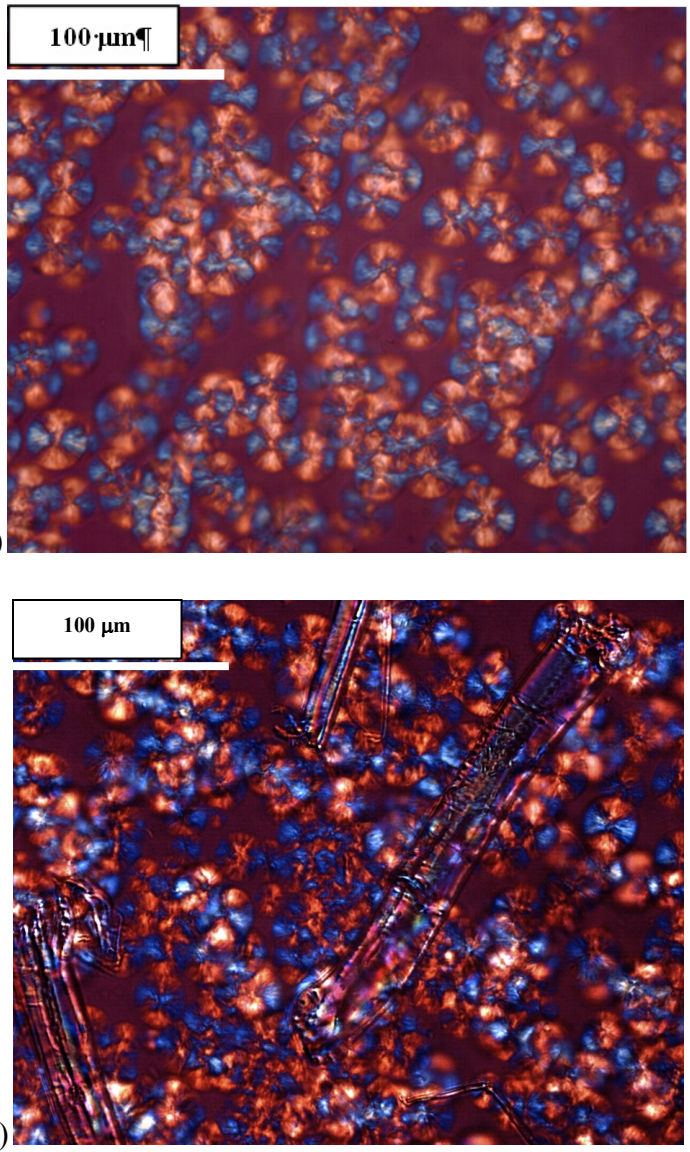

Figure 7.2: Polarized optical micrographs of films after 400s of isothermal crystallization at 120 °C for a) compounded PLA and b) 5 wt% flax fiber composites. Micrographs were obtained by polarized optical microscopy

The curves describing the half-time of crystallization as a function of temperature (Fig. 4.9) had all a similar parabolic shape and met all the same optimal crystallization temperatures. The u-shape can be explained by the presence of two driving forces. On one hand, molten-to-crystalline phase transition is promoted by lowering the temperature (higher degrees of supercooling). On the other hand, polymer chain mobility is elevated as temperature rises. Then, the temperature at

which the best compromise between both driving forces is found corresponds to the highest crystallization rate of the material. The addition of flax fiber was shown to have a remarkable effect in the edges of the curves. The reduction in the half-time of crystallization at temperatures lower than the optimal T_c (left side of the curve) might be mainly explained by the increase of nucleating points formed in the highly supercooled polymer. The increased mobility of the polymer chains at higher temperatures (right side of the curves) allow them to reach easily the nuclei. However, considering that the thermal transitions of biocomposites, i.e. glass transition and melting temperatures, remained unchanged on the whole range of flax fiber loading explored, it is possible that the local mobility of the polymer chains was not strongly affected by the presence of flax fibers at the molecular level.

Crystallization measured by rheometry

Crystallization has been commonly studied by differential scanning calorimetry, which basically is a technique that measures the heat flow necessary to maintain the same temperature in an analyzed sample and a reference during thermal transitions. However, sample size for DSC experiments is extremely small in comparison with plastic objects of common usage. On the other hand, rheometers are equipped with very precise temperature control devices and allow the testing of considerably larger samples, in different flow geometries, under various thermal and shear-flow histories which may allow studying the crystallization phenomenon in conditions closer to industrial processing. However, extracting information related to crystallinity from rheological curves in the presence of crystallization remains a field of future development.

In an effort to correlate the morphology of samples to specific upturns of the complex viscosity curve, preliminary SEM observations of the surface of rheological samples carefully removed from the rheometer after crystallization tests were carried out. For this, the disc was embedded in epoxy resin and a systematic polishing procedure was performed with sandpaper from macrogrits starting at 60 up to microgrits of about 300. Figure 7.3 shows an example of such micrographs, where spherulites of several microns can be easily observed. A systematic etching of the surface might be useful to correctly remove the amorphous phase and highlight the crystalline structural features.

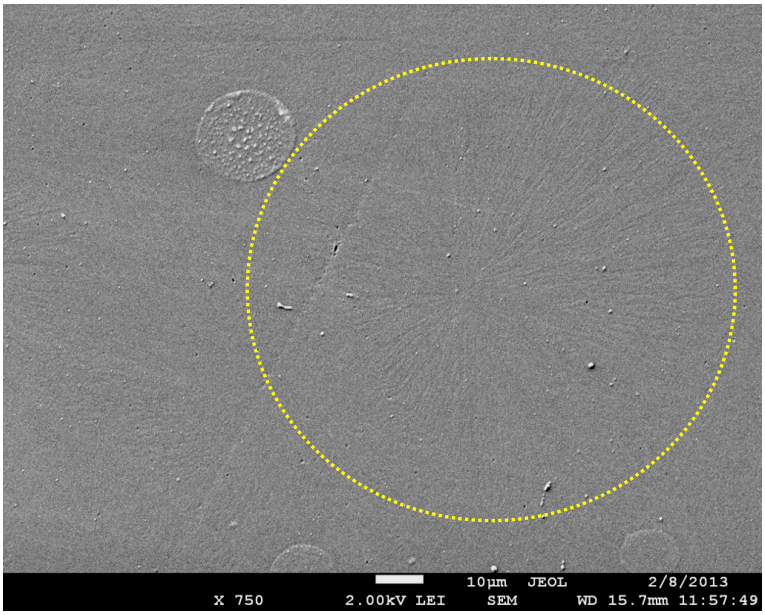

Figure 7.3: SEM micrograph of the surface of a sample crystallized in the rheometer at 130 °C. Sample was removed after the crystallization experiment and the surface was polished before observation.

Cellulose nanocomposites

The migration from the micro to nanoscale represents a major challenge in the industry of polymer composites. Homogenously dispersed nanoparticles have the potential to improve the mechanical performance at very low content without affecting the optical properties of the neat matrix.

Several attempts to disperse well cellulose nanocrystals in hydrophobic matrices have been extensively reported in the literature. However, the inherent necessity of using water for reaching the dispersion and stabilization of CNC suspensions is still a major concern. The novel two-step process explored in this project offers a feasible way to adequately disperse nanocrystals. Despite the fact that TEM observations could not be successfully achieved, observations using FEG-SEM at high magnification allowed the identification of superposed individual nanocrystals. Figure 7.4 shows a few single nanocrystals observed at the highest PEO:CNC ratio tested. The marked effect in the dispersion when decreasing the molecular weight of PEO indicated that the chain length of the polymer carrier had a significant effect on the encapsulation of nanocrystals;

therefore, molecular weight should be considered as a key parameter in the effectiveness of the polymer carrier.

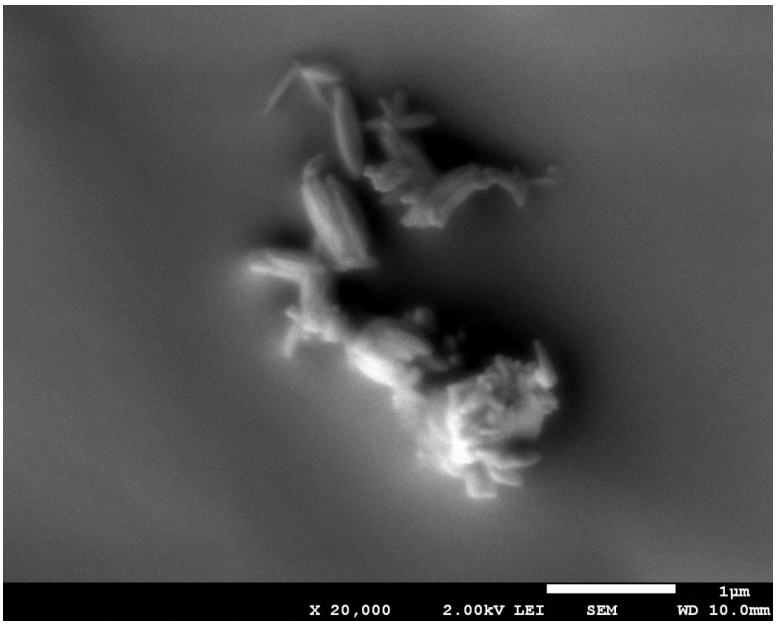

Figure 7.4:.FEG-SEM micrograph of microtomed surface of PLA/ 1 wt%CNC/86.5 wt% L-PEO (blend #4).

CHAPTER 8 CONCLUSIONS AND RECOMMENDATIONS

8.1 CONCLUSIONS

This research aimed at developing new fully biobased and biodegradable composites and nanocomposites. The objectives proposed at the beginning of this project were achieved and the main results are summarized in three scientific articles. The conclusions of this dissertation can be summarized as follows:

Melt compounding of fully biobased and biodegradable flax-fiber reinforced PLA composites was successfully achieved in a wide fiber loading range, from 1 to 20 wt%. The addition of fibers led to the increase of the melt viscosity of compounded PLA, for example, 10 wt% flax fibers resulted in a viscosity increase of 50% compared with compounded PLA, i.e. from 3000 to 4500 Pa.s. Thermal stability was also modified by the presence of such reinforcements; monitoring rheological properties over time showed that the complex viscosity dropped about 0.1% per minute in the case of compounded PLA and 2% per minute at fiber loading of 10 wt%.

Processing had a strong effect in the size reduction of flax fiber; the length of as-received flax fibers, ~1mm, was reduced by 75% and the mean diameter dropped from 70 to about 30 μm. Most fiber bundles were broken up and an important population of single fibers was noted. The aspect ratio dropped from ~30 to ~15. Length and diameter distributions were found to be narrower after compounding, indicating that fiber breakage led to more monodisperse reinforcement. Despite the fact that the aspect ratio decreased by half after compounding, tensile properties demonstrated the potential of flax fiber as a reinforcement for the PLA matrix. Young modulus rose ~50% in the presence of 20 wt% flax fibers, while tensile strength exhibited ~10% increase for the same loading.

The addition of flax fibers accelerated the crystallization rate of PLA upon isothermal and non-isothermal conditions. The reduction of the half-time of isothermal crystallization was controlled by the increase in flax fiber content; this behavior was remarkable on the edges of the crystallization temperature interval, i.e. T_c < 100 °C and T_c > 110 °C. The highest isothermal crystallization rates were observed between 100 and 110 °C for all systems, and less significant reductions of $t_{1/2}$ in the presence of the fibers were found in this interval. Despite the accelerated

crystallization observed in PLA biocomposites, the total crystallinity remained nearly constant for all systems, around 36%.

PLA-g-MA was not found to have a notable effect as a compatibilizer for the PLA-based flax fiber systems. Its addition resulted in more brittle composites. Surprisingly, SEM observations of fracture surfaces after tensile testing evidenced good fiber/matrix interactions in the case of non-compatiblized biocomposites and, similar fracture mechanisms were observed with and without PLA-g-MA.

In the second part of this research, rheological properties of PLA and PLA-5 wt% flax fiber composites were studied in the molten state, and subsequently, upon supercooling conditions in order to promote crystallization during rheological testing. The Arrhenius equation was found to describe properly the melt viscosity as a function of temperature for both systems. The presence of fibers slightly increased the flow activation energy of the compounded matrix, which exhibited a value of ~75 kJ/mol; this result was in a close agreement with a previous study using a similar PLA grade. Accurate predictions of the initial complex viscosity values were obtained at lower supercooling degrees, i.e. higher crystallization temperatures. As T_c was lowered, the crystallization phenomena took place earlier leading to important differences between the predicted and measured data. Complex viscosity (η^*), storage (G') and loss modulus (G'') curves showed sigmoidal shapes similar to those describing the degree of crystallinity as a function of time. The nucleating effect of flax fibers was remarkable at low degree of supercooling; particularly, at 130 and 140 °C the test duration was reduced by more than 50% when comparing PLA to its 5wt% composite.

The empirical method proposed for the calculation of induction time was found to overestimate the values of this parameter at high crystallization rates. Comparison between the results obtained by rheometry and DSC techniques indicated that, at $T_c > 130$ °C, the standardized residual method brought reliable calculation of t_{ind}. Further analyses correlating the evolution of rheological properties with the half-time of crystallization or the degree of crystallinity were not possible to achieve, mainly due to the lack of adequate models for the systems explored in this study. Under shear-flow conditions, crystallization of compounded PLA at 140 °C was found to be improved in the whole range of shear rate explored, i.e. 0.5 – 4 s^{-1}. The highest shear rate led

to the largest reduction in induction time, which accounted for about 75% compared to the quiescent crystallization of PLA.

Nanocomposites based on ternary blends of PLA, PEO and CNC were prepared following a novel two-step process combining solution-mixing and melt-mixing procedures. PEO of high and low molecular weight was found to play a key role in the enhancement of CNC/PLA interactions, as a consequence, remarkable improvements of the dispersion of nanocrystals in the PLA matrix were successfully achieved. The extend of agglomerate breakup and nanolevel dispersion was controlled by the PEO:CNC ratio present in the ternary blend. The higher the PEO:CNC ratio, the better the nanocrystals were dispersed. It was demonstrated that the direct melt mixing route did not allow the presence of single nanocrystals.

PLA nanocomposites based on L-PEO/CNC binary blends exhibited remarkable improvements in the crystallization rate of compounded matrix. The presence of L-PEO led to a double effect in the final nanocomposites, it plasticized the PLA matrix and it promoted the interactions between CNC and PLA polymer chains at the same time. This synergistic effect results in enhanced crystallization and thermomechanical behavior. Upon cooling at 10 °C/min such nanocomposites achieved full crystallization, meanwhile neat PLA did not exhibit any crystallization peak under the same cooling rate. During the rubbery transition, the storage modulus showed a faster and earlier recovery compared with the compounded matrix, mainly due to the cold crystallization phenomenon taking place as temperature rises.

Finally, the novel process explored in the third part of this research is a potential alternative to the production of well-dispersed CNC in hydrophobic matrices via a melt-compounded route. It however requires a polymer carrier that is miscible with the main matrix.

8.2 ORIGINAL AND MAIN CONTRIBUTIONS

A comprehensive study of the crystallization and thermomechanical properties of PLA-based flax fiber composites was performed in order to contribute to the understanding of the intrinsic fiber/matrix interactions for such systems. It was demonstrated, by means of various characterization methods that flax fibers act as nucleating agent, leading to the acceleration of the crystallization rate of PLA. However, the maximum degree of crystallinity remained similar to that of the compounded PLA.

The evolution of viscoelastic properties in the presence of crystallization for compounded PLA and its flax fiber composites has not been addressed before in the scientific literature. The validation of an empirical method to calculate the induction time from rheological measurements allowed the identification of the supercooling conditions from which the method gave reliable results. A preliminary study of shear-flow induced crystallization of PLA was also performed.

The novel two-step process detailed in the third part of this research is a potential solution for obtaining well-dispersed cellulose nanocrystals in a partially hydrophobic matrix such as PLA. It represents a step forward to the development of PLA-based CNC nanocomposites via a melt-compounding route. To our knowledge, no work has proposed a similar approach for PLA nanocomposites. It has been demonstrated that the synergistic effect between plasticization and dispersion of nanoparticle resulting from the presence of PEO is a key parameter in the enhanced properties of PLA nanocomposites.

8.3 RECOMMENDATIONS

The following aspects are recommended for future studies in this field:

- Scale up of the melt-compounding of PLA-based flax fiber composites at higher reinforcement loading would provide additional insights about the potential issues in industrial processing and the adequate conditions needed for specific applications.
- Crystallization developed during or right after industrial polymer processing may differ importantly from results obtained by thermal analysis. Therefore, the investigation of the crystallinity development under processing and molding conditions would bring valuable information regarding the nucleating potential of flax fiber for industrial applications.
- Since it has been demonstrated that PEO improved CNC/PLA interactions and considering the similarity of chemical structures of nanocrystals and natural fibers, it would be interesting to evaluate the potential of PEO as a compatibilizer for flax fiber reinforced-systems.
- It would be greatly helpful to couple rheometry to microscopic techniques for further studies regarding the crystallinity of polymer systems under different flow/temperature histories.

- Considering the improvements achieved in the morphology and properties of PLA nanocomposites, it is recommended to explore the effect of different molecular weights of PEO and to optimize the PEO:CNC ratio as a function of the final application of the nanocomposite materials.
- To evaluate the synergistic effects between plasticization and nanocrystal reinforcement at higher contents of CNC, extrusion represents an interesting way of pursuing this study.
- PLA/PEG copolymers have acquired a great interest to modulate the hyphophilic/hydrophobic nature of bioresorbable materials for biomedical applications. The use of such copolymers as a means to obtain well-dispersed PLA nanocomposites should be explored in the future.

REFERENCES

[1] R. Auras, B. Harte, and S. Selke, "An overview of polylactides as packaging materials," *Macromolecular Bioscience,* vol. 4, pp. 835-864, Sep 2004.

[2] K. Madhavan Nampoothiri, N. Rajendran Nair, and R. Pappy John, "An Overview of the Recent Developments in Polylactide (PLA) Research," *Bioresource Technology,* vol. 101, pp. 8493-8501, 2010.

[3] D. E. Henton, P. Gruber, J. Lunt, and J. Randall, "Polylactic Acid Technology," in *Natural Fibers, Biopolymers, and Biocomposites*, A. K. Mohanty, M. Misra, and L. T. Drzal, Eds., ed: CRC Press Taylor & Francis Group, 2005, pp. 527-577.

[4] M. Jamshidian, E. A. Tehrany, M. Imran, M. Jacquot, and S. Desobry, "Poly-Lactic Acid: Production, Applications, Nanocomposites, and Release Studies," *Comprehensive Reviews in Food Science and Food Safety,* vol. 9, pp. 552-571, Sep 2010.

[5] R. Mehta, V. Kumar, H. Bhunia, and S. N. Upadhyay, "Synthesis of poly(lactic acid): A review," *Journal of Macromolecular Science-Polymer Reviews,* vol. C45, pp. 325-349, Oct-Dec 2005.

[6] D. Garlotta, "A Litterature Review of Poly(Lactic Acid)," *Journal of Polymers and the Environment,* vol. 9, pp. 63-84, April, 2001 2001.

[7] D. R. Witzke, "Introduction to Properties, Engineering, and Prospects of Polylactide Polymers," Doctor of Philosophy, Chemical Engineering, Michigan State University, 1997.

[8] G. Perego, G. D. Cella, and C. Bastioli, "Effect of molecular weight and crystallinity on poly(lactic acid) mechanical properties," *Journal of Applied Polymer Science,* vol. 59, pp. 37-43, 1996.

[9] P. Combette and I. Ernoult, *Physique des polymères* vol. I. Structure, Fabrication, Emploi: Presse Internationales Polytechnique, 2005.

[10] H. B. Li and M. A. Huneault, "Effect of nucleation and plasticization on the crystallization of poly(lactic acid)," *Polymer,* vol. 48, pp. 6855-6866, Nov 2007.

[11] S. Saeidlou, M. A. Huneault, H. B. Li, and C. B. Park, "Poly(lactic acid) crystallization," *Progress in Polymer Science,* vol. 37, pp. 1657-1677, Dec 2012.

[12] R. Wool, *Polymer Interfaces: Structure and Strength*: Carl Hanser Verlag, 1995.

[13] H. Tsuji and Y. Ikada, "Blends of isotactic and atactic poly(lactide)s: 2. Molecular-weight effects of atactic component on crystallization and morphology of equimolar blends from the melt.," *Polymer,* vol. 37, pp. 595-602, Feb 1996.

[14] H. Tsuji and Y. Ikada, "Properties and morphologies of poly(-lactide): 1. Annealing condition effects on properties and morphologies of poly(-lactide)." *Polymer,* vol. 36, pp. 2709-2716, 1995.

[15] D. M. Bigg, "Properties and Engineering of Polylactide," presented at the Society of Plastics Engineers: Annual Technical Conference, 1996.

[16] J.-R. Sarasua, R. E. Prud'homme, M. Wisniewski, A. Le Borgne, and N. Spassky, "Crystallization and Melting Behavior of Polylactides," *Macromolecules,* vol. 31, pp. 3895-3905, 1998.

[17] M. Yasuniwa, S. Tsubakihara, Y. Sugimoto, and C. Nakafuku, "Thermal analysis of the double-melting behavior of poly(L-lactic acid)," *Journal of Polymer Science Part B: Polymer Physics,* vol. 42, pp. 25-32, 2004.

[18] J. J. Kolstad, "Crystallization Kinetics of Poly(i-lactide-co-meso-lactide)," *Journal of Applied Polymer Science,* vol. 62, pp. 1079-1996, 1996.

[19] S. C. Schmidt and M. A. Hillmyer, "Polylactide stereocomplex crystallites as nucleating agents for isotactic polylactide," *Journal of Polymer Science Part B: Polymer Physics,* vol. 39, pp. 300-313, 2001.

[20] Y. Ikada, K. Jamshidi, H. Tsuji, and S. H. Hyon, "Stereocomplex formation between enantiomeric poly(lactides)," *Macromolecules,* vol. 20, pp. 904-906, 1987.

[21] J. Huang, M. S. Lisowski, J. Runt, E. S. Hall, R. T. Kean, N. Buehler*, et al.*, "Crystallization and Microstructure of Poly(l-lactide-co-meso-lactide) Copolymers," *Macromolecules,* vol. 31, pp. 2593-2599, 1998.

[22] S. Baratian, E. S. Hall, J. S. Lin, r. Xu, and J. Runt, "Crystallization and Solid-State Structure of Random Polylactide Copolymers: Poly(L-lactide-co-D-lactide)s," *Macromolecules,* vol. 34, pp. 4857-4864, 2001.

[23] H. Abe, Y. Kikkawa, Y. Inoue, and Y. Doi, "Morphological and Kinetic Analyses of Regime Transition for Poly[(S)-lactide] Crystal Growth," *Biomacromolecules,* vol. 2, pp. 1007-1014, 2001.

[24] R. Vasanthakumari and A. J. Pennings, "Crystallization kinetics of poly(l-lactic acid)," *Polymer,* vol. 24, pp. 175-178, 1983.

[25] C. Baley. Fibres naturelles de renfort pour matériaux composites [Online]. Available: http://www.techniques-ingenieur.fr/base-documentaire/materiaux-th11/plastiques-et-composites-ti100/

[26] A. Bismarck, S. Mishra, and T. Lampke, "Plant Fibers as Reinforcement for Green Composites," in *Natrural Fibers, Biopolymers, and Biocomposites*, A. K. Mohanty, M. Misra, and L. T. Drzal, Eds., ed: CRC Press Taylor & Francis Group, 2005, pp. 37-108.

[27] M. J. John and S. Thomas, "Biofibres and biocomposites," *Carbohydrate Polymers,* vol. 71, pp. 343-364, 2008.

[28] N. Chand and M. Fahim, *Tribology of natural fiber polymer composites*: Woodhead Publishing Limited, 2008.

[29] A. K. Bledzki and J. Gassan, "Composites reinforced with cellulose based fibres," *Progress in Polymer Science (Oxford),* vol. 24, pp. 221-274, 1999.

[30] X. Li, L. G. Tabil, and S. Panigrahi, "Chemical treatments of natural fiber for use in natural fiber-reinforced composites: A review," *Journal of Polymers and the Environment,* vol. 15, pp. 25-33, Jan 2007.

[31] A. Bismarck, I. Aranbefwi-Askargorta, and J. Springer, "Surface Characterization of Flax, Hemp and Cellulose Fibers; Surface Properties and the Water Uptake Behavior," *Polymer Composites,* vol. 23, pp. 872 - 894, 2002.

[32] A. Dufresne, "Cellulose-Based Composites and Nanocomposites," in *Monomers, Polymers and Composites from Renewable Resources* É. F. d. P. e. INPG, Ed., ed, 2008, pp. 401-418.

[33] A. C. O'Sullivan, "Cellulose: the structure slowly unravels," *Cellulose,* vol. 4, pp. 173-207, 1997.

[34] R. A. Festucci-Buselli, W. C. Otoni, and C. P. Joshi. (2007, Structure, organization, and functions of cellulose synthase complexes in higher plants. *Brazilian Journal of Plant Physiology 19(1),* 1-13.

[35] J. W. S. Hearle and W. E. Morton, *Physical properties of textile fibres*, Fourth edition ed.: Woodhead Publishing Limited, 2008.

[36] P. Zugenmaier, "Conformation and packing or various crystalline cellulose fibers," *Prog. Polym. Sci.,* vol. 26, pp. 1341-1417, 2001.

[37] H. L. Bos, M. J. A. Van Den Ever, and O. C. J. J. Peters, "Tensile and compressive properties of flax fibres for natural fibre reinforced composites," *Journal of Materials Science,* vol. 37, pp. 1683-1692, 2002.

[38] M. A. S. Azizi Samir, F. Alloin, and A. Dufresne, "Review of recent research into cellulosic whiskers, their properties and their application in nanocomposite field," *Biomacromolecules,* vol. 6, pp. 612-626, 2005.

[39] A. Arbelaiz, B. Fernandez, G. Cantero, R. Llano-Ponte, A. Valea, and I. Mondragon, "Mechanical properties of flax fibre/polypropylene composites. Influence of fibre/matrix modification and glass fibre hybridization," *Composites Part a-Applied Science and Manufacturing,* vol. 36, pp. 1637-1644, 2005.

[40] G. Siqueira, J. Bras, and A. Dufresne, "Cellulose Whiskers versus Microfibrils: Influence of the Nature of the Nanoparticle and its Surface Functionalization on the Thermal and Mechanical Properties of Nanocomposites," *Biomacromolecules,* vol. 10, pp. 425-432, 2009.

[41] M. A. S. Azizi Samir, F. Alloin, J.-Y. Sanchez, N. El Kissi, and A. Dufresne, "Preparation of Cellulose Whiskers Reinforced Nanocomposites from an Organic Medium Suspension," *Macromolecules,* vol. 37, pp. 1386-1393, 2004.

[42] D. Bondeson, I. Kvien, and K. Oksman, "Strategies for Preparation of Cellulose Whiskers from Microcrystalline Cellulose as Reinforcement in Nanocomposites," in *Cellulose Nanocomposites: Processing, Characterization and Properties.*, K. Oksman and M. Sain, Eds., ed, 2006, pp. 10-25.

[43] I. Kvien, B. S. Tanem, and K. Oksman, "Characterization of cellulose whiskers and their nanocomposites by atomic force and electron microscopy," *Biomacromolecules,* vol. 6, pp. 3160-3165, Nov-Dec 2005.

[44] A. Chakraborty, M. Sain, and M. Kortschot, "Cellulose Microfibers as Reinforcing Agents for Structural Materials," in *Cellulose Nanocomposites: Processing, Characterization and Properties*, ed, 2006, pp. 169 - 186.

[45] A. Junior de Menezes, G. Siqueira, A. A. S. Curvelo, and A. Dufresne, "Extrusion and characterization of functionalized cellulose whiskers reinforced polyethylene nanocomposites," *Polymer,* vol. 50, pp. 4552-4563, 2009.

[46] R. Zuluaga, J.-L. Putaux, A. Restrepo, I. Mondragon, and P. Ganon, "Cellulose microfibrils from banana farming residues: isolation and characterization," *Cellulose,* vol. 14, pp. 585-592, 2006.

[47] G. Guhados, W. Wan, and J. Hutter, "Measurement of the Elastic Modulus of Single Bacterial Cellulose Fibers Using Atomic Force Microscopy," *Langmuir,* vol. 21, pp. 6642-6646, 2005.

[48] L. Wagberg, G. Decher, M. Norgren, T. Lindstrom, M. Ankerfors, and K. Axnas, "The build-up of polyelectrolyte multilayers of microfibrillated cellulose and cationic polyelectrolytes," *Langmuir,* vol. 24, pp. 784-795, Feb 2008.

[49] K. Fleming, D. Gray, S. Prasannan, and S. Matthews, "Cellulose crystallites: A new and robust liquid crystalline medium for the measurement of residual dipolar couplings," *Journal of the American Chemical Society,* vol. 122, pp. 5224-5225, May 2000.

[50] D. Y. Kim, Y. Nishiyama, and S. Kuga, "Surface acetylation of bacterial cellulose," *Cellulose,* vol. 9, pp. 361-367, 2002.

[51] S. J. Eichhorn, "Cellulose nanowhiskers: promising materials for advanced applications," *Soft Matter,* vol. 7, pp. 303-315, 2011.

[52] S. Kalia, A. Dufresne, B. M. Cherian, B. S. Kaith, L. Averous, J. Njuguna*, et al.*, "Cellulose-Based Bio- and Nanocomposites: A Review," *International Journal of Polymer Science,* 2011.

[53] D. Klemm, F. Kramer, S. Moritz, T. Lindstrom, M. Ankerfors, D. Gray*, et al.*, "Nanocelluloses: A New Family of Nature-Based Materials," *Angewandte Chemie-International Edition,* vol. 50, pp. 5438-5466, 2011.

[54] S. Paunonen, "Strength and barrier enhancements of composites and packaging boards by nanocelluloses - A literature review," *Nordic Pulp & Paper Research Journal,* vol. 28, pp. 165-181, 2013.

[55] N. Lin, J. Huang, and A. Dufresne, "Preparation, properties and applications of polysaccharide nanocrystals in advanced functional nanomaterials: a review," *Nanoscale,* vol. 4, pp. 3274-3294, 2012.

[56] T. Nishino, K. Hirao, M. Kotera, K. Nakamae, and H. Inagaki, "Kenaf reinforced biodegradable composite," *Composites Science and Technology,* vol. 63, pp. 1281-1286, Jul 2003.

[57] M. Shibata, K. Ozawa, N. Teramoto, R. Yosomiya, and H. Takeishi, "Biocomposites made from short abaca fiber and biodegradable polyesters," *Macromolecular Materials and Engineering,* vol. 288, pp. 35-43, 2003.

[58] K. Oksman, M. Skrifvars, and J. F. Selin, "Natural fibres as reinforcement in polylactic acid (PLA) composites," *Composites Science and Technology,* vol. 63, pp. 1317-1324, 2003.

[59] E. Bodros, I. Pillin, N. Montrelay, and C. Baley, "Could biopolymers reinforced by randomly scattered flax fibre be used in structural applications?," *Composites Science and Technology,* vol. 67, pp. 462-470, Mar 2007.

[60] B. Bax and J. Mussig, "Impact and tensile properties of PLA/Cordenka and PLA/flax composites," *Composites Science and Technology,* vol. 68, pp. 1601-1607, Jun 2008.

[61] C. Baley, "Analysis of the flax fibres tensile behaviour and analysis of the tensile stiffness increase.," *Composites Part a-Applied Science and Manufacturing,* vol. 33, pp. 939-948, 2002.

[62] T. Huber and J. Mussig, "Fibre matrix adhesion of natural fibres cotton, flax and hemp in polymeric matrices analyzed with the single fibre fragmentation test," *Composite Interfaces,* vol. 15, pp. 335-349, 2008.

[63] A. Le Duigou, I. Pillin, A. Bourmaud, P. Davies, and C. Baley, "Effect of recycling on mechanical behaviour of biocompostable flax/poly(L-lactide) composites," *Composites Part a-Applied Science and Manufacturing,* vol. 39, pp. 1471-1478, Sep 2008.

[64] R. A. Shanks, A. Hodzic, and D. Ridderhof, "Composites of poly(lactic acid) with flax fibers modified by interstitial polymerization," *Journal of Applied Polymer Science,* vol. 101, pp. 3620-3629, Sep 2006.

[65] J. T. Lee, M. W. Kim, Y. S. Song, T. J. Kang, and J. R. Youn, "Mechanical Properties of Denim Fabric Reinforced Poly(lactic acid)," *Fibers and Polymers,* vol. 11, pp. 60-66, Feb 2010.

[66] M. Avella, G. Bogoeva-Gaceva, A. Bularovska, M. E. Errico, G. Gentile, and A. Grozdanov, "Poly(lactic acid)-based biocomposites reinforced with kenaf fibers," *Journal of Applied Polymer Science,* vol. 108, pp. 3542-3551, Jun 2008.

[67] M. N. G. Belgacem, Alessandro, "Surface Modification of Cellulose Fibres," in *Monomers, Polymers and Composites from Renewable Resources*, É. F. d. P. e. INPG, Ed., ed, 2008, pp. 385-400.

[68] K. Weissenbach and H. Mack, "Silane Coupling Agents," in *Functional Fillers for Plastics*, M. Xanthos, Ed., ed: WILEY-VCH Verlag GmbH & Co. KGaA, 2005, pp. 59-83.

[69] J. Biagiotti, D. Puglia, L. Torre, J. Kenny, A. Arbelaiz, G. Cantero*, et al.*, "A Systematic Investigation on the Influence of the Chemical Treatment of Natural Fibers on the Properties of Their Polymer Matrix Composites," *Polymer Composites,* vol. 25, pp. 470-479, 2004.

[70] F. Marti-Ferrer, F. Vilaplana, A. Ribes-Greus, A. Benedito-Borras, and C. Sanz-Box, "Flour rice husk as filler in block copolymer polypropylene: Effect of different coupling agents," *Journal of Applied Polymer Science,* vol. 99, pp. 1823-1831, Feb 2006.

[71] V. Favier, H. Chanzy, and J. Y. Cavaille, "Polymer nanocomposites reinforced by cellulose whiskers," *Macromolecules,* vol. 28, pp. 6365-6367, 1995.

[72] K. Oksman, A. P. Mathew, D. Bondeson, and I. Kvien, "Manufacturing process of cellulose whiskers/polylactic acid nanocomposites," *Composites Science and Technology,* vol. 66, pp. 2776-2784, 2006.

[73] D. Bondeson and K. Oksman, "Polylactic acid/cellulose whisker nanocomposites modified by polyvinyl alcohol," *Composites Part A: Applied Science and Manufacturing,* vol. 38, pp. 2486-2492, 2007.

[74] D. Bondeson and K. Oksman, "Dispersion and characteristics of surfactant modified cellulose whiskers nanocomposites," *Composite Interfaces,* vol. 14, pp. 617-630, 2007.

[75] L. Petersson, I. Kvien, and K. Oksman, "Structure and thermal properties of poly(lactic acid)/cellulose whiskers nanocomposite materials," *Composites Science and Technology,* vol. 67, pp. 2535-2544, 2007.

[76] N. E. Zafeiropoulos, C. A. Baillie, and F. L. Matthews, "A study of transcrystallinity and its effect on the interface in flax fibre reinforced composite materials," *Composites Part a-Applied Science and Manufacturing,* vol. 32, pp. 525-543, 2001.

[77] C. Bernal, "Deformation and Fracture Behavior of Natural Fiber Reinforced Polypropylene," in *Polyolefin Composites*, D. Nwabunma and T. Kyu, Eds., ed: John Wiley & Sons, Inc., 2008, pp. 178-203.

[78] E. Hermida and V. Mega, "Transcrystallization kinetics at the poly(3-hydroxybutyrate-co-3-hydroxyvalerate)/hemp fibre interface," *Composites Part A: Applied Science and Manufacturing,* vol. 38, pp. 1387-1394, 2007.

[79] C. Wang and C.-R. Liu, "Transcrystallization of polypropylene composites: nucleating ability of fibres," *Polymer,* vol. 40, pp. 289-298, 1999.

[80] D. G. Gray, "Transcrystallization of polypropylene at cellulose nanocrystal surfaces," *Cellulose,* vol. 15, pp. 297-301, Apr 2008.

[81] A. P. Mathew, K. Oksman, and M. Sain, "The effect of morphology and chemical characteristics of cellulose reinforcements on the crystallinity of polylactic acid," *Journal of Applied Polymer Science,* vol. 101, pp. 300-310, Jul 2006.